Numerical Simulations of Phase Transitions in Condensed Matter

David William Greig

A thesis submitted in fulfilment of the requirements

for the degree of Doctor of Philosophy

to the

University of Edinburgh

1995

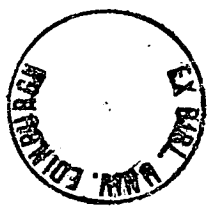

Abstract

This thesis concerns the use of classical molecular dynamics techniques, in computer simulations, to the study structure and phase transitions in various materials.

The equations required to determine the motion of atoms and molecules in the molecular dynamics simulations are discussed. Atom-atom pairwise additive potentials are used to describe the van der Waals type forces between atoms and molecules. The Parrinello-Rahman description of the equations of motion of particles in a periodically repeating cell are formulated. Quaternions are used to describe the orientations of molecules.

The melting transition in a two-dimensional cluster of krypton atoms is simulated. The structural changes on heating are examined in some detail and the possibility of a second-order melting transition and the existence of a hexatic phase between the solid and liquid phases is discussed.

The formation of a solid from a rapidly cooled liquid-like phase is investigated. Simulations of krypton atoms in a periodically repeating cell and in a cluster are performed to examine the effects of boundary conditions. Simulations on mixtures of krypton and argon atoms, in equal proportion, in both a periodically repeating cell and in a cluster are performed. The solid structures formed are discussed in terms of glass and crystalline ordering.

The orientational order-disorder transition and plastic phase in adamantane is studied. The molecular reorientation in the plastic phase is examined. Molecules occupy

two possible orientations which are related by inversion. By restricting molecules to these two orientations an Ising-like model for adamantane is produced and the order-disorder phase transition is examined in a Monte Carlo simulation. Comparison of the the molecular dynamics and Monte Carlo models is made. The disordered phase and reverse phase transition is discussed in terms of orientational frustration and domain formation.

The suitability of using pairwise additive van der Waals type potential to represent the interaction between C_{60} molecules is assessed. The plastic phase of C_{60} is successfully modelled, however, the unit cell at low temperature predicted in the simulation is not consistent with experimental results. A discussion of other possible models of intermolecular potential is given.

Declaration

This thesis has been composed by myself and it has not been submitted in any previous application for a degree. The work reported within was executed by me, unless otherwise stated.

August 1995

Acknowledgements

Thanks to: Stuart Pawley for supervision and encouragement; Charlotte Cheung for the initial work on Chapter 2 and for being generally nice; the Edinburgh Parallel Computing Centre for use of their resources; Stewart Clark for help with the colour pictures; all in the Condensed Matter group and others in the Dept. of Physics; my family.

Contents

Chapter 1

Molecular Dynamics

> *...for the whole burden of philosophy seems to consist in this - from the phenomena of motions to investigate the forces of nature, and then from these forces to demonstrate the other phenomena...*
>
> *Principia Mathematica*, Isaac Newton.

1.1 Introduction

The above quotation shows that Newton appreciated the essence of the technique of molecular dynamics. For a system of particles, if all the forces which act on each particle can be calculated then it is possible to predict the trajectories of these particles and thereby examine certain physical phenomena exhibited by part or all of that system. We may recognise this as the principle of determinism. If a system, better called an ensemble, contains particles which are atoms or molecules then by calculating the trajectories of the particles under changing thermodynamic conditions it is possible to predict how the structure of matter will change, *i.e.* to predict phase transitions. If the forces can be adequately described within the regime of classical physics then nothing beyond Newton's laws of motion are required to predict the trajectories of the particles. Indeed Newton, who spent a large part of his life in the pursuit of alchemy, may have wished, or even intended, that his laws of motion could be used to predict

the transformation of matter.

To predict the continuous trajectories of the particles would require an exact analytic solution of all the equations of motion for all particles. In a one-particle system the solution should be trivial, in a two-particle system a solution is generally possible, but in a system of three or more interacting particles analytic solutions become increasingly unlikely. A numerical solution must therefore be found. In a molecular dynamics simulation the following procedure is used; for an ensemble in which the initial positions and momenta of all particles are known, all the forces acting on each particle are calculated and the new positions and momenta of the particles after a discrete time interval, the time-step δt, are predicted according to these forces. This procedure is repeated for many time-steps over which certain phenomena may be witnessed. The technique essentially involves numerical integration of the equations of motion. Although the mathematics of this was known to or developed by Newton, a molecular dynamics simulation for a solid containing 100 particles for 1000 time-steps requires about 1.8 million individual calculations. Allowing 20s per calculation, this would require about three working years devoted to doing nothing but this simulation. The first molecular dynamics simulation therefore was required to await the invention of electronic computers.

The first computer simulation of a condensed matter ensemble was by Metropolis *et al.* [1] in the early 1950's using the statistical mechanical Monte Carlo method to simulate an ensemble of hard spheres. In the latter part of that decade advances in computing allowed the more computationally intensive molecular dynamics technique to be used, the first simulation being performed by Alder and Wainright [2] again on an ensemble of hard spheres. The first simulation of an atomistic condensed matter system was by Rahman in 1964 [3] who simulated liquid argon using the Lennard-Jones potential. From that time on molecular dynamics has been used to simulate a wide range for phenomena in an even wider range of materials, the size and complexity of such simulations increasing with the rapid expansion in the speed and memory of

computers.

In the subsequent chapters of this thesis molecular dynamics simulations are used to study phase transitions in four different kinds of condensed matter. In Chapters 4 and 5, other numerical simulation techniques, namely Monte Carlo and lattice dynamics, are used in conjunction with molecular dynamics simulations. In this first chapter, since it is the basis of the work to be presented, the formulation of the techniques of molecular dynamics simulations will be discussed.

1.2 Potential and Force

A molecular dynamics simulation will only give useful results if the theoretical model of the inter-particle forces is an accurate representation of the real physical forces. In many cases the the complex quantum mechanical interactions between atoms can be reduced to a simple formula for the variation in potential between particles which depends on the distance between atoms and some particular parameters for the energy of interaction. For all simulations which will be discussed in this thesis pairwise additive potentials are used. This is a potential interaction between particles in which the total force on a particle is represented by the sum of all forces between the particle and its neighbours.

For simulations on molecular ensembles, the interatomic bonds within the molecules are assumed to be rigid so that only intermolecular forces need be considered. In this case the total force acting on a molecule is the sum of the forces between all atoms in that molecule and all the atoms of its neighbouring molecules. The approximation to a rigid molecule is valid if the displacements of atoms due to molecular vibrations are small on the scale of the separation of atoms between molecules. This is true for the cage-like structure of adamantane and C_{60}, to be discussed later, but for molecules like n-butane [16] in which the CH_2 and CH_3 groups have large amplitude twisting motions with respect to each other, intramolecular forces must also be calculated.

Particle interactions due to coulombic and van der Waals forces can generally be described by pairwise additive potentials. Metallic potentials are not pairwise additive, but can be constructed in a form which is effectively pairwise additive [6]. Covalent solids require the use of a quantum mechanical molecular dynamics technique [7].

For all the atoms and molecules in the simulations to be discussed the most significant interactions are from van der Waals forces. These forces can be successfully described by the fluctuating dipole-dipole model due to London [4], in which the attractive part of the potential falls off as the inverse radius of atomic separation to the power 6. The potential must also include repulsive terms which fall off more rapidly than the attractive part, the best-known version of this being the Lennard-Jones potential [5],

$$\phi(r) = 4\epsilon(-\frac{r_o^6}{r^6} + \frac{r_o^{12}}{r^{12}}) = \frac{-A}{r^6} + \frac{B}{r^{12}} \tag{1.1}$$

where ϵ has dimensions of energy and r_o dimensions of length.

The first derivative of the potential gives an expression for the force of interaction between two particles. The force on particle i from particle j is

$$\vec{F}_{ij} = \frac{1}{r_{ij}}\frac{d\phi(r_{ij})}{dr}(\vec{s}_i - \vec{s}_j) \tag{1.2}$$

where $\vec{s}_i$ is the position vector of the centre of particle i in the co-ordinates being used and r_{ij} is the separation of the two particles. Since this force is Newtonian $F_{ji} = -F_{ij}$, a fact which can be used to reduce the amount of computation required when forces are calculated.

In molecular ensembles the torque acting about a molecule's centre due to all the forces acting on it must also be calculated. This is the sum of the torques about the molecular centre acting on each of the atoms in that molecule, due to all the forces

acting on those atoms, explicitly

$$\underline{\tau}_{ij} = \sum_{n_i=1}^{N_{Ai}} \sum_{n_j=1}^{N_{Aj}} -(F_{xn_in_j}, F_{yn_in_j}, F_{zn_in_j}) \times (x_{n_i}, y_{n_i}, z_{n_i}) \tag{1.3}$$

where $\underline{\tau}_{ij}$ is the torque vector between molecule i containing N_{Ai} atoms and molecule j containing N_{Aj} atoms, $(F_{xn_in_j}, F_{yn_in_j}, F_{zn_in_j})$ is the force on atom n_i in molecule i due to atom n_j in molecule j, and $(x_{n_i}, y_{n_i}, z_{n_i})$ are the co-ordinates of atom n_i relative to the centre of molecule i.

1.3 Temperature

The temperature of an ensemble containing N particles is determined from the Boltzmann definition;

$$< E_{tran} > = \sum_{i=1}^{N} \frac{1}{2} \frac{m_i |v_i|^2}{N} = \frac{3}{2} k_B T_T \tag{1.4}$$

where $< E_{tran} >$ is the average translational kinetic energy of a particle, k_B the Boltzmann constant and T_T is the translational temperature. In molecular ensembles there are rotational degrees of freedom also, requiring a rotational temperature, T_R, to be defined,

$$< E_{rot} > = \sum_{i=1}^{N} \frac{1}{2} \frac{\underline{\omega_i}^T \underline{\underline{\tilde{I}_i}} \underline{\omega_i}}{N} = \frac{3}{2} k_B T_R \tag{1.5}$$

where $\tilde{I}_i$ is the inertia tensor of molecule i. If the molecules are not linear, the thermodynamic temperature of the ensemble is defined to be the average of the translational

and rotational temperatures, $T = \frac{1}{2}(T_T + T_R)$. Changing temperature from T_1 to T_2 is done by rescaling all components of translational and angular velocities by the factor $\sqrt{(T_2/T_1)}$.

In the simulations to be performed only 32-1024 particles are involved, a sample size which is not nearly large enough for a statistically correct Maxwell-Boltzmann distribution of particle energies to be attained. The use of a 'temperature' in a simulation is a method of finding the average amount of kinetic energy in the ensemble. Comparing temperatures calculated in simulations to experimental values is rarely strictly valid. However, since we are concerned with the study of phase transitions induced by heating or cooling, the use of a temperature when presenting results is intuitively correct.

1.4 Equations of Motion

1.4.1 Clusters

In a cluster the ensemble has a free space boundary in all directions, *i.e.* a surface. Initially the particles are arranged, as in nature, so as to minimise the surface area in a disc in two dimensions or a spherical globule in three dimensions. The equations of motion simply follow Newton's laws

$$\ddot{\vec{s}}_i = \frac{1}{m_i}\sum_{j\neq i}^{N}\vec{F}_{ij} \tag{1.6}$$

and

$$\dot{\underline{\omega}}_i = \tilde{I}_i^{-1}\sum_{j\neq i}^{N}\underline{\tau}_{ij} \tag{1.7}$$

where $\ddot{\vec{s}}_i$ and $\dot{\underline{\omega}}_i$ are the linear and angular accelerations of particle i, derived from the forces and torques expressed in (1.2) and (1.3).

A computational problem encountered with clusters is that they possess an overall angular momentum which causes the cluster to rotate with respect to the Cartesian axes; an undesirable effect which complicates analysis. A particle i at $\vec{r}_i(x_i, y_i, z_i)$ relative to the centre of the cluster has a velocity $\vec{v}_i(\dot{x}_i, \dot{y}_i, \dot{z}_i)$ and so will have an angular momentum about the centre of the cluster. The total angular momentum of a cluster of N particles is therefore

$$\underline{L} = \sum_{i=1}^{N} -m_i(\vec{v}_i \times \vec{r}_i). \tag{1.8}$$

In a cluster of very large (infinite) extent there would be an overall cancellation of velocities, however, since we have at most only 1024 particles the angular momentum can be significant and so must be removed. The inertia tensor of the cluster [8] is determined as

$$\tilde{J} = \sum_{i=1}^{N} m_i \begin{pmatrix} y_i^2 + z_i^2 & -x_i y_i & -x_i z_i \\ -x_i y_i & x_i^2 + z_i^2 & -y_i z_i \\ -x_i z_i & -y_i z_i & x_i^2 + y_i^2 \end{pmatrix} \tag{1.9}$$

so that the angular velocity with which the cluster rotates about its centre will be given by,

$$\underline{\Omega} \;=\; \tilde{J}^{-1}\underline{L} \tag{1.10}$$

The rotation of the cluster can then be prevented by removing the part of the linear velocity of each atom which is due to the overall angular velocity of the cluster, explicitly

$$\vec{v}_i' = \vec{v}_i - (\underline{\Omega} \times \vec{r}_i) \tag{1.11}$$

where $\vec{v}_i'$ is the corrected velocity of particle i.

1.4.2 Periodic Boundary Conditions

When periodic boundary conditions are applied in a simulation the formulation of the equations of motion due to Parrinello and Rahman [9] is followed. The particles are contained within a periodically repeating cell with edges defined by vectors $\vec{a}, \vec{b}$ and $\vec{c}$, in Cartesian space. The length and direction of these vectors are allowed to change with time and with thermodynamic conditions so that the cell can adopt the shape of any parallelepiped of any size. If the components of $\vec{a}, \vec{b}$ and $\vec{c}$ form the metric tensor $\underline{h}$,

$$\underline{h} = \begin{pmatrix} a_1 & b_1 & c_1 \\ a_2 & b_2 & c_2 \\ a_3 & b_3 & c_3 \end{pmatrix}$$

then the volume of the cell is $\Omega = det\underline{h} = \vec{a} \cdot \vec{b} \times \vec{c}$. The position vector of the centre of mass of particle i is described by $\vec{s}_i$ in terms of fractional co-ordinates which is related to the position vector in Cartesian co-ordinates $\vec{r}_i$ by $\vec{r}_i = \xi_i \vec{a} + \eta_i \vec{b} + \zeta_i \vec{c} = \underline{h}\vec{s}_i$, where ξ_i, η_i, ζ_i are the fractional co-ordinates of particle i, which have values between -0·5 and 0·5. The Lagrangian of the system is

$$L = \frac{1}{2}\sum_i^N m_i \dot{\vec{s}}_i{}' \underline{G} \dot{\vec{s}}_i + \frac{1}{2} W Tr(\dot{\underline{h}}' \dot{\underline{h}}) - \sum_i^N \sum_{j>i}^N \phi(r_{ij}) - p_{ext}\Omega \tag{1.12}$$

where $\underline{G} = \underline{h}'\underline{h}$ so that $r_{ij}^2 = (\vec{s}_i - \vec{s}_j)'\underline{G}(\vec{s}_i - \vec{s}_j)$, p_{ext} is the externally applied hydrostatic pressure, $\phi(r_{ij})$ is the pair potential discussed on p.3, and W is a constant which has the dimensions of mass.

From the solution of (1.12) the equation of motion for the centre of mass of particle i is

$$\ddot{\vec{s}}_i = \frac{1}{m_i}\sum_{j\neq i}^{N} F_{ij} - \underline{G}^{-1}\dot{\underline{G}}\dot{\vec{s}}_i \tag{1.13}$$

where $\dot{\underline{G}} = \frac{d}{dt}(\underline{h}'\underline{h}) = \dot{\underline{h}}'\underline{h} + \underline{h}'\dot{\underline{h}}$. The first term in (1.13) can be recognised as (1.6), the equation of motion with free space boundaries, while the second term accounts for the motion of the sides of the cell superimposed on the motion of the particles.

The equation of motion for the cell defined by $\underline{h}$ is

$$\ddot{\underline{h}} = \frac{1}{W}(\underline{\pi} - p_{ext})\underline{\sigma} \tag{1.14}$$

where $\underline{\pi}$ is the stress tensor defined as

$$\underline{\pi} = \frac{1}{\Omega}\left(\sum_{i}^{N} m_i\vec{v}_i\vec{v}_i - \sum_{i}^{N}\sum_{j>i}^{N}\frac{1}{r_{ij}}\frac{d\phi(r_{ij})}{dr}(\vec{r}_i - \vec{r}_j)(\vec{r}_i - \vec{r}_j)\right) \tag{1.15}$$

where $\vec{v}_i = \underline{h}\dot{\vec{s}}_i$ and the summation of each term produces a 3×3 dyadic tensor. Using x_{ij}, y_{ij}, z_{ij} for the components of $\vec{r}_i - \vec{r}_j$ and $\dot{x}_i, \dot{y}_i, \dot{z}_i$ for the components of $\vec{v}_i$, then the terms in (1.15) are explicitly

$$(\vec{r}_i - \vec{r}_j)(\vec{r}_i - \vec{r}_j) = \begin{pmatrix} x_{ij}x_{ij} & x_{ij}y_{ij} & x_{ij}z_{ij} \\ y_{ij}x_{ij} & y_{ij}y_{ij} & y_{ij}z_{ij} \\ z_{ij}x_{ij} & z_{ij}y_{ij} & z_{ij}z_{ij} \end{pmatrix} \quad \& \quad \vec{v}_i\vec{v}_i = \begin{pmatrix} \dot{x}_i\dot{x}_i & \dot{x}_i\dot{y}_i & \dot{x}_i\dot{z}_i \\ \dot{y}_i\dot{x}_i & \dot{y}_i\dot{y}_i & \dot{y}_i\dot{z}_i \\ \dot{z}_i\dot{x}_i & \dot{z}_i\dot{y}_i & \dot{z}_i\dot{z}_i \end{pmatrix}$$

The stress tensor expresses the internal pressures on the sides of the cell, as the tensor p_{ext} expresses the external pressure. The tensor $\underline{\sigma}$ is comprised of the components of $\vec{b} \times \vec{c}$, $\vec{c} \times \vec{a}$ and $\vec{a} \times \vec{b}$ (in the same way as $\underline{h}$ is comprised of the components of $\vec{a}, \vec{b}$ and $\vec{c}$), where the cross-products express the surface areas perpendicular to the directions across which the pressures act.

For a system in equilibrium, $\ddot{\underline{h}}$ in (1.14) will be slow to vary and zero on average. Examining (1.15), the first term is dependent on the kinetic (thermal) energy of the particles whereas the second term depends on the potential energy (forces) between particles. A change in temperature will increase or decrease the kinetic term in the stress tensor so that the potential term in the stress tensor must change so as to re-establish equilibrium. Since the potential energy of the particles depends only on their separation, an expansion or contraction of the cell or a structural change will occur when the temperature changes or similarly when the pressure is changed.

The constant W is a consequence of the application of periodicity and has no exact physical definition. The value of W is generally chosen to be of the order of the total mass, M, of all the particles in the cell (often $W = \frac{M}{10}$). If a simulation starts with a cell with a volume significantly larger or smaller than the desired volume for equilibrium at the particular simulation temperature, then, if a harmonic crystalline solid is being simulated, the volume of the box will exhibit a harmonic oscillation. This effect is often encountered when temperature is first rescaled. Nosé and Klein [10] give the period of these oscillations, $\mathcal{T}$, as being

$$\mathcal{T} \approx 2\pi\sqrt{\frac{W}{3LB}}$$

where L is the typical linear dimension of the cell and B is the bulk modulus. If $\mathcal{T}$ can be determined from the simulation then the bulk modulus may be estimated.

The oscillations are a transient effect, disappearing eventually due to anharmonicity in the solid. However, depending on the particular solid being simulated, these oscillations can persist for times which are long on the time-scale of the simulation, and the amplitude of the oscillation can be large enough to interfere with the equilibration process. The oscillations can be damped out by systematically reducing the velocity of the sides of the cell on each step thus,

$$\dot{\underline{h}}' = \dot{\underline{h}}(1 - \beta)$$

where $\dot{\underline{h}}'$ is the damped velocity and β is a damping constant, $0 \leq \beta \leq 1$.

The tensor $\underline{h}$ is 3x3 and therefore has 9 degrees of freedom, which determine the size, skew and rotation in Cartesian space, however, only 6 degrees of freedom are required to uniquely determine the size and shape of the cell. The extra degrees of freedom can be interpreted as a rotation of the cell with respect to Cartesian axes, which does not relate to any physical property of the ensemble. Although the rotation is small over a single time-step, if the simulation is run for a long time (more than 10^6 time steps) the cumulative effects of such rotations can eventually produce a large rotation about a single direction; this rotation is inconsistent with the boundary conditions and will corrupt the simulation data. To avoid this the lower diagonal of $\underline{h}$ is always set to zero, so that there are now only 6 degrees of freedom and the infinitesimal rotations on the cell are removed on each step. When $\delta\underline{h}$, the change in $\underline{h}$ over a time interval δt, is calculated from (1.14), the new $\underline{h}$ is given by

$$\underline{h}(t + \delta t) = \underline{h}(t) + \begin{pmatrix} \delta h_{11} & \delta h_{12} - \delta h_{21} & \delta h_{13} - \delta h_{31} \\ 0 & \delta h_{22} & \delta h_{23} - \delta h_{32} \\ 0 & 0 & \delta h_{33} \end{pmatrix} \tag{1.16}$$

which removes the infinitesimal rotation of the cell.

1.4.3 Molecular Orientation

In simulations of molecular ensembles molecular orientations are represented by quaternions [14, 15]. Originated by Hamilton in 1863 as an extension of complex numbers a quaternion is described by four co-ordinates and has the advantage over Euler angles for describing orientations by avoiding singularities.

A rotation of $\alpha, 0 \leq \alpha/2 < 2\pi$, of a solid body about the unit vector $\vec{r}$ is described by the quaternion,

$$\underline{p} = (\cos(\frac{\alpha}{2}), \vec{r}\sin(\frac{\alpha}{2})). \tag{1.17}$$

This can be written as $\underline{p} = (L_4, \vec{L})$, where $\vec{L} = (L_1, L_2, L_3)$ is a three-dimensional vector in Cartesian space and L_4 is the fourth quaternion co-ordinate. If $\underline{p}' = (L_4', \vec{L}')$ then,

$$\underline{p} + \underline{p}' = (L_4 + L_4', \vec{L} + \vec{L}') \tag{1.18}$$

and

$$\underline{pp}' = (L_4 L_4' - \vec{L} \cdot \vec{L}', L_4\vec{L}' + L_4'\vec{L} + \vec{L} \times \vec{L}') \tag{1.19}$$

are the rules for addition and multiplication of quaternions.

If we write a Cartesian position vector $\vec{v}$ (for an atom in a molecule) as the quaternion $\underline{q} = (0, \vec{v})$, then transforming $\vec{v}$ to $\vec{v}'$ by the rotation described by $\underline{p}$ is equivalent to transforming $\underline{q}$ to $\underline{q}'$ by the similarity transform $\underline{q}' = \underline{pqp}^{-1}$, where $\underline{p} = \underline{p}^{-1}$ since $\underline{p}$ has unit norm. If the Cartesian part of $\underline{pqp}^{-1}$ is evaluated explicitly, by following the multiplication rule of (1.19), a 3x3 transform matrix, T, such that $\vec{v}' = T\vec{v}$ is formed

$$\vec{v}' = \begin{pmatrix} L_1^2 - L_2^2 - L_3^2 + L_4^2 & 2(L_1L_2 - L_3L_4) & 2(L_1L_3 + L_2L_4) \\ 2(L_1L_2 + L_3L_4) & -L_1^2 + L_2^2 - L_3^2 + L_4^2 & 2(L_2L_3 - L_1L_4) \\ 2(L_1L_3 - L_2L_4) & 2(L_2L_3 + L_1L_4) & -L_1^2 - L_2^2 + L_3^2 + L_4^2 \end{pmatrix} \vec{v}. \quad (1.20)$$

If the transform matrix is denoted $R(L_i)$, then an atomic position is defined as $R(L_i)\vec{v}$. If this atom then makes a rotation in time δt described by the matrix $\Omega(\delta t)$, its new position is,

$$\Omega(\delta t)R(L_i)\vec{v} = R(L_i')\vec{v}$$

where L_i' are the components of the quaternion describing the new orientation, and

$$L_i' = L_i + \dot{L}_i\delta t. \quad (1.21)$$

If the molecule has angular velocity $\underline{\omega}$, a small angular displacement in time δt is $\frac{1}{2}\underline{\omega}\delta t$. As a quaternion this displacement is $(1, \frac{1}{2}\underline{\omega}\delta)$, $L_4 \simeq 1$ since the angle of rotation is very small, giving the quaterion describing the rotated position as

$$L_i' = (1, \frac{1}{2}\underline{\omega}\delta t)(L_4, \underline{L}) = (L_4 - (\underline{\omega}\cdot\underline{L})\frac{\delta t}{2}, \underline{L} + (\underline{\omega}L_4 + \underline{\omega}\times\underline{L})\frac{\delta t}{2}). \quad (1.22)$$

Comparing (1.21) and (1.22) we find $(\dot{L}_4, \underline{\dot{L}})$,

$$\underline{\dot{L}} = \frac{1}{2}(\underline{\omega}L_4 + \underline{\omega}\times\underline{L}) \quad (1.23)$$

$$\dot{L}_4 = -\frac{1}{2}\underline{\omega}\cdot\underline{L} \tag{1.24}$$

Differentiating (1.23) and (1.24) with respect to time we establish the differential equations of motion for molecular orientation in terms of quaternions, $(\ddot{L}_4, \underline{\ddot{L}})$,

$$\underline{\ddot{L}} = \frac{1}{2}(\underline{\dot{\omega}}L_4 + \underline{\omega}\dot{L}_4 + \underline{\dot{\omega}}\times\underline{L} + \underline{\omega}\times\underline{\dot{L}}) \tag{1.25}$$

$$\ddot{L}_4 = -\frac{1}{2}(\underline{\dot{\omega}}\cdot\underline{L} + \underline{\omega}\cdot\underline{\dot{L}}) \tag{1.26}$$

1.5 Solving the Equations of Motion

In establishing the equations of motion we have found a set of coupled differential equations which we can use to predict the motion of atoms or molecules in an ensemble. To do this numerical integration in discrete time-steps, δt, must be used. For this we employ the algorithms derived by Beeman [11]

$$u(t+\delta t) = u(t) + v(t)\delta t + \frac{1}{6}(4\frac{\delta^2 u(t)}{\delta t^2} - \frac{\delta^2 u(t-\delta t)}{\delta t^2})\delta t^2 \tag{1.27}$$

$$v(t+\delta t) = v(t) + \frac{1}{6}(2\frac{\delta^2 u(t+\delta t)}{\delta t^2} + 5\frac{\delta^2 u(t)}{\delta t^2} - \frac{\delta^2 u(t-\delta t)}{\delta t^2})\delta t \tag{1.28}$$

where u is a positional co-ordinate and v a velocity co-ordinate, t is the current time, $t + \delta t$ the next time for which values of u and v are predicted and $t - \delta t$ denotes values for the previous time-step. These algorithms are also applicable to incrementing quaternion co-ordinates and the co-ordinates of the cell in the Parrinello-Rahman method. A simpler algorithm due to Verlet [12] is often used, which has the same level of approximation, but only uses positions. (1.27) and (1.28) are versions of the Runge-Kutta method for numerical solution of differential equations [13] generalised to calculate stable trajectories for solid particles. Time steps are generally in the order of 0.001 to 0.01ps depending of the mass of the particle and the temperature of the simulation.

The time development of particle co-ordinates will of course depend on the initial positions and velocities and thereby on the temperature of the ensemble. Convergence of the solution of equations is often judged from when the potential energy of the ensemble reaches a steady minimum value after a large number of time-steps (10^3-10^5) from the initial calculation. The ensemble is then considered to be in equilibrium at either the nominal temperature to which initial velocities were set, or an average temperature found once equilibrium is obtained. There are however no hard and fast rules for determining when an ensemble is in equilibrium, and indeed one of the benefits of molecular dynamics simulations is the ability to model highly dynamic and non-equilibrium states of matter.

1.6 Computers

It is true to say that, until recently, the size and complexity of molecular dynamics simulations has depended on the computing facilities available, and that only large and expensive supercomputers could reasonably be used. Parallel supercomputers are particularly well suited to performing molecular dynamics calculations. There are two types of parallel computer, Multi-Instruction Multi-Data (MIMD) machines, in

which there are 10-100 high-performance processors capable of carrying out independent tasks simultaneously, and Single-Instruction Multi-Data (SIMD) machine in which 4,000-64,000 processors all carry out the same task. The general strategy for applying molecular dynamics methods on parallel machines is to distribute the data for the various particles over the processors and simultaneously calculate as many of the forces as possible. During the time when the work for this thesis was performed, fast serial work-stations became available. These machines contain a single very fast processor and, although they have very much less processing capability than supercomputers, they are much cheaper (tens of thousands compared to a few million pounds), and can therefore be more readily dedicated to a single task.

Previously the efficiency of programming was paramount to the success of a molecular dynamics simulation, necessitating in-depth analysis of the application of programs to machine architecture, however, since modern parallel languages are generally an extension of standard FORTRAN or C, and since such machines often have a lifespan of only a few years before being superseded, programming details rapidly become irrelevant. Fast serial machines only require code in standard machine languages. It should be enough therefore to limit the discussion on computers to stating what machines were used and their relative performance. The simulations of two-dimensional krypton in Chapter 2, adamantane in Chapter 4 and C_{60} in Chapter 5 were all performed on the CM200 Connection Machine at the Edinburgh Parallel Computing Centre. This is a SIMD machine with 16,384 processors. The simulations on inert gas clusters in Chapter 3 and the Monte Carlo simulations of adamantane in Chapter 4 both used Hewlett Packard 700 series work-stations in the Department of Physics. As a rough guide to the processing time required in such simulations, the CM200 can perform 10,000 steps for 256 adamantane molecules (6656 atoms) in 3 hours and 40 minutes and a Hewlett Packard machine can perform 10,000 steps on 256 atoms in 20 minutes.

Chapter 2

Two-Dimensional Melting

The little Hexagon meditated on this for a while and then said to me;'But you have been teaching me to raise numbers to the third power: I suppose 3^3 *must mean something in Geometry; what does it mean?' 'Nothing at all', I replied, 'not at least in Geometry; for Geometry has only Two Dimensions.'*

Flatland, Edwin Abbott Abbott.

2.1 Introduction

In simple terms a solid will melt when the particles of which it is comprised have enough kinetic energy to overcome the bonding forces which hold them together, such that the particles become free to diffuse between each other and a liquid is formed. If the solid is crystalline then melting is also characterised by the loss of long-range translational order. In terms of lattice vibrations, at low temperature the atoms make small amplitude harmonic oscillations about their minimum energy positions. As temperature increases large amplitude anharmonic vibrations are generated, and the number of long-wavelength modes increases also. The increasingly anharmonic behaviour of the solid and the dominance of long-wavelength oscillations is associated with defect formation, thermal expansion, and eventually melting in a first-order transition.

A more complex theory of melting addresses how long-range translational order is

lost. Melting can be instigated from the surface (or grain boundary) [17], where with increasing temperature atoms diffuse to vacant surface sites leaving vacancies in the bulk into which other atoms can diffuse. Eventually vacancies occur throughout the solid, removing translational order and allowing particles to diffuse, *i.e.* forming a liquid phase. The formation of defects (dislocations, vacancies and interstitials) are of particular interest in the melting transition, since their formation disrupts the long-range order in a solid. In defect-mediated melting [18] dislocations form spontaneously in the bulk of the solid, increasing in density as the the melting temperature is approached, until the solid becomes saturated by dislocations, hence removing translational order and forming a liquid. This latter theory is associated with the phenomenon of premelting [19] where dislocations form at temperatures well below the melting point.

As well as these general theories, there has been great interest in what happens when a melting transition is confined to two-dimensions. Theories of two-dimensional melting are claimed to originate from work by Feynman who in an attempt to gain insight into solving three-dimensional problems, would often try to solve a two-dimensional version first [20, 35]. Kosterlitz and Thouless [21], and later Nelson, Halperin and Young [22, 23, 24] (KTNHY) found solutions for magnetic, crystalline and superfluid properties for the continuum field of a two-dimensional hexagonal lattice. Two-dimensional melting was predicted to be a two-stage process of a continuous (second-order) phase transition from solid to liquid *via* an intermediate hexatic phase. In the transition from the solid to the hexatic phase, long-range translational order is removed by the formation of dislocations. In a hexatic phase an anisotropic liquid is formed in which atoms are free to diffuse, but some short-range translational order is retained as six-fold co-ordination of some atoms and their neighbours, somewhat like a smectic liquid-crystal. In the transition from the hexatic phase to an isotropic liquid the short-range order is lost by disclinations; disclination is when atoms lose their regular six-fold co-ordination with neighbours to become unco-ordinated with five, six or seven irregularly distributed neighbours.

In the twenty years since this theory was first mooted, much work has been done to confirm or otherwise confound its validity. Experiments have provided evidence of continuous melting transitions for krypton and argon monolayers on a graphite substrate [27, 28], but first order melting for xenon [29]. Monte Carlo and renormalisation group methods have been employed to study dislocation formation on a hexagonal lattice, which support the KTNHY theory [30, 31] or a modified version in which first or second-order melting occurs depending on whether the core dislocation energy is small or large [32, 33, 34]. With small core dislocation energy, dislocations aggregate rapidly to form multiple grain boundaries which saturate the solid at the melting point creating a first-order melting transition which pre-empts the transition predicted by the KTNHY theory. Studies of Lennard-Jones systems, mainly using molecular dynamics simulations, contradict the KTNHY theory, suggesting first-order melting with possible solid-liquid phase co-existence near the melting point rather than a hexatic phase [35, 36].

For a detailed review of previous work see Standburg [25] and Abraham [26].

2.2 Simulation Details

Calculations were performed on a cluster of 1024 Krypton atoms initially arranged in a hexagonally close-packed disc with interatomic spacing of 2.02Å and random velocities corresponding to a temperature of 20K. Atoms interact *via* the Lennard-Jones potential with A=2937 kcal/mole $Å^{-6}$, B=6393405 kcal/mole $Å^{-12}$. Calculations for the initial cluster were made for 30,000 time-steps of 0.005ps at 20K until equilibrium was attained. A time-step of 0.005ps was maintained throughout the simulation. Temperature was then increased, initially in 10K intervals, with at least 8000 steps performed at each temperature, checking about every 1000 steps to observe whether equilibrium was being approached or else the cluster was melting.

In the KTNHY theory and most previous simulations periodic boundary conditions

have been used, since it is assumed that this approximates bulk behaviour of an ensemble; unless the ensemble is large, however, periodicity will only remove surface effects. We choose to study a cluster because it retains a surface, which all real solids possess, and this surface may play an important part in the melting process. The disadvantage of the cluster is the high proportion of atoms in surface sites compared to bulk sites and a melting point lower than experiments on bulk samples, due to the small size of the ensemble. In periodically repeating ensembles, melting temperatures can be higher than experiment with unphysical superheating occurring. Simulations of large clusters are not common and we have found only one previous simulation of a two-dimensional cluster. Choquard and Clerouin [37], using a logarithmic interaction between 511 particles on a disk, predict a first-order melting transition preceded by premelting effects which are the spontaneous formation of dislocations.

2.3 Analysis Techniques.

The **co-ordination number** is a determination of short-range order, found by counting the number of neighbouring atoms found within a certain radius of each atom and averaged for all atoms in the cluster. A radius of 5.52Å was chosen since it is halfway between the first and second nearest neighbours in the hexagonal close-packed structure. In the perfect structure, an atom in the bulk of the cluster has a co-ordination number of 6. The average co-ordination number for the initial close-packed cluster is found to be 5.771, less than 6 due to the atoms on the surface.

In periodic ensembles the volume is a well defined quantity, but in clusters the presence of a surface, which changes shape and so is not well defined, requires a numerical method to estimate volume, or, in a two-dimensional ensemble, **area**. The area occupied by an atom is taken to be a circle of radius 2.02Å, the close-packed separation. The cluster is considered to be covered by a grid of squares (500×500 squares with sides of length 0.4Å); every square more than half covered by an atom is considered to

be filled and those less than half covered considered empty. The position of the surface is then determined by finding the first and last squares in each row and each column of squares which are filled. All squares outside the surface are now discounted and the area of the cluster estimated by counting the total number of squares, both filled and empty, within the surface and multiplying by the area of a single square. The **density** of the perfect structure, using a hexagonal unit cell with sides of length 4.04Å, is 5.9286 a.m.u.Å^{-2}. Using our method, the density of the initial cluster described above is determined to be 5.9129 a.m.u.Å^{-2}, a discrepancy of only 0.26% from the theoretical value.

It is useful if **defect formation** can be visualised. Defect formation (dislocations and vacancies) can be associated with the formation of extra vacant areas in the cluster compared to the initial close-packed structure. In Figure 2.1 the upper diagram shows two rows of atoms in close-packed configuration and the lower diagram the same atoms with a dislocation introduced. If the radius associated with an atom is now chosen as 2.325Å (the dashed line in Figure 2.1) then the slight overlap between the disc-shaped atoms exactly covers the 9.2% vacant area in the close-packed structure. If the grid method used to find the area is used once again, the unfilled squares within the surface now represent excess area due to deviation from close-packing. Using a suitable graphics package, unfilled squares within the cluster and around the surface are plotted coloured black, so that the distribution of the vacant areas within the cluster can be visualised. Random thermal displacement of atoms would appear as disperse individual black squares, whereas for defect formation identifiable patterns should emerge. In the lower diagram of Figure 2.1 the vacant areas are filled in as black showing the pattern expected to be observed if a dislocation is formed.

Figure 2.2 shows a cluster with a grain boundary produced by a molecular dynamics simulation. The atoms were started on a square lattice and allowed to anneal at 20K into a hexagonal structure. Equilibrium was achieved after 200ps of simulation time. On examination the cluster was found to have a grain boundary dividing it. Figure 2.2

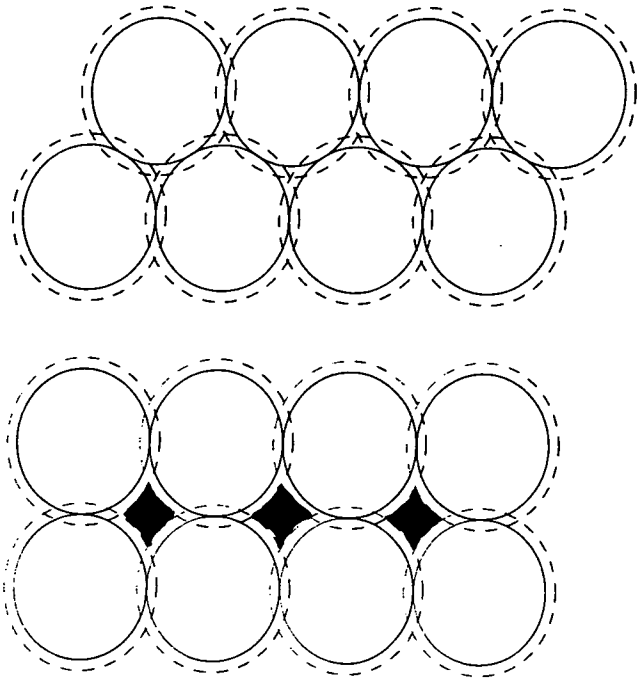

Figure 2.1. Dislocation formation.

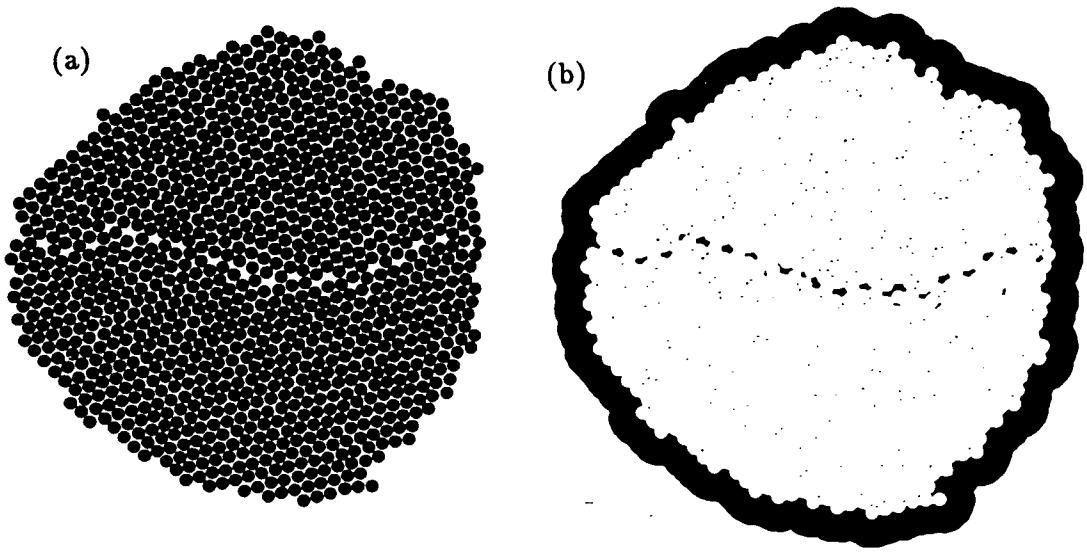

Figure 2.2. Cluster with grain boundary (a) atoms (b) defects.

(a) shows this cluster with the atoms represented as black discs of diameter 4.04Å and Figure 2.2(b) the same cluster pictured using the method described above. The grain boundary can clearly been seen running through the cluster.

The **pair distribution function (p.d.f.)** can be used to visualise the short-range order of the cluster. Each atom is taken in turn to be at the centre of a circle of radius 13Å and a point is plotted within the circle which corresponds to the position of each of that atom's neighbouring atoms found within that radius. The superposition of all these points shows the spatial and orientational distribution of the nearest neighbour ordering within the cluster (see Figure 2.6).

The dynamical state of the atoms in a cluster near equilibrium can be observed by plotting the **trajectories** of the atoms over a suitable period of simulation time. In Figure 2.5 the trajectories are plotted over 10ps.

2.4 Results

Figure 2.3(a) shows the total potential energy for the krypton cluster in equilibrium as temperature increases from 20K. Equilibrium is adjudged to be when the potential energy of the cluster shows small fluctuations about an average value measured over 20ps of simulation time but shows no overall upward or downward trend. Fluctuations in potential are less than 1% of the average value when in equilibrium. Calculated temperatures show considerable fluctuation, so a mean value is found again over 20ps of simulation time and the range of error calculated. The mean values are shown in Table 2.1 with the nominal value in brackets. The temperature is set by rescaling velocities once only, on the initial step for each temperature in the simulation. Although temperature fluctuations range from $\pm$1K to $\pm$3K from the mean value, most mean values are within 0.2K of the nominal temperature. Figures 2.3(b) and (c) show the variation with temperature of average co-ordination number and the density of the cluster. Since these values are measured just once at the end of the simulation of each

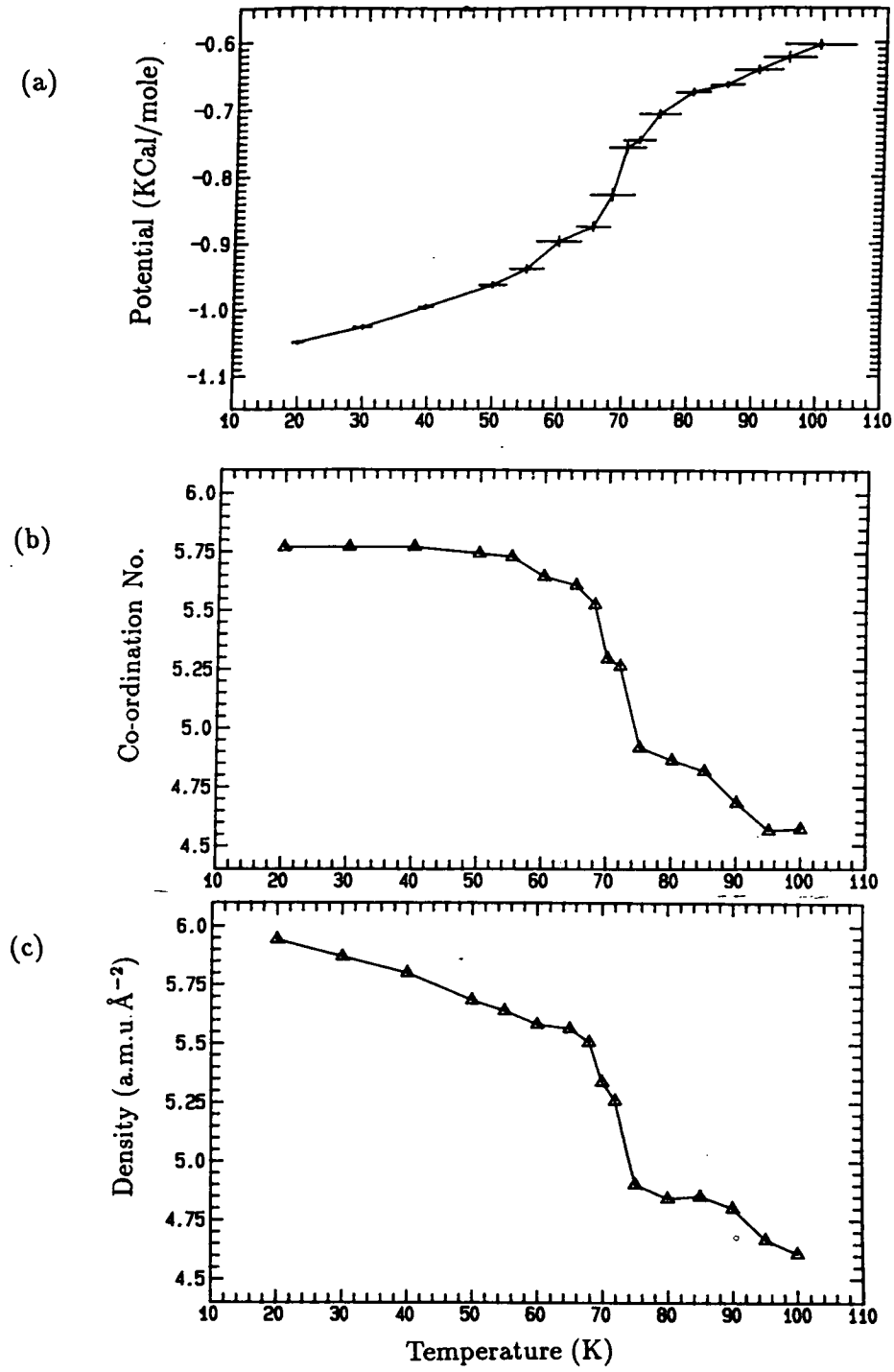

Figure 2.3. (a) Potential energy (b) average co-ordination number and (c) density against temperature.

Mean Temp. (K)	Time (ps)	Mean Temp. (K)	Time (ps)
19.891 (20)	185	70.135 (70)	533
29.967 (30)	74	71.967 (72)	573
39.639 (40)	62	75.009 (75)	82
49.867 (50)	74	80.036 (80)	45
55.042 (55)	103	84.309 (85)	45
59.915 (60)	280	90.127 (90)	45
65.150 (65)	143	94.875 (95)	45
67.989 (68)	142	99.710 (100)	45

Table 2.1. Mean temperatures and simulation times.

temperature no errors are estimated for these quantities.

All graphs show sharp changes in the values measured between 68K and 75K with a brief levelling off between 70K and 72K. The simplest interpretation of this is that a first-order melting transition occurs in the temperature range 68K to 75K. However the lack of any obvious discontinuity between two consecutive temperatures in this range and an apparent stabilisation of values between 70K and 72K suggests a more complicated melting process may occur. A detailed examination of changes in the structure of the cluster on heating is therefore required.

Figure 2.4 shows defect formation in the cluster, Figure 2.5 shows atomic trajectories and Figure 2.6 shows the pair distribution functions (p.d.f) for the temperatures shown in the diagrams. At 40K the cluster remains disc shaped; there are some isolated black dots within the cluster showing where atoms have significant thermal displacements. At 50K some black areas occur in lines, which can be identified as thermally induced dislocations (*cf.* Figure 2.1). The surface is noticeably less smooth than at 40K which explains the slight drop in co-ordination number from 5.771 between 20K and 40K to 5.743 at 50K.

At 60K as well as increasing disorder at the surface, the density of defects within the solid increases, and dislocations appear to aggregate. The trajectories and p.d.f. at this temperature show that the cluster remains solid, since atomic displacements are

small and centred on hexagonally arranged sites. Some atoms show a directionality in their motion which will correspond to the direction of slippage where a dislocation has been formed.

Further disordering is evident at 68K; some vacancies occur below the surface layer and there is further aggregation of dislocations which now form patterns similar to the grain boundary in Figure 2.2(b), only somewhat smaller. At 68K the p.d.f. shows that overall hexagonal ordering is maintained. Although underlying hexagonal order can still be seen in the trajectories in Figure 2.5, atoms have larger displacements and it appears that different parts of the cluster have an overall co-operative directional motion superimposed on the random atomic motions. This may be due to the cluster being divided by grain boundaries formed by aggregating dislocations, with the different grains moving in different directions. The cluster certainly has a granular appearance when viewed *via* trajectories at this temperature.

At 70K vacancies now occur within the bulk of the cluster and some atoms can be distinguished as white discs showing that they are now separated from neighbouring atoms and so are free to diffuse. There are also several remaining isolated solid areas (white patches), surrounded by defects. Some atoms show large random motion with trajectories crossing, characteristic of diffusive motion in a liquid, but other atoms have smaller displacements similar to those at 68K and so remain in a solid formation. The p.d.f. for a liquid would show no directional translational order but instead a continuous distribution of points with a narrow circular band at the first nearest neighbour radius and a broader band at the second nearest neighbour radius. In the p.d.f. at 70K the groups are more widely dispersed and are merging so that the hexagonal pattern is only just distinguishable. This is can be explained by the superposition of the hexagonal pattern for a solid and the continuous distribution for a liquid. Since six-fold co-ordination remains for solid areas we cannot tell whether any short-range order is retained and therefore whether the liquid is anisotropic or isotropic

There is evidence, therefore, that in the melting transition there is a region of

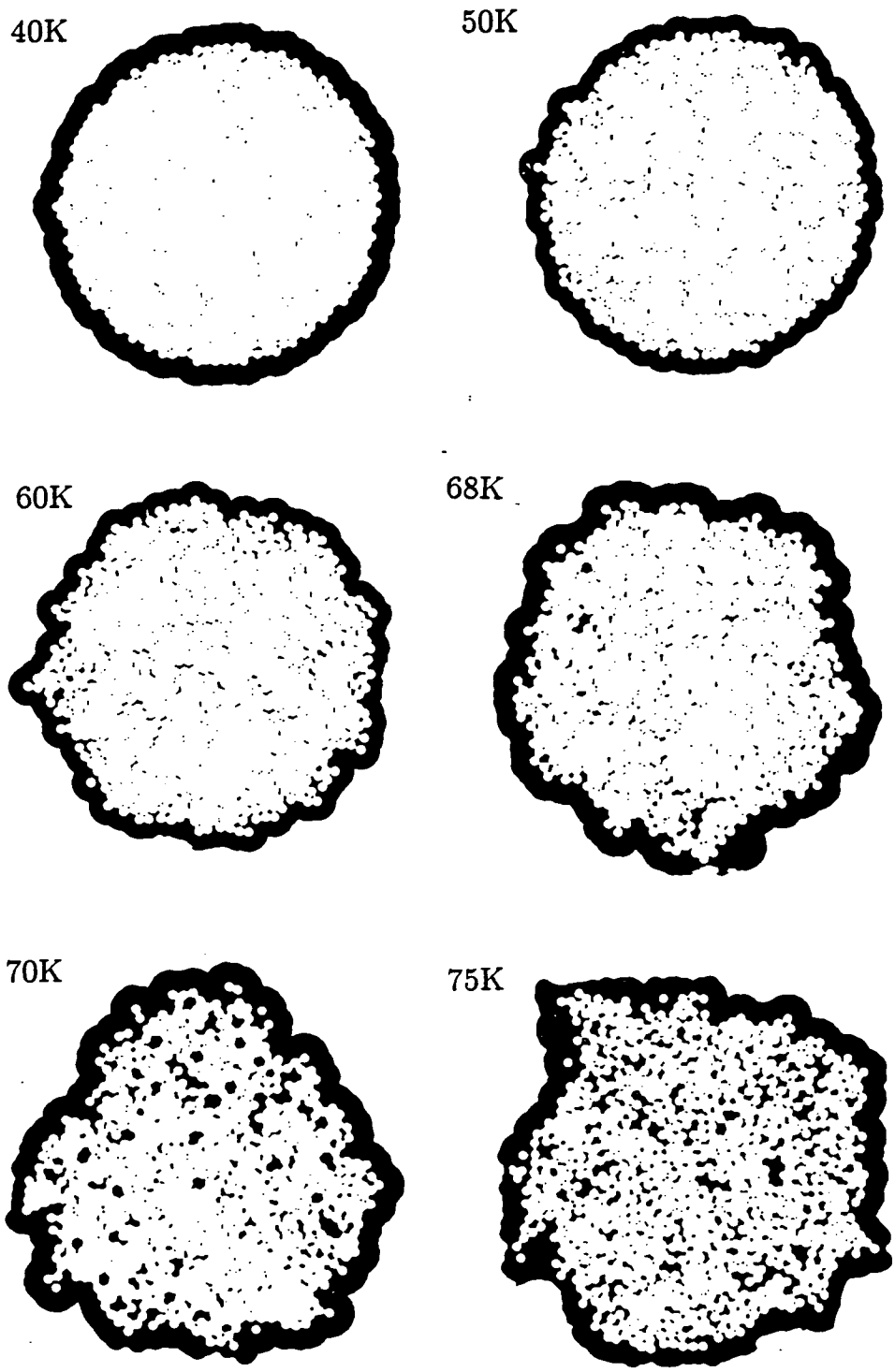

Figure 2.4. Structure of cluster at 40K, 50K, 60K, 68K, 70K and 75K.

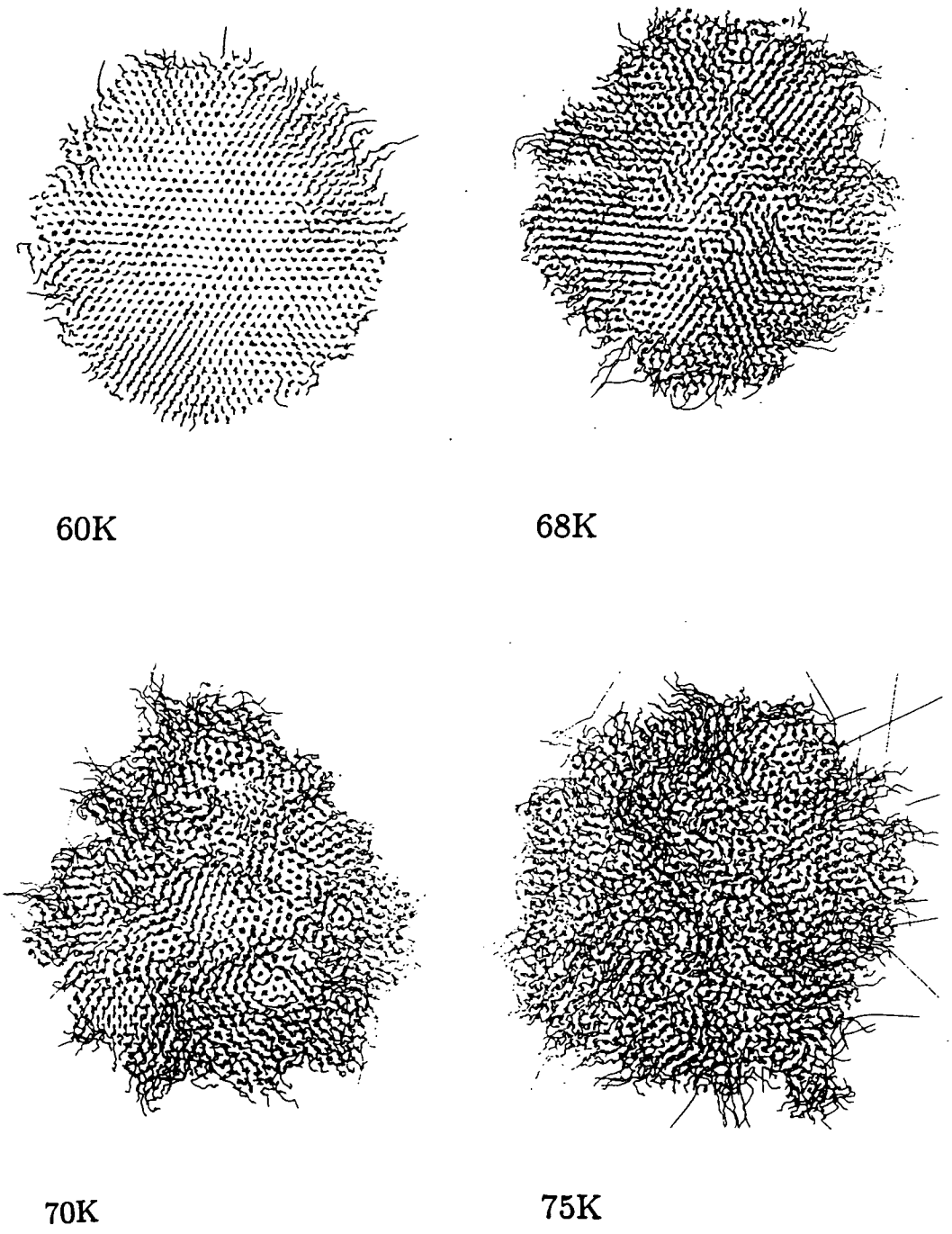

Figure 2.5. Trajectories over 10ps at 60K, 68K, 70K and 75K.

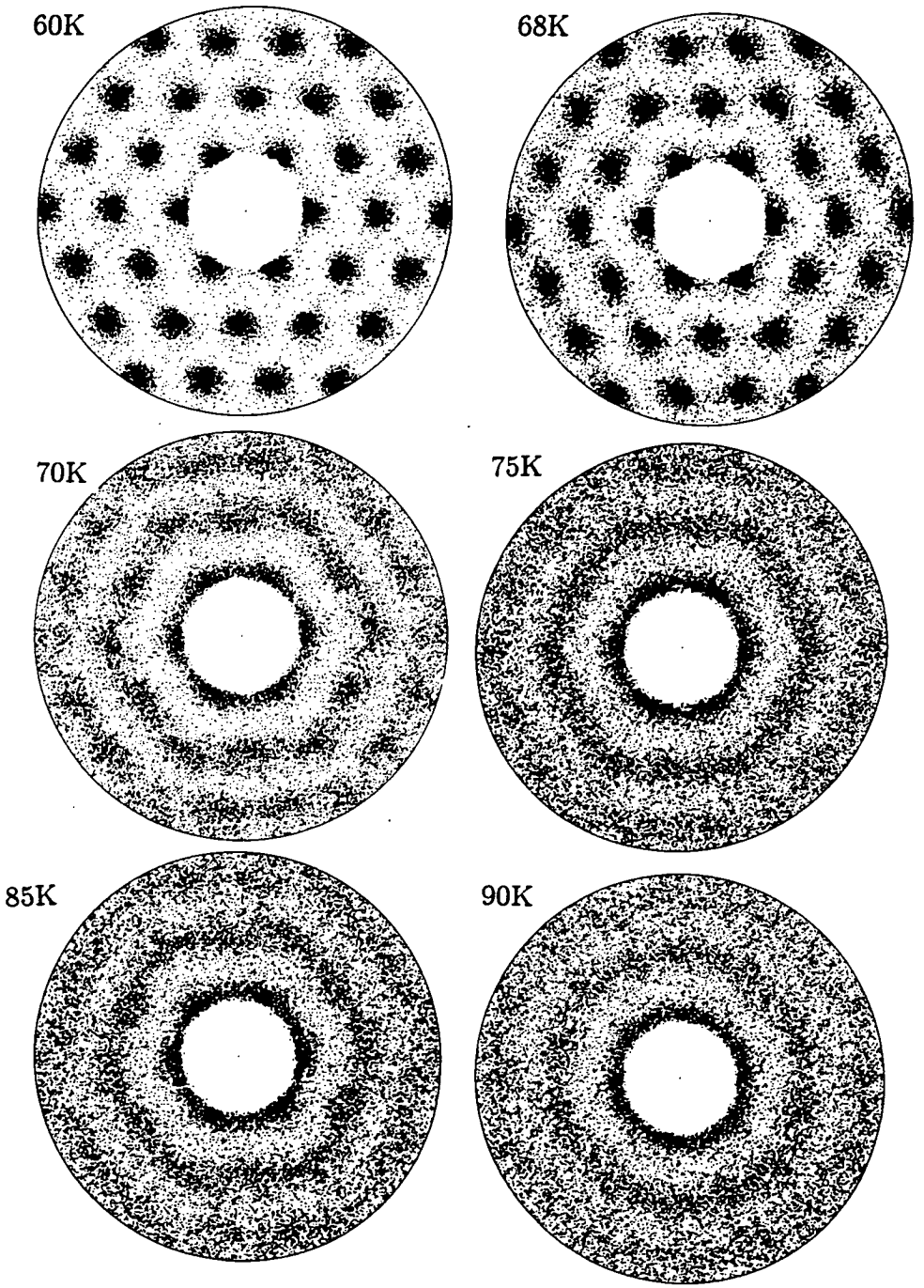

Figure 2.6. P.d.f. at 60K, 68K, 70K, 75K, 85K and 90K.

solid-liquid phase co-existence. A solid heated well above its melting point will rapidly transform into a liquid, however, near the melting point the transition from solid to liquid is slow and may require a very long simulation time. It is possible that at 70K and 72K, although equilibrium appears to have been achieved, the solid regions are slowly melting and the cluster will eventually become liquid. To test this, the simulation was continued at 70K and 72K after apparent equilibrium was found. The total simulation time at each temperature is shown in the Table 2.1. All measured values and figures were made near the end of the time at each temperature.

At 70K around 250ps were required to equilibrate the cluster after heating from 68K. On heating to 72K equilibration took 100ps with only a very small change in potential, density and co-ordination number observed. The simulations were then run for a further 280ps at 70K and 470ps at 72K. At both temperatures potential remained near the initial equilibrated value, no significant changes in density or co-ordination number were observed, and the solid areas in the cluster persisted. When heated to 75K a considerable decrease in potential is immediately noticeable, and equilibrium is found after only 60ps. On the time-scale of a molecular dynamics simulation for 1024 atoms 500ps is a long time. If a slow melting transition was occurring at 70K then heating to 72K should be enough to melt the remaining solid within the time of the simulation as heating from 72K to 75K did. We can therefore state that a long-lived solid-liquid co-existence phase does occur in this simulation.

Any remaining large solid areas have disappeared at 75K. The cluster has noticeably expanded compared to 70K, there is no longer any long-range translational order evident, and all atomic trajectories show large displacement diffusive motion suggesting the cluster is now liquid. In the p.d.f at 75K there are no longer any distinct groupings of dots showing loss of any solid areas. The first and second nearest neighbour bands still have an overall hexagonal shape, rather than circular, which implies some short-range order must exist at 75K. The hexagonal shape is consistent with some atoms remaining six-fold co-ordinated out to second nearest neighbours, but are still able

to make large displacement motion, hence continuous bands, as opposed to distinct groups, are observed in the p.d.f.. Evidence of a hexatic phase is found at 75K, or more likely a phase in which regions of a hexatic anisotropic liquid and an isotropic liquid co-exist.

The six-fold short-range order is still observable in the p.d.f. for 85K, but at 90K the bands are now more diffuse and circular in shape. There is also a drop in the average co-ordination number, from 4.818 at 85K to 4.683 at 90K, suggesting the cluster is now mostly a puddle of isotropic liquid. There is therefore a final transition from an anisotropic to an isotropic liquid between 85K and 90K, which, because no large discontinuities in density or potential are observed, may be a second-order transition.

2.5 Conclusions

The melting of a two-dimensional cluster of Krypton atoms, in this simulation, occurs in three stages: a first-order transition between 68K and 70K from a solid phase to an intermediate phase where solid and liquid co-exist, the liquid probably being anisotropic; another first-order transition between 72K and 75K where the remaining solid melts and the cluster enters a phase which is liquid but in which some short-range order remains, a hexatic anisotropic liquid phase; finally, a second-order (continuous) transition from an anisotropic to an isotropic liquid phase completed between 85K and 90K, in which the short-range order is lost. Well below the first stage of the melting transition, premelting effects can be observed as the formation of dislocations at 50K and above. Melting is mediated by loss of order from the surface inwards and by the removal of translational order by dislocations in the bulk. There is some evidence that dislocations aggregate to form grain boundaries which produce the first stage of the melting transition; the smaller grains melt, but larger grains remain as solid regions, hence the solid-liquid co-existence phase is entered.

The results of our simulations should now be discussed in terms of the theories of

two-dimensional melting discussed at the start of this chapter. The initial first-order transitions observed appear to be most in agreement with the theory due to Saito, where a two-dimensional hexagonal crystal with bonding energy of the order of the Lennard-Jones interaction for Krypton has a first-order melting transition induced by grain boundary formation. The solid-liquid co-existence phase has been observed in molecular dynamics simulations by Abraham, using a Lennard-Jones potential and a constant density ensemble with periodic boundary conditions. As mentioned earlier, applying such restrictions in a simulation can suppress certain effects, surface melting effects of course, but also vacancy and dislocation formation in the bulk. Neither Saito nor Abraham found evidence for a hexatic phase above the melting transition.

The observation of defect formation in the solid before melting and of a hexatic phase with a second-order transition to an isotropic liquid phase are in direct agreement with the KTNHY theory. This theory also predicts that the transition from the solid to the hexatic phase is second-order (continuous), whereas we find sizable discontinuities in density and potential which imply a first-order transition between these phases. It is possible that this behaviour is a finite size effect due to the use of a cluster. The first-order transition occurs when the grain boundaries extend throughout, *i.e.* saturate, the entire cluster; the temperature at which saturation occurs will depend on the size of the cluster. In a much larger cluster, or a bulk sample, this saturation effect may not happen until a somewhat higher temperature, possibly higher than the temperature at which the isotropic liquid phase is reached. If this is the case, the loss of translational order due to defect formation would be continuous with temperature, in full agreement with the KTNHY theory.

To test this hypothesis simulations of the melting of larger and smaller clusters is required. In a smaller cluster the saturation effect would be more significant, creating more obviously discontinuous change in the area and potential of the cluster, and no solid-liquid co-existence would occur. In a larger cluster the discontinuities observed should be smaller and the temperature range for which solid-liquid co-existence occurs

would be greater. In a very large cluster (with a considerable bulk region), if the KTNHY theory is correct, then no discontinuities in area or potential energy would be observed and the change from solid to anisotropic liquid would be continuous.

Although in principle this is a simple simulation, by employing careful analysis much interesting information can be gleaned. It is also a good illustration of the worth of using clusters in simulations in condensed matter physics. Real materials have a large bulk but also a surface (and often grain boundaries also). In applying periodic boundary conditions, effects associated with surfaces and grain boundaries are removed and long-range effects in bulk, such a dislocations, are restricted to the length between cyclic boundaries. In phenomena such as melting, as we have seen, these are important effects. In our simulations we could perform long studies on a 1024 atom cluster. With advances in supercomputing, in the near future detailed simulations of 10,000+ atoms should become commonplace, moving the study of clusters into the size region of microcrystals, and thus allowing bulk and surface effects to be studied in detail.

Chapter 3

Solidification

And the loss of fire is called cooling, and the contraction which follows it is called a state of solidity.
Plato, Timaeus.

3.1 Introduction

In Chapter 2 we saw how a melting transition occurs in an ensemble with a surface and argued that results could be radically different compared to when periodic boundary conditions are applied. Another phenomenon which may be affected by what conditions are applied to a simulation is that of solidification. We shall use the term solidification to mean 'formation into a solid', and largely avoid other phrases such as freezing or nucleation, since no detailed study of the nature of the phase from which the solid forms or how this process occurs shall be made.

3.2 Simulation Details

Four (three-dimensional) ensembles are studied; 256 krypton atoms with periodic boundary conditions, 256 krypton atoms in a cluster, a mixture of 128 krypton and 128 argon atoms with periodic boundary conditions and a mixture of 128 krypton and

	A (KCal/mole Å^{-6})	B (KCal/mole Å^{-12})
Kr-Kr	2937.00	6393405.0
Kr-Ar	2366.01	4222192.2
Ar-Ar	1906.03	2788327.8

Table 3.1. Parameters for Lennard-Jones potential.

	Lattice Parameter (Å)	Melting Temperature (K)
Krypton	5.72	116.5
Argon	5.26	83.9

Table 3.2. Data for krypton and argon.

128 argon atoms in a cluster. Inert gas atoms are used since their interactions can be well represented by the Lennard-Jones potential (p.4). The parameters used are listed in Table 3.1. For the interaction of krypton and argon the geometric mean of the A and B parameters is taken, *e.g.* $A_{KrAr} = \sqrt{A_{Kr}A_{Ar}}$. In Table 3.2 some experimental data on krypton and argon is given [38].

We require all simulations to begin from an initial ensemble which is liquid-like, *i.e.* with average atomic separations which are only slightly larger than that for the solid and with a random distribution of atoms so that there is no translation order. The liquid-like state is achieved by starting the atoms on face-centred cubic lattice sites but with an enlarged lattice parameter of 6.0Å and with random velocities which correspond to a temperature of 140K, which is well above the melting temperature of both krypton and argon. Each simulation begins with 10,000 steps of time-step 0.005ps at 140K, after which the initial lattice order has disappeared and the atoms are randomly distributed. A time-step of 0.005ps is used throughout all the simulations.

For clusters, to prevent evaporation at the initially high temperature, any atom which escapes too far from the centre of the cluster has the direction of its velocity reversed so that it returns towards the surface of the cluster; the cluster is in essence contained within a sphere from which no atom can escape. So long as the sphere is

significantly larger than the cluster (*e.g.* in the cluster simulations to be discussed the sphere has a radius of 17Å for clusters of about 14Å radius) the pressure applied to the cluster remains effectively zero and the only effect of the sphere is to retain the atoms.

Since only a relatively brief investigation of the solidification process is proposed here, we shall mainly be interested in the final solid structure resulting from the very rapid cooling of an initially liquid-like ensemble. This is done by quenching, *i.e.* rescaling the atomic velocities, from 140K to 40K. The simulations are then continued at 40K until a stable average potential energy is observed. The ensemble is then assumed to be in equilibrium and no further large structural changes will occur. The ensemble is then cooled to 1K, to reduce the thermal motion of atoms, and the structure of the ensemble is analysed.

3.3 Analysis Techniques

The most straightforward analysis method is a **pictorial representation** in which all or part of the ensemble is viewed with the atoms represented as spheres of a radius which is half the nearest neighbour separation in the face-centred close-packed structure found in experiments. For krypton the radius is 2.02Å and for argon 1.86Å.

The **radial distribution function (r.d.f.)** is a well known method of determining the spatial distribution of atoms in an ensemble and thereby any translational ordering. For an ensemble containing N atoms the r.d.f. used here is defined as

$$g(r) = \sum_{i=1}^{N} \frac{n_i(r, r+\delta r)}{V(r, r+\delta r)} \tag{3.1}$$

where $n_i(r, r+\delta r)$ is the number of atoms in the radial shell between r and $r+\delta r$ from atom i and $V(r, r+\delta r) = \frac{4}{3}\pi[(r+\delta r)^3 - r^3]$ is the volume of that shell. The r.d.f. is determined for N intervals of δr, from a minimum to a maximum radial distance, such

that $\delta r = (r_{max} - r_{min})/N$. For the length scales involved in the simulations we choose r_{min}=2.0Å, r_{max}=10.0Å and N=80, so that the r.d.f. has a resolution of 0.1Å.

In the **pair distribution function (p.d.f.)** the presence of translational order is investigated by plotting the directional co-ordination between an atom and its neighbours. The method is similar to that for the two-dimensional p.d.f. (p.20) except a three-dimensional distribution must now be represented on a two-dimensional page. First the unit vector in the direction from the position of atom i at (x_i, y_i, z_i) to the position of a neighbouring atom j at (x_j, y_j, z_j), with radial separation R_{ij}, is calculated; explicitly

$$(x_{ij}, y_{ij}, z_{ij}) = (x_j - x_i, y_j - y_i, z_j - z_i)/R_{ij}.$$

If this is done for all atoms and their nearest neighbour atoms, then what we have is a set of points, $X_{ij}(x_{ij}, y_{ij}, z_{ij})$, all of which lie on a unit sphere. To represent these points as a two-dimensional distribution function we use the **equal area projection**. To project the three-dimensional point X_{ij} to the point $X_p(x_p, y_p)$ in the xy plane, we define r_1 as the chord from the 'north pole' of the unit sphere at $(0, 0, 1)$ to X_{ij},

$$r_1 = \sqrt{x_{ij}^2 + y_{ij}^2 + (1 - z_{ij})^2} = \sqrt{2(1 - z_{ij})}$$

and r_2 as the distance of X_{ij} from the z-axis in the xy plane

$$r_2 = \sqrt{x_{ij}^2 + y_{ij}^2}.$$

The equal area projection of X_{ij} is,

$$(x_p, y_p) \quad = \quad (x_{ij}, y_{ij}) \times [r_1/r_2]. \tag{3.2}$$

The p.d.f. is constructed for up to twenty-four neighbour atoms for each atom, within a cut-off radius of 12.0Å.

3.4 Krypton in a Cell and a Cluster

When krypton solidifies it forms a close-packed face-centred cubic crystal; this is a well known result verified in many experiments. We shall therefore be looking for the presence of such a structure in the simulations in this section.

For the simulation of 256 krypton atoms in a periodically repeating cell 490ps were required to equilibrate the ensemble at 40K. A view down the z-axis through the central section of the ensemble is shown in Figure 3.1(a) and Figure 3.2(a) shows the p.d.f. of the ensemble. Since all the points in the p.d.f. are arranged in distinct groups, there is a regular arrangement of atoms and their neighbours; the solidified structure is therefore crystalline. The final dimensions of the cell occupied by the atoms is 23.94Å×23.93Å×23.94Å, suggesting a cubic structure.

In solid krypton the expected nearest-neighbour atomic separation for the face-centred cubic structure is $r_n = a/\sqrt{2}$ =4.04Å. The r.d.f. in Figure 3.3(a) shows a large peak at 4.0Å, which corresponds to the nearest neighbour separation distance, within the 0.1Å resolution of the r.d.f.. Some of the distances between atoms in the face-centred cubic structure of krypton are listed in Table 3.3. Were the ensemble to have a face-centred cubic structure the r.d.f. should show a peak near 5.7Å, the cubic lattice parameter; at this distance however the r.d.f. shows a distinct dip. The structure cannot therefore be face-centred cubic.

Let us now compare the peak values of the r.d.f. with neighbour distances for a body-centred cubic structure, as given in Table 3.4. The body-centred cubic lattice parameter would be 4.66Å and the second nearest neighbour peak in the r.d.f. would be at this distance. Although there is no obvious peak at this distance it is possible that imperfections in the structure have broadened this peak so that it has partially merged with the larger nearest-neighbour peak. The third nearest-neighbour peak would be expected at 6.59Å and indeed a small peak is evident at this distance.

If we look again at Figure 3.1(a) the position of a body-centred cubic unit has

(a)

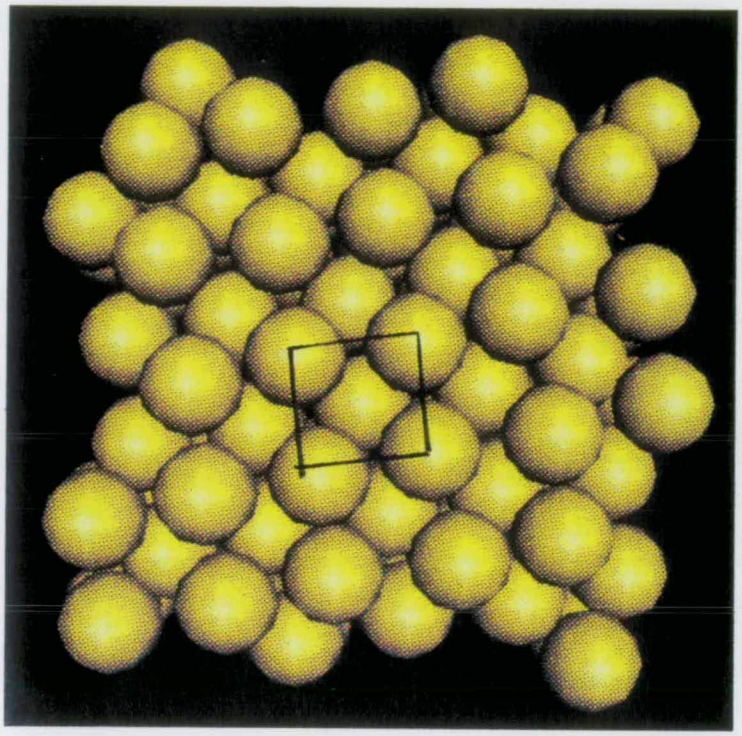

(b)

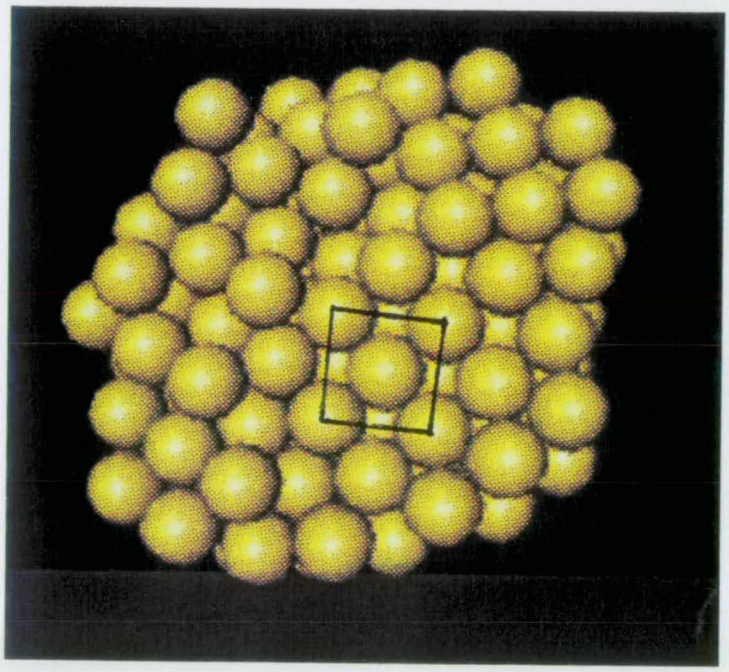

Figure 3.1. Solid krypton in (a) periodic cell (b) cluster.

Neighbour	Distance	Å
$\frac{1}{2}\frac{1}{2}0$	r_n	4.04
100	$\sqrt{2}r_n = a$	5.72
$1\frac{1}{2}\frac{1}{2}$	$\sqrt{\frac{3}{2}}a$	7.00
110	$\sqrt{2}a$	8.08

Table 3.3. Neighbour distances for face-centred cubic structure.

Neighbour	Distance	Å
$\frac{1}{2}\frac{1}{2}\frac{1}{2}$	r_n	4.04
100	$\frac{2}{\sqrt{3}}r_n = a$	4.66
110	$\sqrt{2}a$	6.59
$\frac{3}{2}\frac{1}{2}\frac{1}{2}$	$\frac{\sqrt{11}}{2}a$	7.73

Table 3.4. Neighbour distances for body-centred cubic structure.

been marked and we may convince ourselves that a body-centred cubic structure is discernible. In the p.d.f. the centres of the four largest groups of dots are approximately the same distance from the centre of the circle and are all separated from each other by 90°, which is consistent with the projection of pairs of atoms at the centre and the corners of a body-centred unit cell. There are also other smaller groups of points which too have a distribution consistent with cubic ordering. An ensemble of 256 atoms will be comprised of 128 body-centred unit cells; this number of unit cells can not be fitted exactly into a cubic periodic cell which may explain why the axes of the crystalline solid are not aligned with the axes of the periodic cell which contains it. There is also an asymmetry in the density of points in the p.d.f. suggesting that there may be more than one body-centred cubic crystallite present.

For the simulation of 256 krypton atoms in a cluster, 420ps were required to achieve equilibrium at 40K. The groups of points which comprise the p.d.f. of the cluster in Figure 3.2(b) and the view of a cross-section through the cluster in Figure 3.1(b) show that some crystalline ordering is present. The r.d.f. of the cluster in Figure 3.3(b) again

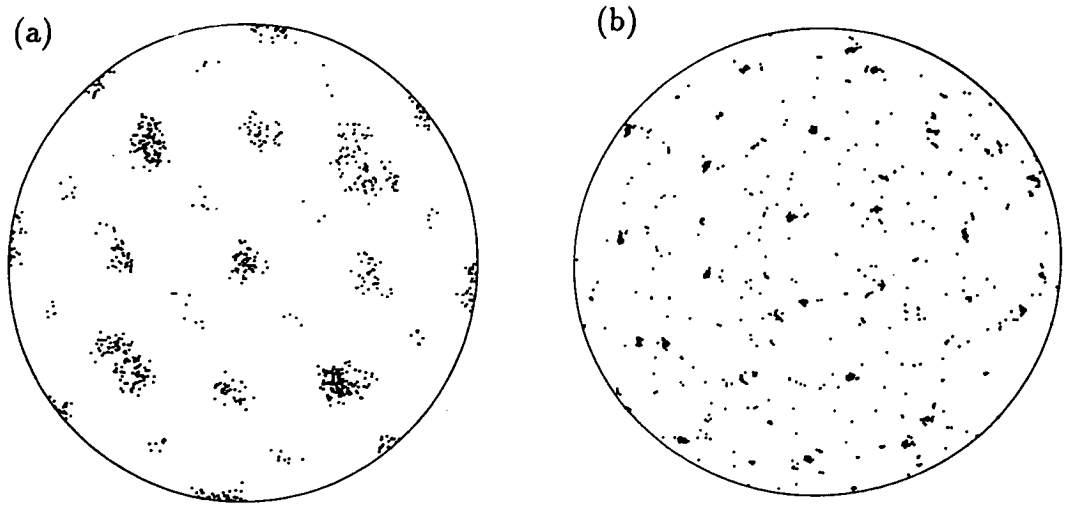

Figure 3.2. P.d.f. for solid krypton in (a) periodic cell (b) cluster.

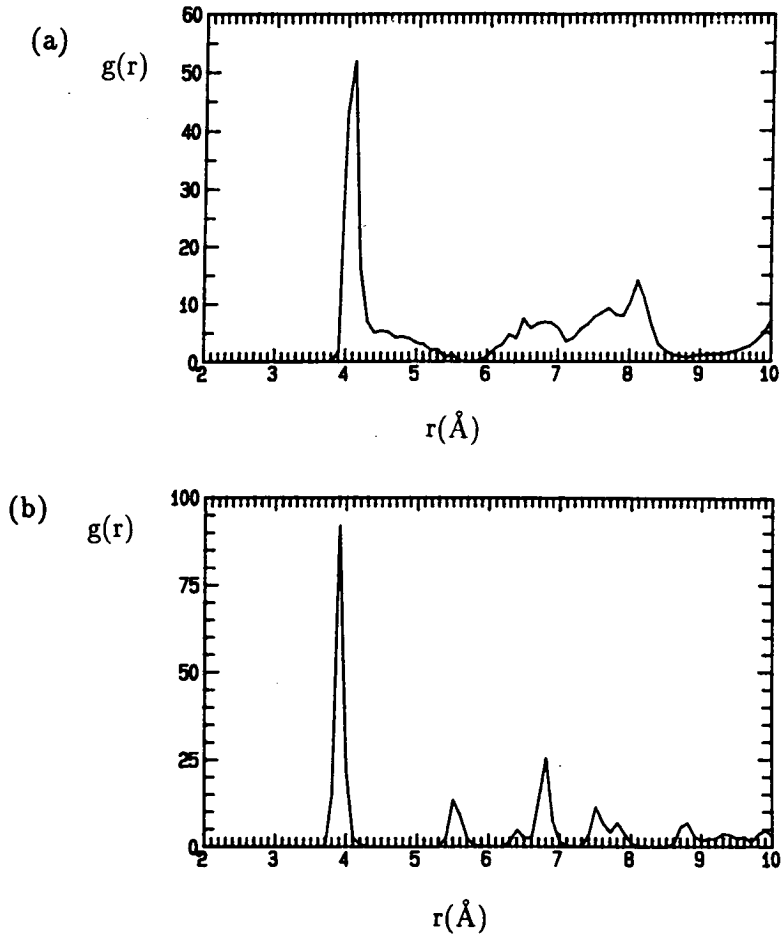

Figure 3.3. R.d.f. for solid krypton in (a) periodic cell (b) cluster.

shows a nearest-neighbour peak at 4.0Å. The second nearest neighbour peak occurs at 5.6Å, which, as discussed above, is consistent, to within 0.1Å, of what is expected for a face-centred cubic structure. Re-examining Figure 3.1(b), we can see that the position of face-centred cubic unit cell has been marked within a region of face-centred cubic structure in the lower part of the cluster.

Solidification, particularly in relation to nucleation, is one of the most obvious and earliest uses of molecular dynamics simulations [39]. Nucleation is the process by which small solid regions, called nucleation centres, form in a liquid; the solid then forms out of the liquid around these nucleation centres. For a review of the subject see Oxtoby [43].

The results of our simulation are in agreement with those of Mandell, McTague and Rahman [40] who observed the formation of a body-centred structure on cooling a liquid comprised of 500 particles interacting *via* a Lennard-Jones potential in an ensemble with periodic boundary conditions applied. When the simulation was repeated with the periodic boundary conditions removed a close-packed structure was found to form, like that found in our cluster simulation. However, Hsu and Rahman [41], again in a simulation of 500 particles in a periodic cell, found that, with a Lennard-Jones potential, the structure formed on cooling was face-centred cubic, in disagreement with the earlier findings of Mandell and McTague.

A body-centred nucleation centre requires the co-ordination of an atom and eight neighbours whereas the face-centred nucleation centre requires the co-ordination of an atom and twelve neighbours. A body-centred nucleation centre should therefore have a higher probability of forming spontaneously, however, a face-centred nucleation centre has a lower potential energy and is thus more stable, which is why in a bulk sample krypton will form a close-packed solid. In simulations the solidification process is sensitive to the small size of the ensemble used; the time required for a solid to form becomes shorter the smaller the ensemble used. If a body-centred nucleation centre

should form, and the ensemble is small enough, the entire ensemble can rapidly form the body-centred structure around this nucleation centre. If this ensemble is periodically repeating then the body-centred structure is space-filling and so will remain stable on the time-scale of a molecular dynamics simulation. The solidification process in small ensembles will therefore depend on cooling rate, potential, initial conditions, size and boundary conditions. Swope and Andersen [42] have performed simulations of very large periodic cells containing 15,000 and 1,000,000 particles. In these simulations 10% of the ensemble formed a body-centred structure, the rest being in face-centred or hexagonally close-packed structures. With slower solidification, *i.e.* annealing, in a large ensemble, body-centred regions are less likely to remain stable and the expected close-packing dominates.

In a cluster a predominantly face-centred structure was found to form on cooling. Unlike the periodic cell, the cluster has a surface. The most energetically favoured state for a cluster is to have a minimum surface area; this is achieved by face-centred close packing of atoms. If a body-centred nucleation centre did form then a body-centred structure could form around it, however, the body-centred structure would transform to a face-centred structure to minimise the surface area and the potential energy of the cluster.

It is reasonable to assume that for a small number of atoms (100-1000) the boundary conditions applied may affect the process of solidification. Simulations of clusters with around 1000 atoms may be sufficient for a detailed study of nucleation as opposed to the very large ensembles required to overcome the effect of periodic boundary conditions. Since they have surfaces, clusters are also suitable for the simulation of annealing effects in crystallisation. Further heating of the solidified cluster, over a long period of time, causes the grain boundaries separating the crystallites of which the cluster is comprised to migrate to the surface and disappear, leaving the cluster as a perfect single microcrystal.

3.5 Krypton and Argon Mixtures

We shall now examine what happens in the solidification of mixtures of krypton and argon in equal proportion. Argon is chosen because, based on a comparison of the nearest neighbour separation in solid form, it is the inert gas atom with size closest to that of krypton.

3.5.1 In a cell

A mixture of 128 krypton and 128 argon atoms in a periodically repeating cell, with an initially random distribution of the two atom types throughout the ensemble, is quenched from 140K to 40K. After 1500ps of simulation time the potential energy of the ensemble had stabilised and equilibrium was assumed. A section through the resulting ensemble is shown in Figure 3.4 and the p.d.f. of all atoms in the ensemble and their eight nearest neighbours, at 1K, is shown in Figure 3.5. No crystalline ordering is evident in either of these figures. If we now look at the r.d.f. of the ensemble, in Figure 3.6, we can see there is a broad peak between 3.5 and 4.1Å, encompassing the nearest neighbour separations for all combinations of krypton and argon atoms, and that there are no further distinct peaks at greater distances. The results of all the analytical methods applied are consistent with the structure of the ensemble being that of an amorphous solid.

In quenching the ensemble what we have observed is a glass transition into an amorphous solid. In experiments such transitions do occur when atomic liquids are cooled rapidly. The study of glass transitions is a large subject [44] which has involved molecular dynamics simulations using the Lennard-Jones potential [45, 46]. A proper analysis of the amorphous solid goes beyond the scope of this thesis, but this result is of interest for comparison with the supercooling of a mixed krypton and argon cluster which follows.

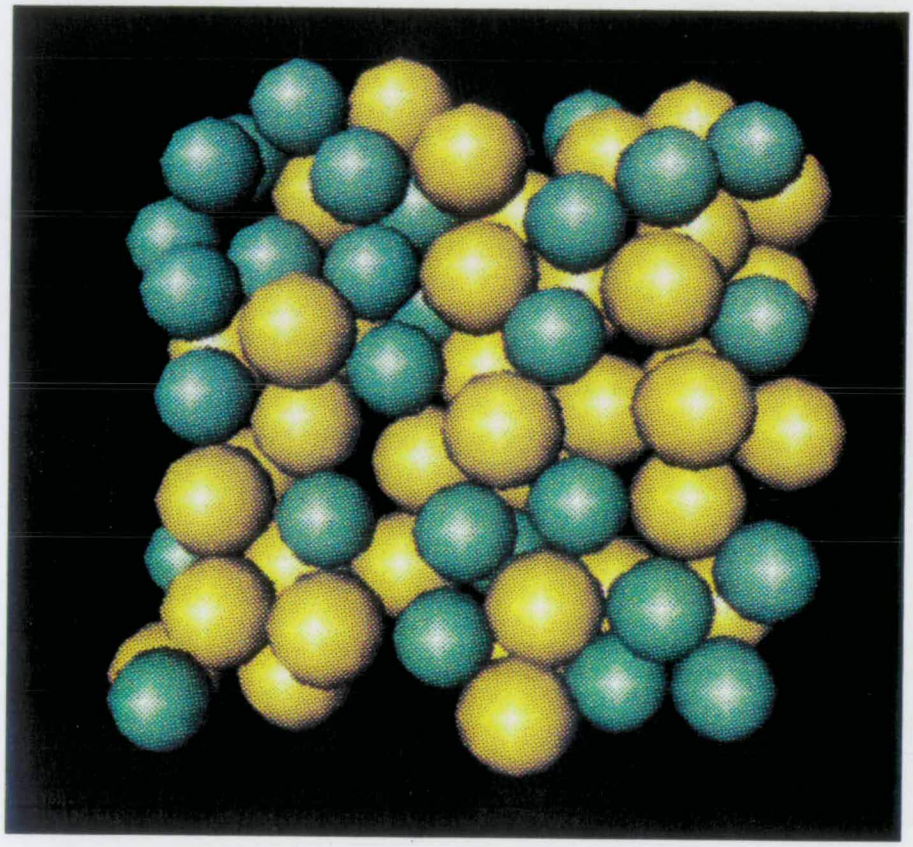

Figure 3.4. Solid krypton and argon in periodic cell.

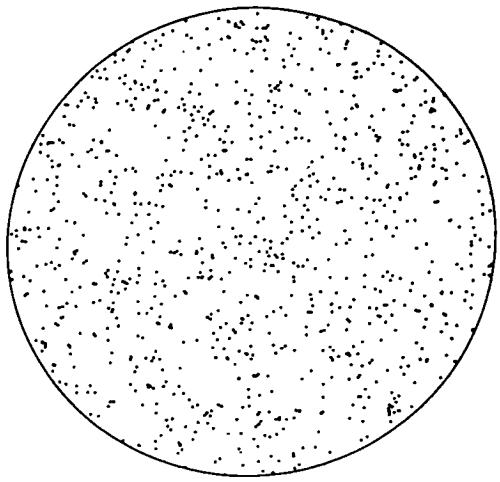

Figure 3.5. P.d.f. for solid krypton and argon in a periodic cell.

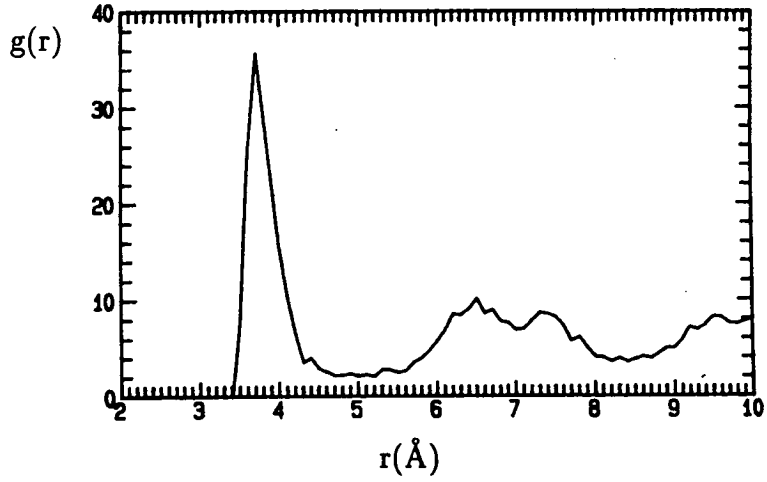

Figure 3.6. R.d.f. for solid krypton and argon in a periodic cell.

3.5.2 In a Cluster

As we saw in Section 3.4 the solidification process in a cluster can be very different from that in a periodic cell containing the same number of atoms. A cluster containing 128 krypton and 128 argon atoms, randomly distributed, is quenched from 140K to 40K. Equilibrium is reached after 1200ps. A cross-section of this cluster is shown in Figure 3.7(a), and Figure 3.8(a) shows the p.d.f. of the cluster constructed as before. If we compare this p.d.f. to the p.d.f. for the body-centred cubic krypton structure in Figure 3.2(a) we can see that the two are similar, suggesting that a body-centred type of ordering may be present in the cluster.

If the structure has cubic order then the [100],[010] and [001] directions are all equivalent. We shall assume that Figure 3.8(a) was constructed with the [001] nearly aligned with the z-axis and now construct two more p.d.f.s, one for the cluster rotated by 90° about the x-axis, so that the [010] is aligned with the z-axis (Figure 3.8(b)) and the other for the cluster rotated by 90° about the y-axis, so that the [100] is aligned with the z-axis (Figure 3.8(c)). The p.d.f. constructed in each of the three directions show a similar distribution of points, particularly for the four largest groupings at 90° intervals about the centre. The crystalline ordering in the cluster is therefore most likely to be cubic.

In Figures 3.9(a),(b) and (c) the p.d.f. in Figure 3.8(a) has been decomposed into Kr-Kr, Kr-Ar and Ar-Ar pairs respectively. The p.d.f. for Kr-Ar shows the strongest ordering with the four groupings at 90° intervals about the centre as the most outstanding feature. This order is consistent with a cubic unit cell in which atoms of one type on the vertices and an atom of the other type in the body-centre, what is commonly known as the CsCl structure.

We can now check if the r.d.f. of the cluster is consistent with the CsCl structure.

(a)

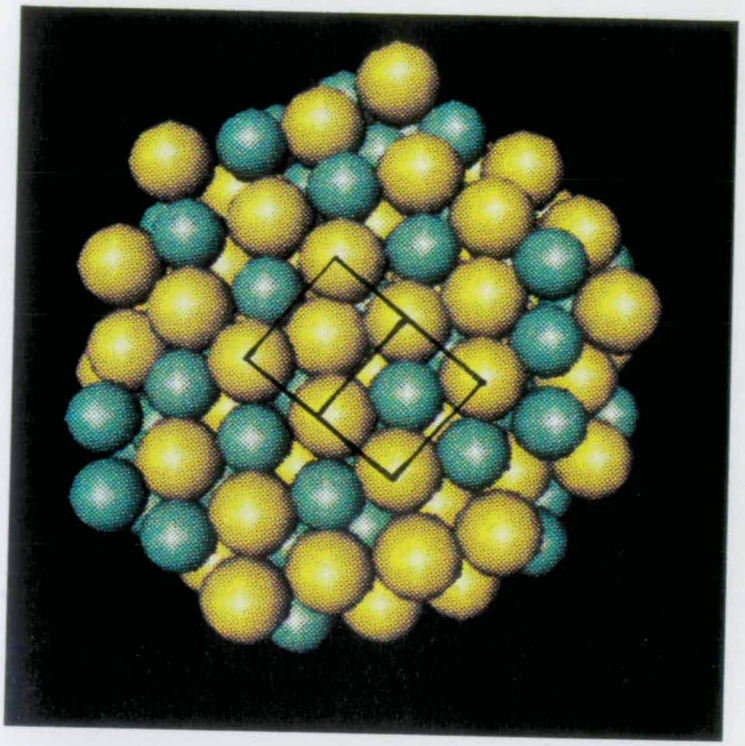

(b)

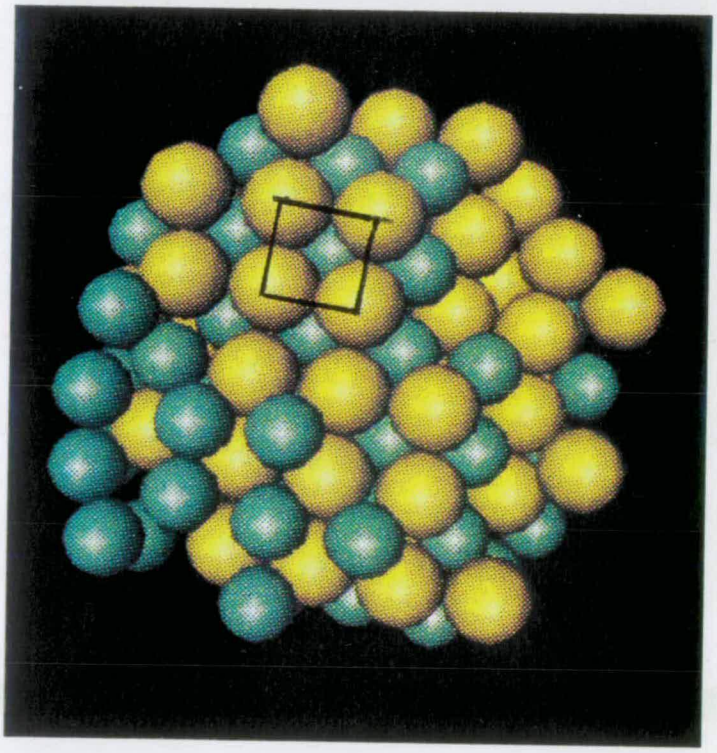

Figure 3.7. Solid krypton and argon clusters (a) quenched (b) annealed.

Neighbour	Distance	Å	Pair
$\frac{1}{2}\frac{1}{2}\frac{1}{2}$	r_n	3.50	Kr-Ar
100	$\frac{2}{\sqrt{3}}r_n = a$	4.04	Kr-Kr,Ar-Ar
110	$\sqrt{2}a$	5.71	Kr-Kr,Ar-Ar
$\frac{3}{2}\frac{1}{2}\frac{1}{2}$	$\frac{\sqrt{11}}{2}a$	6.70	Kr-Ar

Table 3.5. Neighbour distances for CsCl structure.

From the r.d.f. for the whole cluster in Figure 3.10(a) we can measure the peak nearest-neighbour distance, to within 0.1Å, to be 3.5Å. Taking r_n=3.50Å between a krypton-argon pair we can calculate the neighbour distances between various pairs of atoms in the CsCl structure (Table 3.5).

Figure 3.10(b),(c) and (d) show the r.d.f.s for Kr-Kr, Kr-Ar and Ar-Ar respectively. The first neighbour peak occurs in the r.d.f. for Kr-Ar as expected and there is a peak at 6.7Å consistent with the CsCl structure, but there is also another peak just below 4.0Å, merging with the first peak, which is not consistent with the CsCl structure. In the Kr-Kr r.d.f. there is a sizable peak at around 4.0Å, which is between the first and second nearest neighbour distances for the CsCl structure. The Ar-Ar r.d.f. has its largest peaks at 3.7Å and 5.7Å, which is consistent with the CsCl structure.

From the analysis we may conclude that the predominant crystalline order of krypton and argon atoms in the cluster conforms to the CsCl structure. If we re-examine the part of the cluster shown in Figure 3.7(a) we can now recognise it as being a view of a cross-section through a [110] plane. For the two unit cells marked on the figure, that on the lower-right has the CsCl structure, with krypton atoms on the corners and an argon atom at the body-centre, but that on the upper-left has a krypton atom in the body-centre and on the corners. A few unit cells with krypton in the body-centre and on the vertices can explain the unexpected peak in the Kr-Kr r.d.f.. The overall structure of the cluster may be defined as being the CsCl structure discussed above with some disordering of atomic sites, *i.e.* krypton on argon sites and vice-versa.

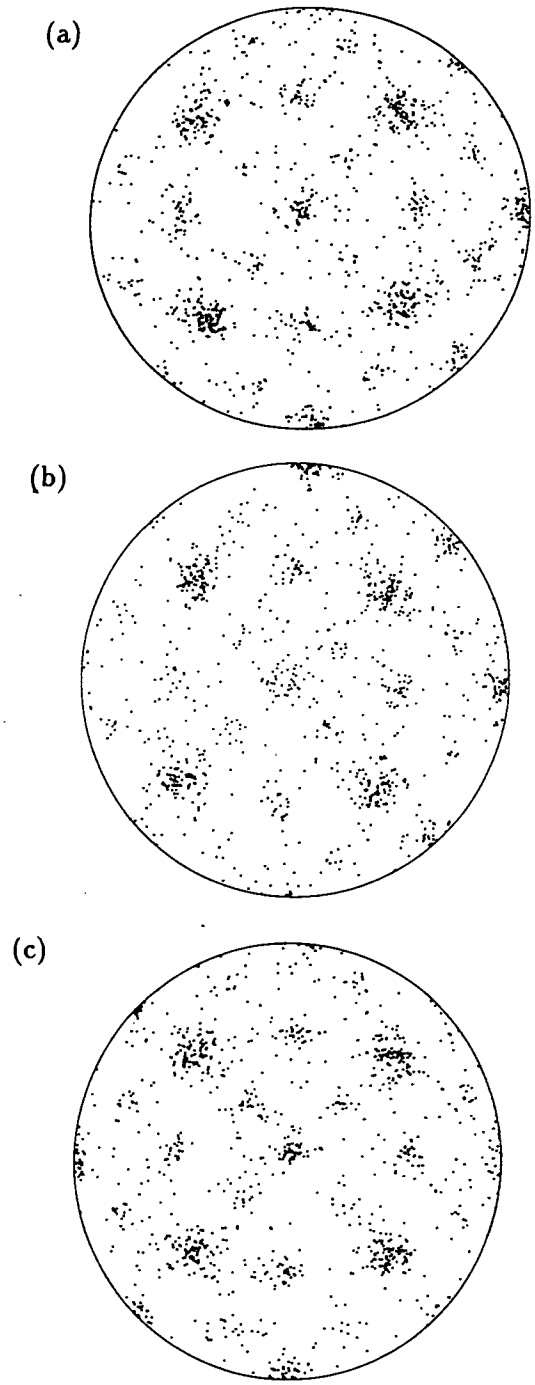

Figure 3.8. P.d.f.s for quenched cluster in (a) 001 (b) 010 (c) 100 directions.

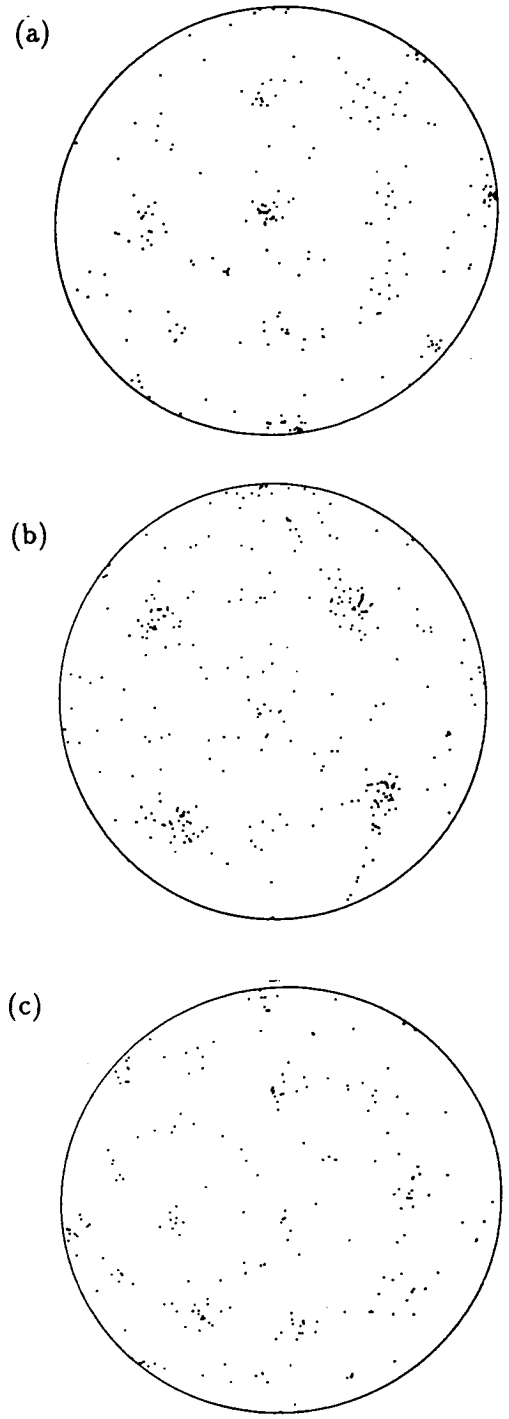

Figure 3.9. P.d.f.s for quenched cluster for (a) Kr-Kr (b) Kr-Ar (c) Ar-Ar

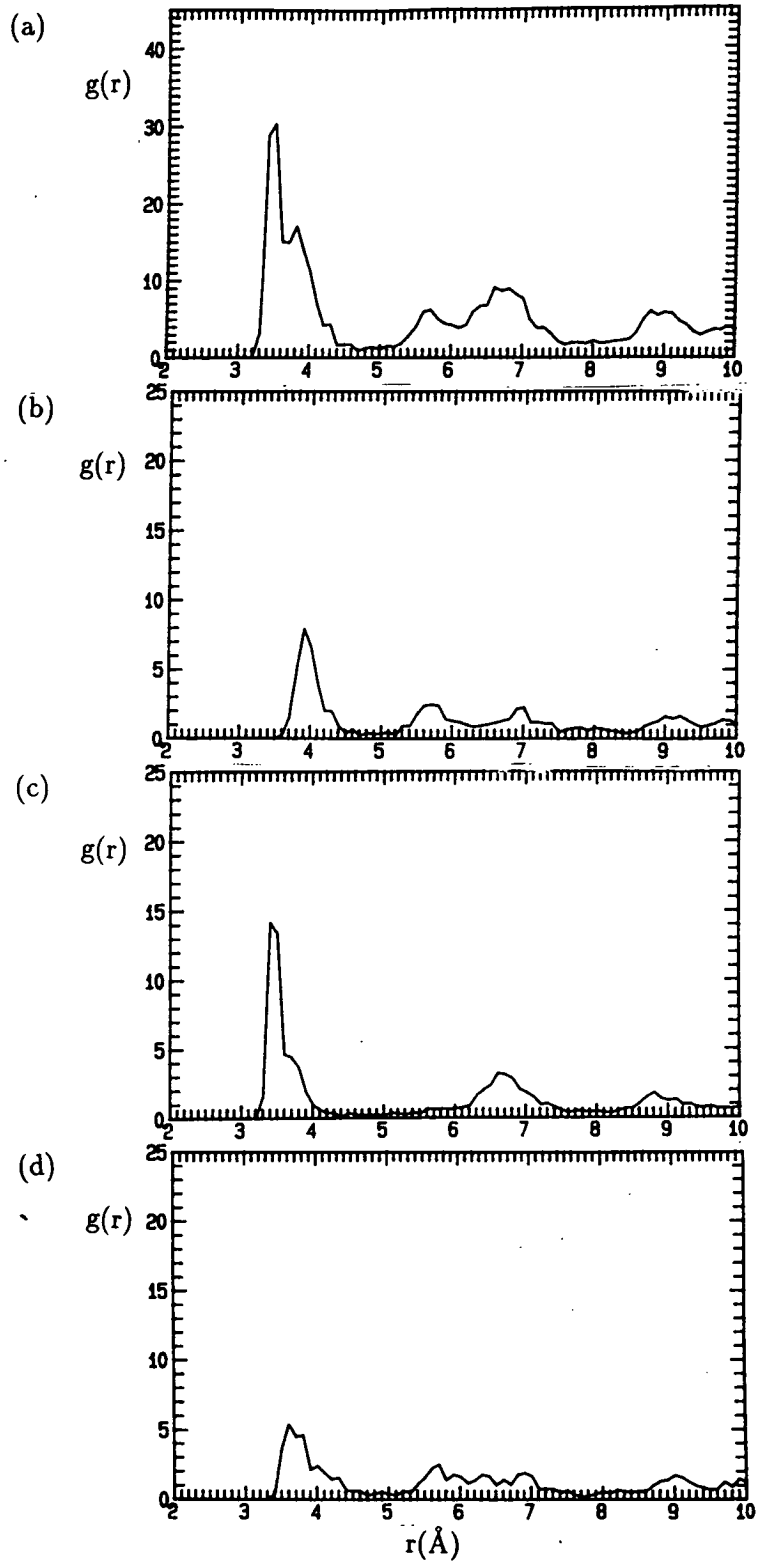

Figure 3.10. R.d.f.s for quenched cluster (a) all (b) Kr-Kr (c) Kr-Ar (d) Ar-Ar.

All the simulations thus far in this chapter have induced solidification by quenching a liquid-like phase. We shall now examine what happens to the cluster of krypton and argon mixture if it is annealed, *i.e.* the temperature is gradually and continuely reduced, rather than quenched. Starting with the same initial configuration as the quenched cluster, the cluster is cooled from 140K to 30K, over 1200ps. The temperature of the cluster was reduced on each step at an average rate of 0.09Kps^{-1}. A cross-section of the resulting structure is shown in Figure 3.7(b) and the p.d.f.s for the all atoms, Kr-Kr, Kr-Ar and Ar-Ar pairs are shown in Figures 3.11(a-d) respectively. Examining these figures we can immediately see evidence of crystallisation in the CsCl structure.

The r.d.f.s for the annealed cluster, constructed in exactly the same fashion as for the quenched cluster, are shown in Figures 3.12(a-d). If we compare these to the r.d.f.s for the quenched cluster in Figures 3.10(a-d) (plotted on the same scale) we can see that the peaks in the r.d.f.s of the annealed cluster are sharper and have greater amplitude than those in the quenched cluster, suggesting that more uniform crystalline order has been formed by annealing. The distances at which the peaks in the r.d.f.s of the annealed cluster occur can be matched to the neighbour distances for the CsCl structure given in Table 3.5. There are still two small anomalous peaks, just below 4.0Å in the Kr-Ar r.d.f. and near 3.7Å in the Ar-Ar r.d.f., but these are smaller than for the quenched cluster and may be attributed to the unordered atoms which are always found near the surface of the cluster. From the analysis we may conclude that the majority of the annealed cluster has formed a crystallite in the CsCl structure.

The simulations performed on clusters of mixtures equal proportion of krypton and argon atoms have predicted that the favoured structure formed on cooling is that of the CsCl structure, which has a cubic unit cell with a krypton atom at $(0,0,0)$ and an argon atom at $(\frac{1}{2},\frac{1}{2},\frac{1}{2})$ and a=4.0±0.1Å. The question now arises, could this structure really form in experiment and if so would it be observable? In experiment, cooling a bulk sample on the nanosecond time-scale of a simulation would result in a glass transition

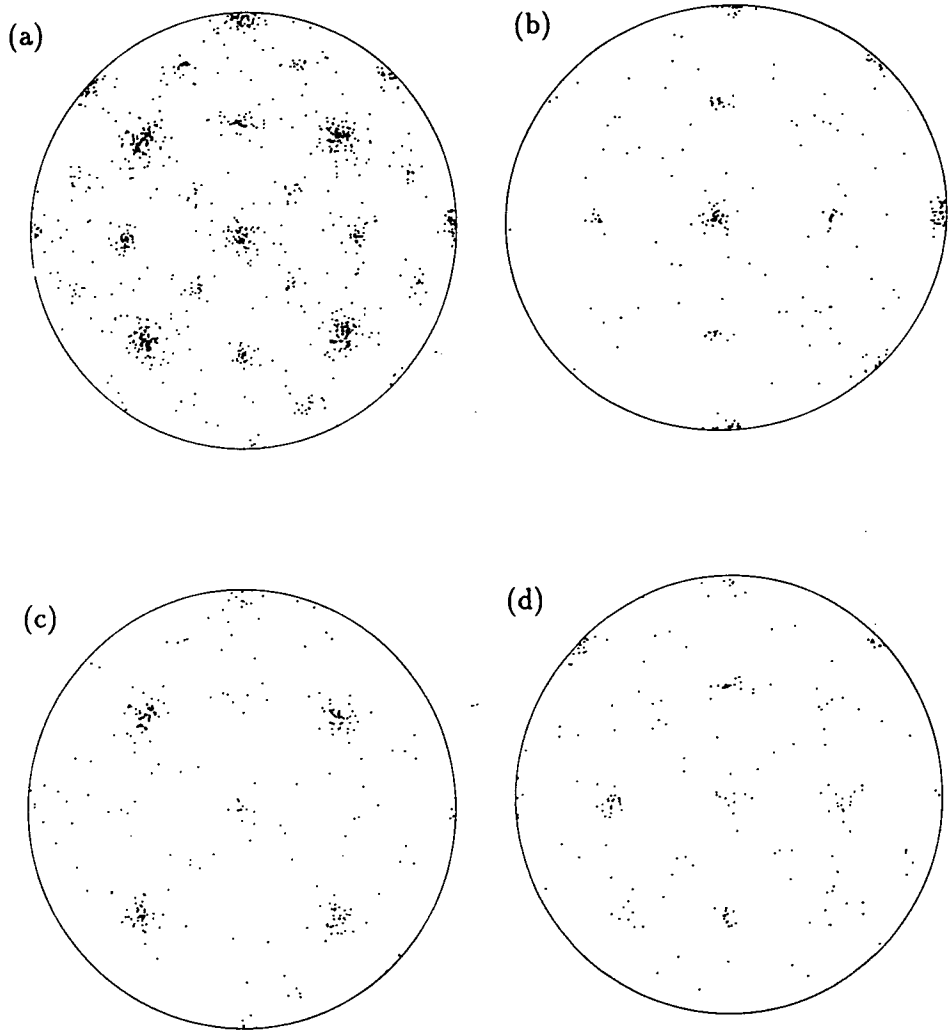

Figure 3.11. P.d.f.s for annealed cluster (a) all (b) Kr-Kr (c) Kr-Ar (d) Ar-Ar.

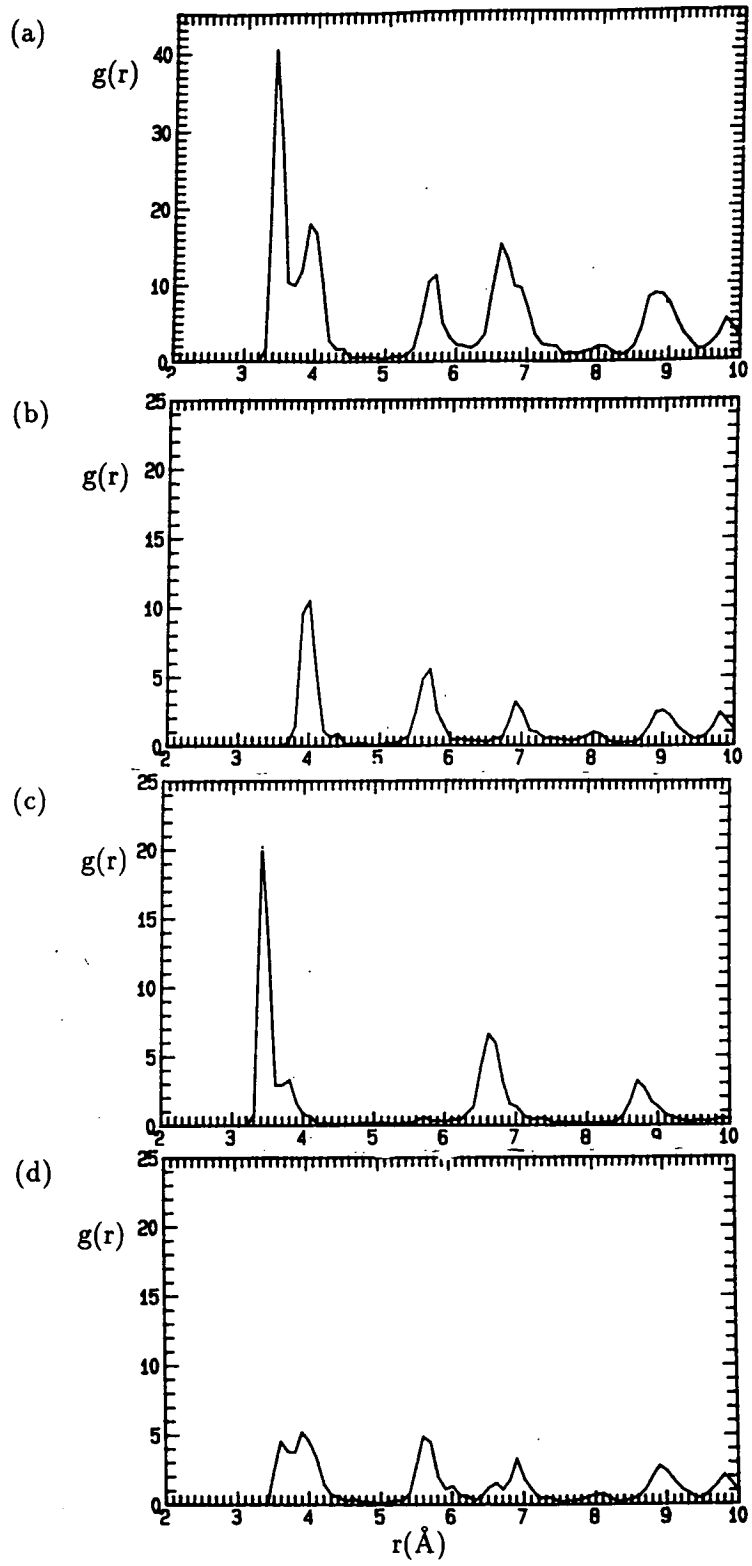

Figure 3.12. R.d.f.s for annealed cluster (a) all (b) Kr-Kr (c) Kr-Ar (d) Ar-Ar.

as discussed previously, however, in such a solid it is possible that some regions of the CsCl cluster could form amongst the majority amorphous structure. In molecular beam experiments clusters of around 250 atoms are formed on time-scales similar to that of molecular dynamics simulations. If it is experimentally possible to achieve an equal mixture of krypton and argon in the molecular beam, then electron diffraction techniques could be used to examine whether the clusters formed do exhibit the CsCl structure. The formation of the CsCl structure by slow annealing of a krypton and argon liquid mixture is unlikely to occur since mixtures of inert gas atoms in liquid form tend to demix [47], so that, due to the difference in freezing temperatures between krypton and argon, crystallites of krypton would most likely form in the still liquid argon.

The simulations of the krypton and argon clusters does demonstrate that the spontaneous formation of crystal structures involving more than one type of atom from a liquid state can be studied by molecular dynamics simulation. A more practical application of this method would be in studying the formation of crystalline metallic alloys [48].

Chapter 4

Adamantane

The scion of gold, which is very hard because of its density and dark in colour, is called adamant.
Ibid.

4.1 Introduction

Adamantane, $C_{10}H_{16}$, is a saturated hydrocarbon molecule consisting of six methylene (CH_2) groups linked by four methine (CH) groups (Figure 4.1(a)). The carbons of the methine groups form a tetrahedral cage, with the methylene groups projecting from the six edges of this tetrahedron (Figure 4.1(b)); the adamantane molecule therefore exhibits tetrahedral symmetry. In Appendix A data for the adamantane molecule is given, including a set of atomic co-ordinates; these co-ordinates describe a molecule for which a 2-fold symmetry axis of the tetrahedral cage is aligned with the Cartesian z-axis, with one edge of the tetrahedron lying along the x-axis and the opposing edge along the y-axis. All orientations are discussed relative to these co-ordinates.

At low temperatures [49] the molecular crystal has a tetragonal unit cell with a=b=6.6Å, c=8.81Å and space group $P\bar{4}2_1c$. The molecules have an ordered arrangement of orientations; all molecules have a 2-fold symmetry axis aligned with the c-axis with alternate layers in this direction in inverted orientations and are rotated by 9°

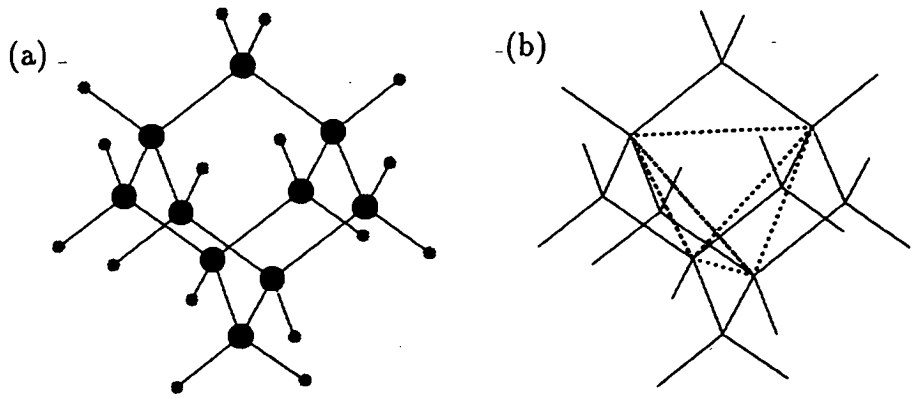

Figure 4.1. Adamantane, (a) molecule (b) tetrahedral symmetry.

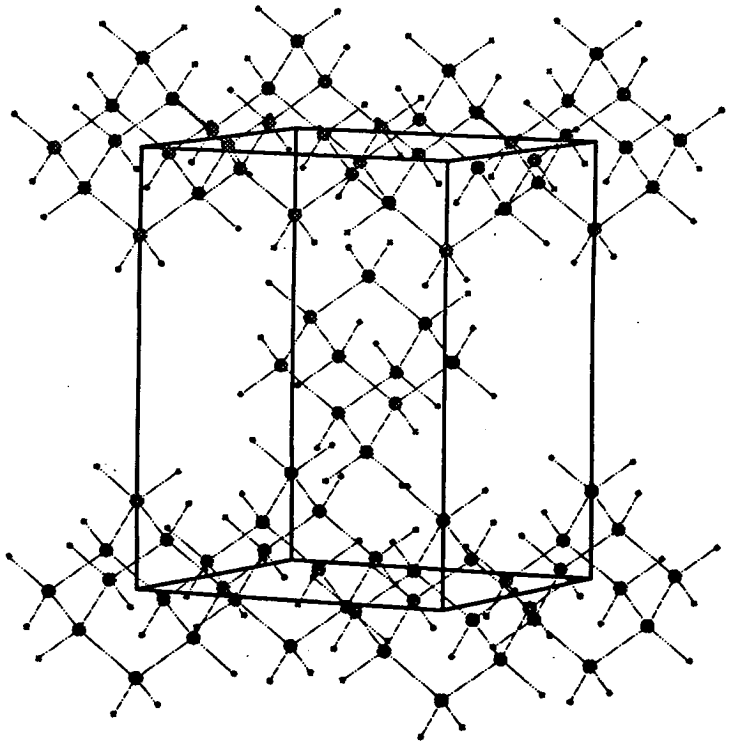

Figure 4.2. The tetragonal unit cell.

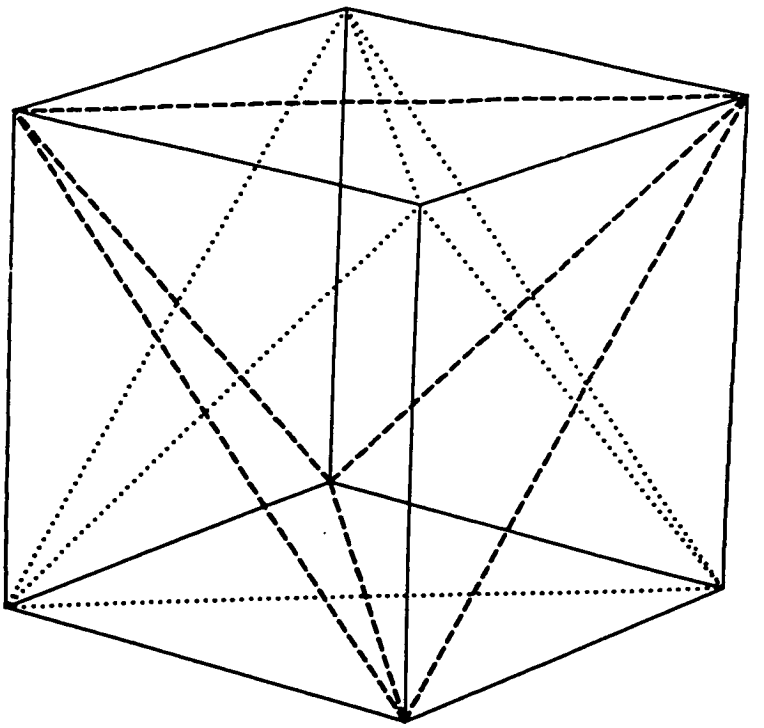

Figure 4.3. The two possible arrangements between a tetrahedron and a cube.

about the c-axis in the opposite sense with respect to the previous layer. The arrangement of the unit cell is shown in Figure 4.2.

At 208.6K there is a first order transition to the orientationally disordered plastic phase. The unit cell is now face-centred cubic, with a=9.45Å where the a and b axes are at 45° to those in the tetragonal phase. The molecules are randomly distributed between two orientations [50, 51], which involve 3-fold symmetry axes of a molecule being aligned with [111] directions of the cubic unit cell. This is a rotationally frustrated state where molecules can make hindered reorientations between these two orientations. The space group in this phase is $Fm3m$.

The two possible orientations which the molecules occupy in the plastic phase can be understood by considering the two unique alignments of the 3-fold symmetry axes of a tetrahedron with the 3-fold symmetry axes of a cube, as shown in Figure 4.3. A 3-fold symmetry axis of a tetrahedron passes through its centre and a vertex. The

same is true for the cube. The co-ordinates listed in Appendix A correspond to the orientation of the dotted line tetrahedron. The dashed line tetrahedron in Figure 4.3 is related to the dotted line tetrahedron by a symmetric inversion. The dashed tetrahedron represents a molecular orientation which has an alignment of molecular 3-folds with $[111], [1\bar{1}\bar{1}], [\bar{1}1\bar{1}]$ and $[\bar{1}\bar{1}1]$ directions and the dotted line tetrahedron represents a molecular orientation which has an alignment of molecular 3-folds with $[1\bar{1}1], [11\bar{1}], [\bar{1}11]$ and $[\bar{1}\bar{1}\bar{1}]$ directions. This gives us a definition of the two molecular orientations relative to the underlying cubic lattice which will be used in the study of reorientations in the simulation. By analogy with spin states in the Ising model, the orientation described by the dashed tetrahedron will be referred to as the 'up' molecular orientation and the inverse orientation, described by the dotted tetrahedron, will be referred to as the 'down' molecular orientation. The two orientations in the ordered tetragonal unit cell are close to the up and down orientations, except for a $\pm 9°$ rotation about the c-axis.

Reynolds [52] has reported the same cubic structure but with local ordering and space group $F\bar{4}3m$ above the phase transition. The most likely order consistent with this space group would involve large domains of molecules all in the same orientation. This work was done on specially prepared single crystals annealed at high temperature in contrast to the other studies in which the crystals were grown by sublimation. Reynolds suggests that ordered domains of up to 300 molecules could be present in the otherwise disordered structure whilst appearing to retain the $Fm3m$ space group.

Several previous computational simulations involving adamantane have been performed. Meyer and Ciccotti [53, 54] used molecular dynamics simulations of 32 and 108 adamantane molecules in a periodically repeating cell interacting *via* the Williams potential (to be discussed later), firstly to calculate some crystallographic properties of the plastic phase and then to study the reorientational motion of molecules. In later work [57], they simulated the transition from the ordered tetragonal to the disordered cubic phase, but found the inverse transition from disordered cubic to ordered tetragonal could not be attained without specifically returning the molecules to near ordered

orientations. Yashonath and Rao [55] use a Metropolis Monte Carlo method to change the positions and orientations of molecules, with interactions centred on the methylene and methine groups, to perform a limited study of the order-disorder transition. Trew and Pawley [56] have performed molecular dynamics simulations on clusters of 128 and 256 molecules, using a potential with interactions centred on the hydrogen atoms. They observed an order-disorder transition close to the temperature found for bulk samples in experiment, but again failed to observe the inverse transition on cooling.

4.2 Simulation Details

As a starting point for the simulations the first objectives are to reproduce the ordered unit cell at low temperature and the transition to a disordered phase on heating. Since much of the simulation will be concerned with disorder and reorientations in the cubic plastic phase the ordered tetragonal unit cell is now chosen to be described relative to the cubic unit cell, having a=b=$\sqrt{2} \times 6.6$Å=9.333Å and c=8.81Å, where the a and b axes are at 45° to those of the tetragonal unit cell, but both c axes are the same. If the molecule at $(0,0,0)$ is near an up orientation then the molecule at $(\frac{1}{2},\frac{1}{2},0)$ is similarly oriented and those at $(\frac{1}{2},0,\frac{1}{2})$ and $(0,\frac{1}{2},\frac{1}{2})$ are in the inverse orientation.

Simulations were performed on a periodically repeating ensemble of $4 \times 4 \times 4$ unit cells, as described above, containing 256 molecules in total. The molecules were given orientations corresponding to the ordered state of the crystals and random velocities and angular velocities corresponding to an average temperature of 140K. The molecules are assumed to be rigid, hence only the inter-molecular forces need be considered. The initial simulation used the Williams pairwise additive atom-atom potential [58] to calculate the forces between all carbon and hydrogen atoms in neighbouring molecules. This potential is similar to the Lennard-Jones potential but has an exponential repulsive term with parameters fitted to data from *ab initio* calculations on various hydrocarbons. The general form is

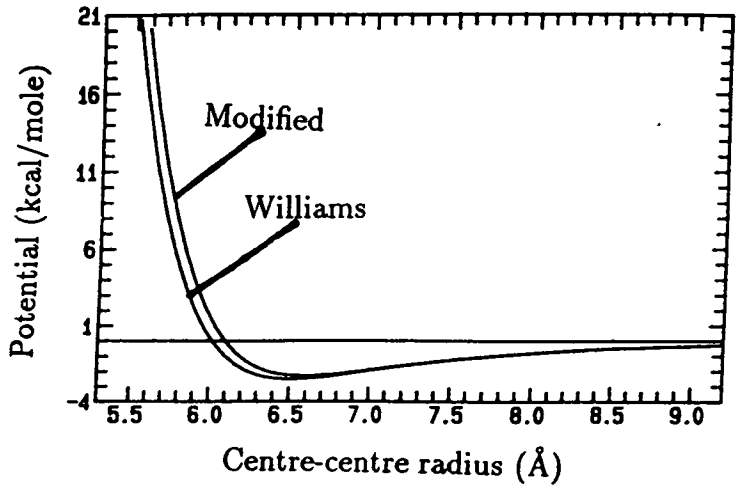

Figure 4.4. Potential between two adamantane molecules

$$\phi(r) = \frac{-A}{r^6} + Be^{-Cr} \tag{4.1}$$

The parameters for carbon-carbon, carbon-hydrogen and hydrogen-hydrogen interaction are given in Table 4.1.

After 6000 steps of 0.02ps the 256 molecule cell was brought to equilibrium at 140K. All the molecules remained close to the ordered orientations they were given initially. The average unit cell was found to be almost tetragonal with a=9.263(1)Å, b=9.282(4)Å, c=8.634(7)Å. The volume of this unit cell is 3.4% smaller than that of the experimental unit cell, which is a significant amount. It was concluded that although the Williams potential could reproduce a stable ordered unit cell for adamantane the lattice parameters found deviated too far from the experimental values. A modification of the potential model was therefore required.

The potential between two nearest neighbour adamantane molecules in the ordered orientations was calculated for a range of centre-centre separations (Figure 4.4). For the Williams potential the minimum energy separation was found to be at 6.335Å compared to the experimental value of 6.4Å. The potential parameters were adjusted to fit the experimental separation (Table 4.2).

	A (kcal/mole Å^{-6})	B (kcal/mole)	C (Å^{-1})
C-C	567.5	83574.09	3.60
C-H	124.92	8760.15	3.67
H-H	27.23	2652.14	3.74

Table 4.1. Parameters for Williams Potential.

	A (kcal/mole Å^{-6})	B (kcal/mole)	C (Å^{-1})
C-C	567.5	86000.0	3.60
C-H	124.92	9200.0	3.60
H-H	27.23	2800.0	3.74

Table 4.2. Parameters for Modified Potential.

Repeating the equilibration procedure using the new potential the unit cell remained close to tetragonal with lattice parameters a=9.383(1)Å, b=9.354(5)Å, c=8.776(1)Å. The volume of this unit cell is now only 0.35% greater than that found from experiment. It is these potential parameters which are used in the simulations.

4.3 Analysis Techniques

The average values of the volume per molecule, the potential energy per molecule and the lattice parameters of the unit cell were calculated during the simulation (Figures 4.5(a,b,c)). The the range of error in the all the parameters measured was estimated by finding the maximum and minimum value of each parameter over 2500 steps. The estimated error in the average values of parameters was then taken to be half the interval between the maximum and minimum values, *i.e.* $err_{av} = (err_{max} - err_{min})/2$.

Some graphical techniques are also employed to examine the behaviour of molecules in the ensemble. In **cage diagrams** (*e.g.* Figure 4.6) a cross-section of the cell is pictured in which the molecules are represented by tetrahedra, the underlying symmetric cage of the adamantane molecule (Figure 4.1(b)). This representation allows us to view the orientations of the adamantane molecules without the obstruction of all the atoms

and the bonds. All such figures show views of the two overlying *ab* face-centred lattice planes, in the centre of the cell, viewed down the *c*-axis (*n.b.* the molecules on the lower plane are drawn smaller than those on the upper plane).

The **orientational distribution function (o.d.f.)** is a graphical method of examining which orientations the molecules favour and the relative occupation of these orientations. As discussed in Section 4.1, the orientational order of a crystalline ensemble of adamantane can be discussed in terms of alignments of the symmetry axes of the molecule and symmetry axes of the unit cell. To construct a suitable o.d.f. therefore, the orientations of the 3-fold symmetry axes of the molecules must be considered. If we consider the molecules as tetrahedra (as in Figure 4.6) and take the centre of each tetrahedron in turn to be at the centre of a unit-sphere, the o.d.f. is constructed by finding the points where the lines from the centre to the vertices of the tetrahedra intersect with the unit sphere. To represent the o.d.f. on the page (*e.g.* Figure 4.7) the points on the northern hemisphere of the unit sphere are projected into the equatorial plane using the equal area projection (p.37). The open circles on the o.d.f.s correspond to the projection of the [111] directions of a cubic lattice.

From **orientational trajectories** the time development of a molecule's orientation can be observed by plotting the trajectory of a fixed point on the molecule. To do this a 3-fold axis of a molecule is chosen (that through the (1,1,1) vertex of the tetrahedron in Figure 4.3) and the point on the o.d.f. formed by this axis is calculated every tenth time step using the method discussed above. Joining these points in sequence gives the orientational trajectory shown in Figure 4.8. In these figures points in both hemispheres are used in the projection, the inner circle being the equator and the outer circle representing the south pole of the sphere. Again the small open circles represent the projection of all the [111] directions of a cubic unit cell.

4.4 Results

4.4.1 Transition to a Disordered Phase

After equilibration at 140K, the simulation was performed for a range of temperatures, increasing in 20K steps, with 6000 steps of 0.02ps at each temperature to re-establish equilibrium. The condition used to assess when the ensemble was in equilibrium was that any expansion or contraction of the cell had occurred and that the volume of the cell showed only small fluctuations about an average value. The volume was considered rather than the potential energy of the ensemble because a plastic phase will be examined in which, for a small sample of molecules, molecular reorientations cause a significant fluctuation in potential energy even in equilibrium.

On heating, a steep increase in volume and a corresponding decrease in potential above 380K can be seen from Figure 4.5. There is also a steep rise in the c lattice parameter. At 420K the c value almost matches those for a and b. Since the angles between the edges of the cell remain very close to 90° throughout the simulation, we can say that a transition from a tetragonal to a cubic unit cell has occurred.

Figure 4.6 shows cage diagrams and Figure 4.7 o.d.f.s for the same temperatures. In the cage diagram at 140K the tetrahedra have a 2-fold axis aligned with the c-axis which is the 4-fold symmetry axis of the tetragonal unit cell. Orientational order is evident with alternate layers in the c direction in inverse orientations. In terms of space groups the $\bar{4}$ axes of the tetrahedra (which are also the 2-fold axes) are aligned with the unique axis of the tetragonal unit cell, hence the ordered configuration found in the simulation is consistent with the $P\bar{4}2_1c$ space group from experiment. Examining the o.d.f. at 140K it can be seen that the groups of points associated with the molecular 3-fold axes show a small rotation away from the cubic [111] directions, corresponding to 9° rotation of the molecules about the c-axis as observed in experiment. The order, size and shape of the low temperature unit cell found in experiments have therefore been closely reproduced in the simulation.

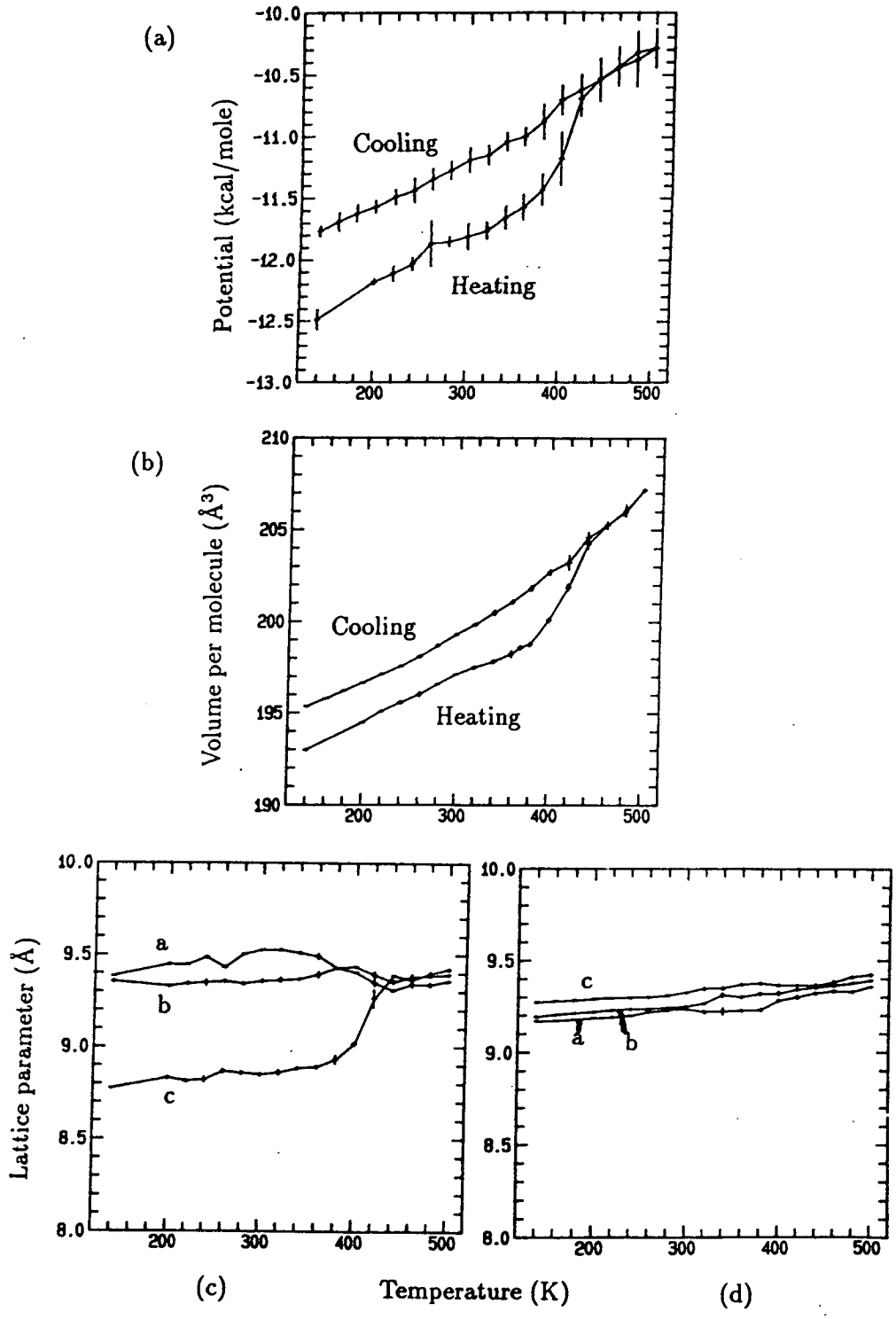

Figure 4.5. (a) Potential (b) Volume and lattice parameters (c) on heating (d) on cooling.

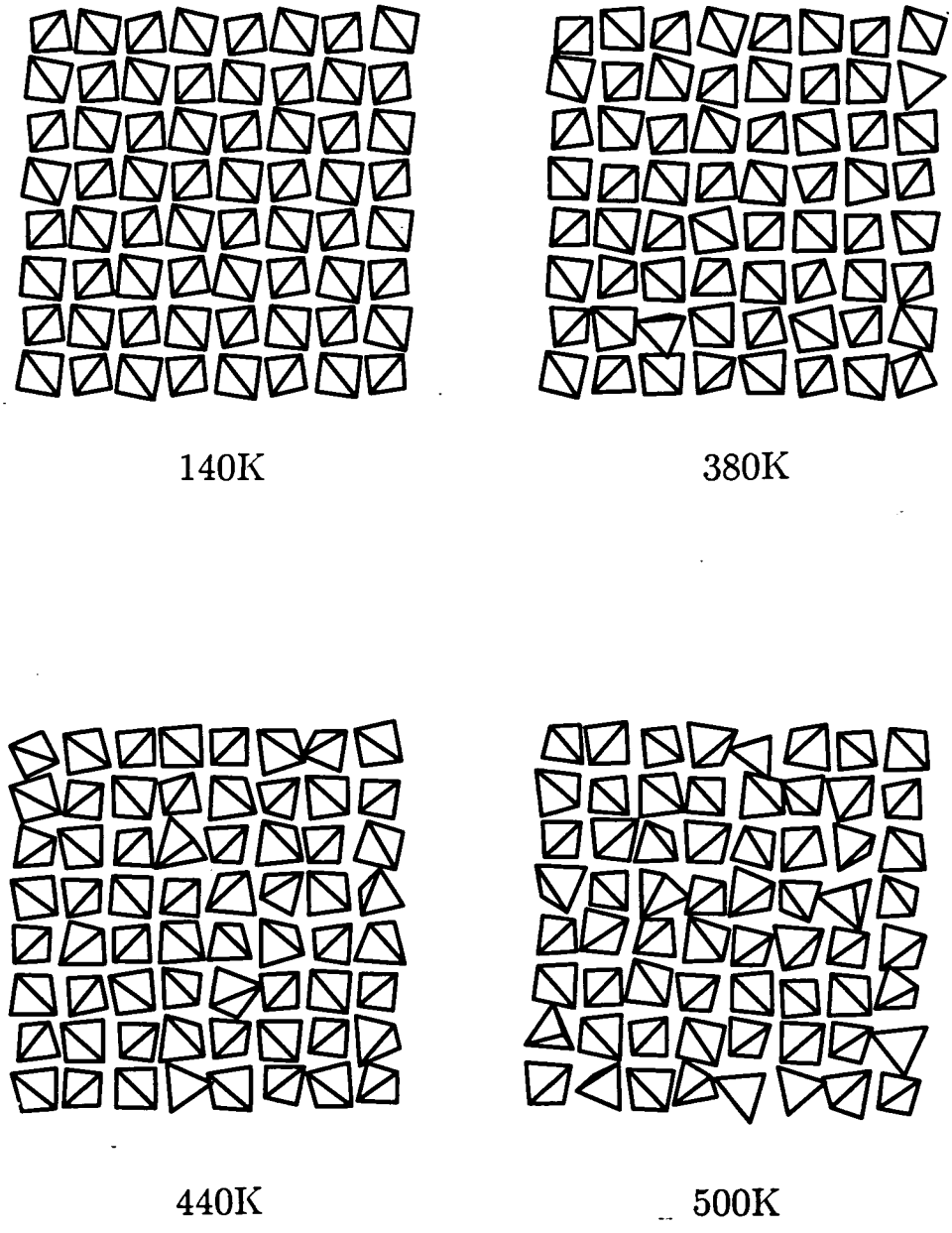

Figure 4.6. *ab* plane centre-section at 140K, 380K, 440K and 500K on heating.

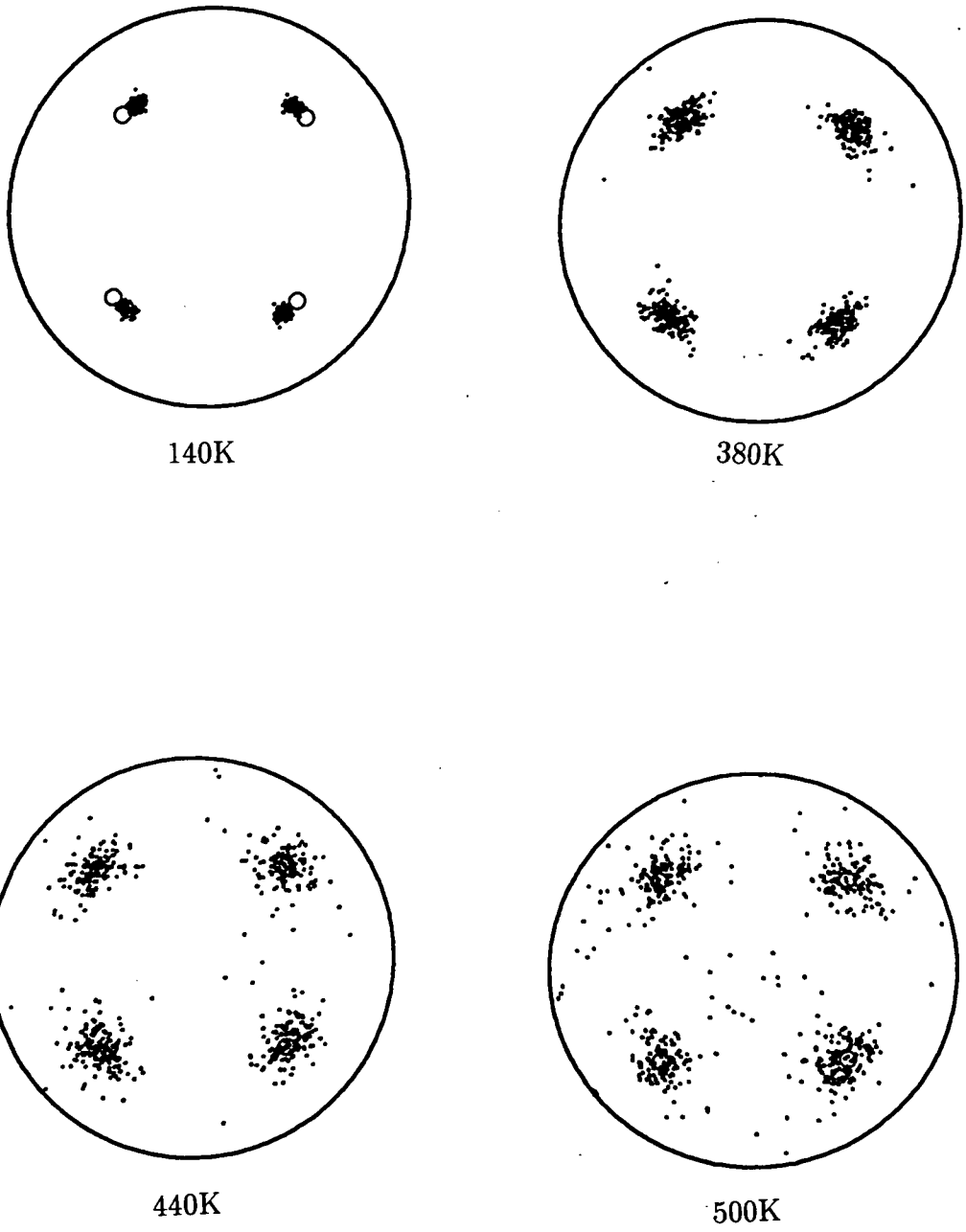

Figure 4.7. o.d.f.s at 140K, 380K, 440K and 500K on heating.

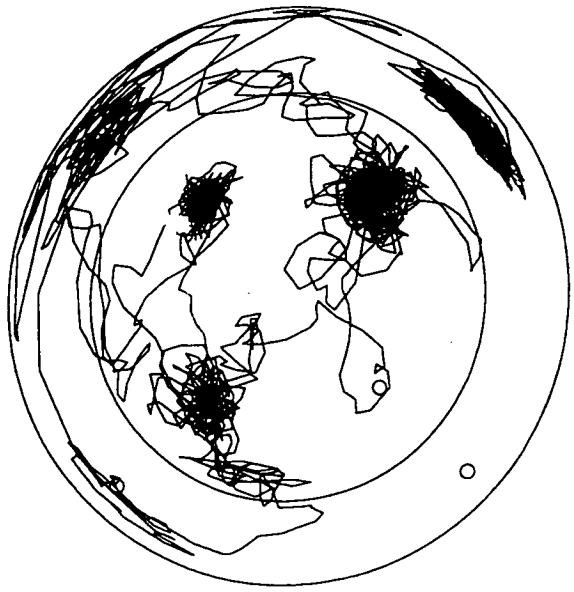

Figure 4.8. Orientational trajectory.

At 380K the groups of dots in the o.d.f.s are more diffuse but still tetragonally distributed. In the cage diagram at the same temperature there are molecules at the top right and bottom left which are no longer aligned with the others and are most probably reorienting. The o.d.f. at 440K shows that the 3-fold symmetry axes of the molecules are aligned with the [111] directions of the now cubic unit cell. Most points lie near the [111] directions, so molecules prefer to occupy either the up or the down orientation, but some points lie outside the large groups indicating that some molecules are reorienting. In Figure 4.7 an up orientation has molecular 3-fold axes aligned with the [111] and $[\bar{1}\bar{1}1]$ unit cell axes (in Figure 4.6 the top edge of the tetrahedron is aligned top left to bottom right) and a down orientation is rotated by 90° about the c-axis with respect to the up so that the molecular 3-folds are aligned with $[1\bar{1}1]$ and $[\bar{1}11]$ directions in the unit cell. No ordered pattern of up and down orientations can be seen, so the solid is now orientationally disordered. The transition from tetragonal

to cubic is therefore also a disordering transition. The unit cell is face-centred cubic. A molecule at any position can be in an up or in a down orientation; no distinction can be made between the orientations of molecules in the unit cell, so the space group is $Fm3m$, as found experimentally.

If we examine the orientational trajectory of a molecule (Figure 4.8) we can see that the molecular 3-fold axis spends most time aligned with one of the [111] directions, but occasionally makes a reorientational jump to align with another [111] direction. In the disordering transition a molecule can make multiple reorientational jumps, rather than a single jump to a different orientation in which it then remains. By comparing the o.d.f. at 500K to that at 440K we can see more evidence of molecules reorienting (more points in the o.d.f. are outwith the large groupings). The cubic phase is therefore a plastic phase.

The simulation has successfully reproduced the low temperature ordering, the order-disorder transition and the plastic phase observed experimentally. An expansion along the c-axis of the cell occurs above 380K accompanied by molecular reorientation and thereby a loss of orientational order. At 420K the unit cell is cubic and has lost the long range orientational order of the tetragonal phase; the ensemble is then in a plastic phase. The tetragonal to cubic transition occurs between 400K and 420K in this simulation. Ciccotti *et al.* [57] performing a molecular dynamics simulation on 2×2×2 unit cells with 32 molecules, using the unaltered Williams potential, found that the cell did not become cubic until 400K, close to our result.

4.4.2 Recooling

The simulation was continued by cooling the same ensemble from 500K back to the starting temperature of 140K, in reductions of 20K. The potential, volume and lattice parameters measured on cooling are shown in Figures 4.5(a,b,d). Above 380K the values measured on cooling match those on heating. Below 380K the values on cooling

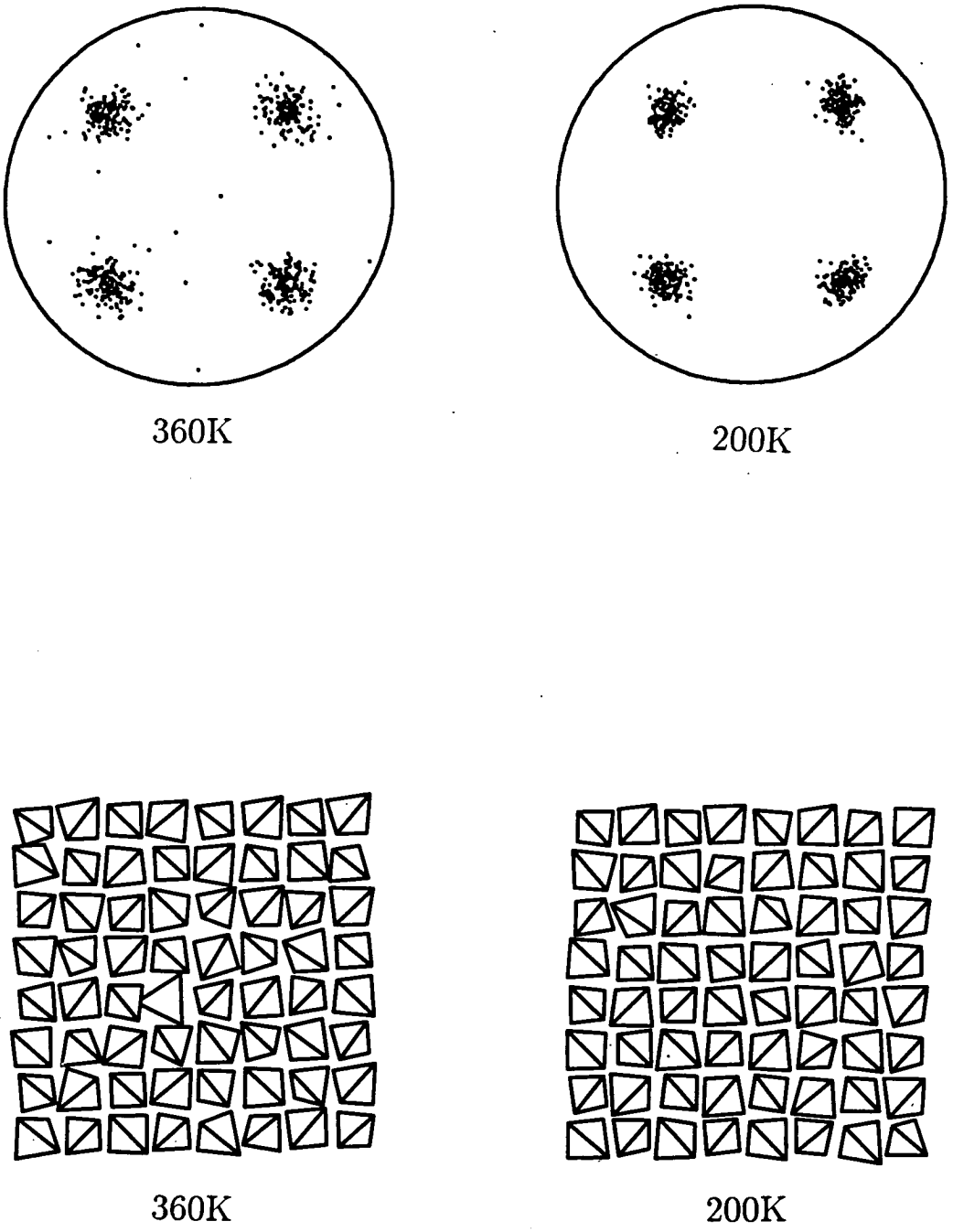

Figure 4.9. O.d.f.s and *ab* plane centre-section at 360K and 200K on cooling.

are consistently above those on heating and show a constant rate of change with temperature. All the lattice parameters retain values in proximity to each other; the unit cell remains cubic and the tetragonal phase is not regained.

In Figure 4.9, at 360K, the molecular orientations retain the up and down orientations, and reorientations can still be observed below the order-disorder transition temperature. The o.d.f. remains consistent with cubic ordering. When cooled to 200K there are no signs of reorientation in Figure 4.9. From the o.d.f., the orientational alignments remain cubic; the cage diagram shows no apparent pattern to the arrangement of up and down orientations suggesting the ensemble is orientationally disordered. The low temperature unit is still consistent with a $Fm3m$ space group.

This result is not consistent with experiments which show the order-disorder transition to be reversible. Further investigation is required to find why the reverse transition does not occur in the molecular dynamics simulation.

4.4.3 Finite-size effects

In the simulation of the transition from the ordered tetragonal to the cubic plastic phase the transition temperature was found to be between 400K and 420K, about 200K higher than observed experimentally. This could be an artefact of the simulation, since with a relatively small ensemble the application of periodic boundary conditions can suppress a phase transition. If this is the case then a simulation on a larger ensemble should produce a lower transition temperature. In a very large ensemble, where the number of molecules is close to the size of a bulk sample (over 10,000) then the transition temperature should be close to that found in experiment, assuming that the potential used accurately represents molecular interactions. A prohibitive amount of computer time would be required to perform a simulation on a larger ensemble with the same exactitude as the simulation discussed above. However, it is possible to simulate the transition in a smaller ensemble. If finite-size effects are significant, the transition temperature should be higher in the smaller ensemble.

A simulation was performed on 2×2×2 unit cells, containing 32 molecules, with the same initial configuration as described in Section 4.2 for 256 molecules. The ensemble was brought to equilibrium over 10,000 steps with a time-step of 0.02ps, at 200K. The temperature was then increased in 20K intervals and equilibrium re-established over 5000 steps, with the same time-step.

Figures 4.10(a,b,c) show the average values for the volume per molecule, potential energy per molecule and lattice parameters of the unit cell against temperature, on heating. The first observation to be made is that the errors estimated in the parameters measured are greater than the errors measured by the same method for 256 molecules. This is to be expected since the size of thermal fluctuations in volume potential are related to the factor $\sqrt{N}/N$. Both volume and potential show steepening increases with temperature. Examining the changes in the lattice parameters on heating, in Figure 4.10(c), we can see that the c parameter rises steeply above 380K. At 440K the a, b and c parameters all have similar values. The transition from a tetragonal to a cubic unit cell occurs between 420K and 440K.

Figure 4.11 shows the o.d.f.s and the molecules in the central ab planes for the ensemble equilibrated at 200K and above the phase transition at 460K. At 200K the tetragonal ordering is the same as for the larger simulation (*cf.* Figures 4.6 and 4.7). At 460K the o.d.f. shows alignments of the 3-fold symmetry axes of the molecules with the cubic [111] directions, while the cage diagram shows evidence of the loss of orientational order and of molecules reorienting. As in the 256 molecule simulation, the cubic phase is a plastic phase.

From the analysis we can state that the transition from the tetragonal to the cubic plastic phase in the 32 molecule ensemble occurs between 420K and 440K, compared with the 256 molecule ensemble in which this transition occurs between 400K and 420K. The conjecture that the transition temperature will rise if the size of the ensemble is reduced appears to be correct. From this result it can be inferred that an increase in the size of an ensemble should decrease the transition temperature. It is doubtful

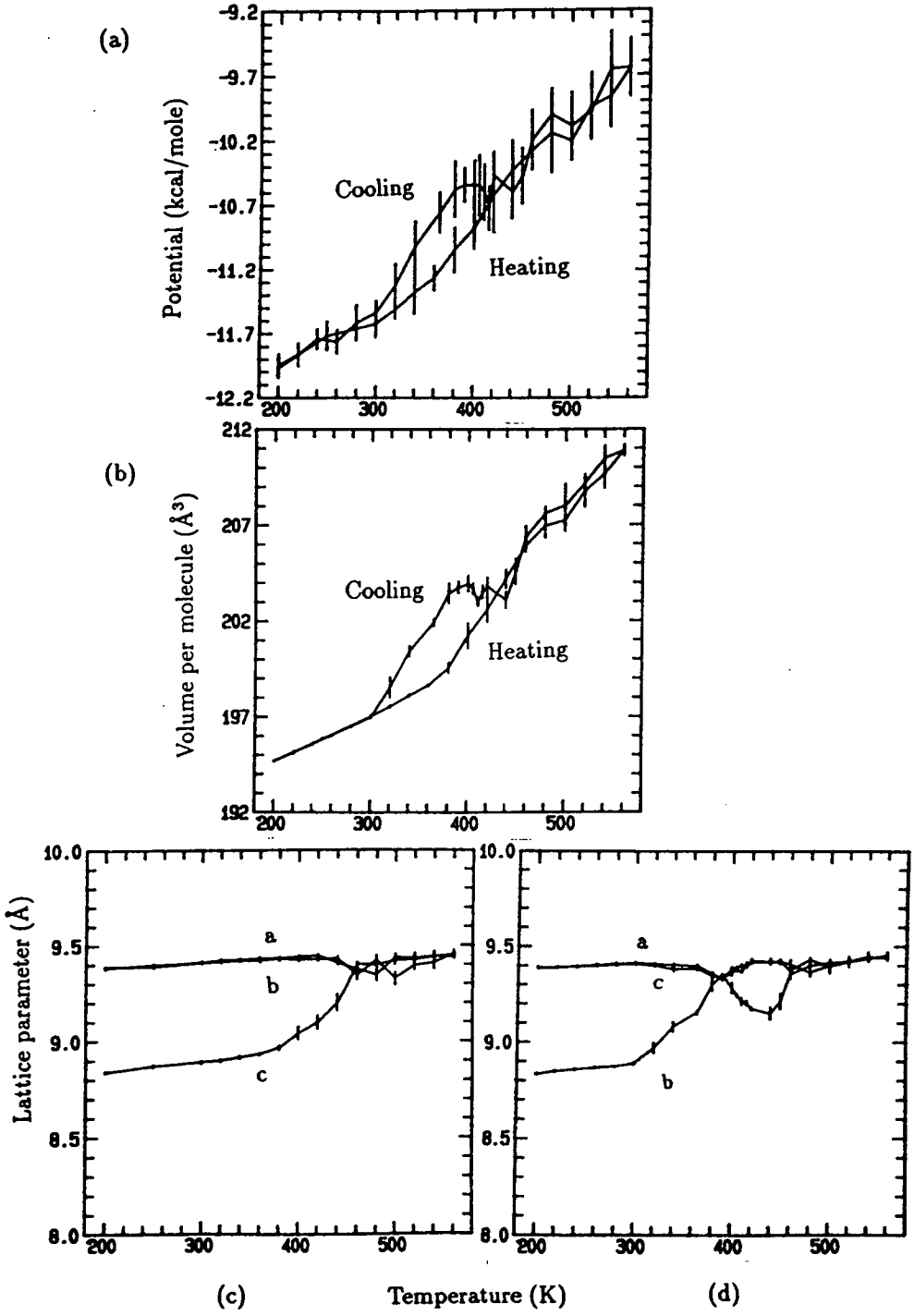

Figure 4.10. (a) Potential (b) Volume and lattice parameters (c) on heating (d) on cooling, for 32 molecules.

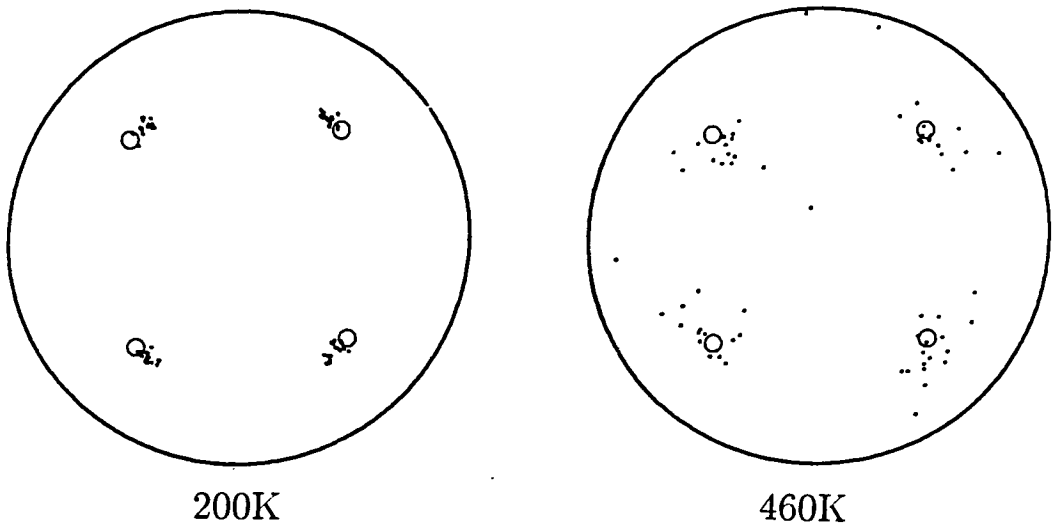

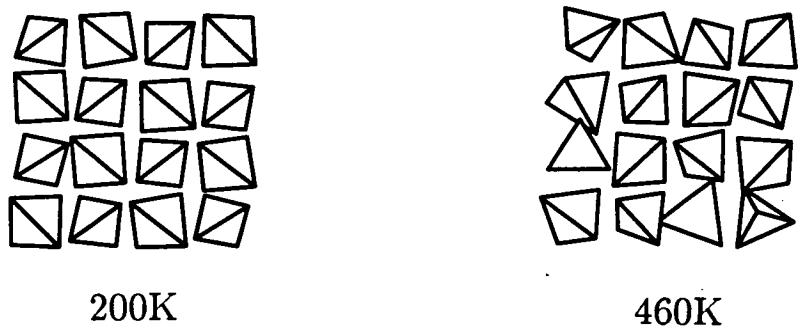

Figure 4.11. O.d.f.s and *ab* plane centre-section at 200K and 460K on heating, for 32 molecules.

that finite-size effects alone could account for the difference of over 200K between the transition temperatures in experiment and by simulation. If we wish to more closely match the experimental transition temperature, a rescaling of the energy parameters of the Williams potential would be required. By rescaling, the rate of thermal expansion would be increased, so that the transition from a tetragonal to cubic phase would occur at a lower temperature, and the potential barrier to molecular reorientation would be decreased, so molecular reorientations would also occur at a lower temperature.

It is also of interest to examine any finite-size effects on recooling the smaller ensemble. Starting from the cubic plastic phase ensemble at 560K, the temperature of the ensemble was decreased in 20K steps, or in 10K steps in temperature regions of interest. The equilibration procedure was the same as that used on heating. Above the order-disorder transition temperature of 440K, the average potential and volume per molecule recorded on cooling (Figures 4.10(a,b)) are similar, within error bounds, to the values recorded on heating. Between 440K and 300K, both potential and volume are greater than the values recorded on heating, but show a steep decline below 380K. Below 300K, the values of the volumes recorded on heating and cooling are almost exactly matched and the values for potential are similar within errors.

At all temperatures on cooling the a and c lattice parameters, (Figure 4.10(d)) consistently match each other and are similar to the values of the a and b lattice parameters recorded on heating. Below 480K, the b lattice parameter drops steeply from its value in the cubic phase, reaching a minimum at 440K, then increasing to once again to match the values of the a and c lattice parameters at 380K. Below 380K the b lattice parameter drops steeply once again levelling off at 300K, below which temperature it matches the values for the c lattice parameter recorded on heating. The shape of the unit cell therefore fluctuates between cubic and tetragonal down to 300K. Below 300K the tetragonal unit cell remained stable. The b-axis is now unique axis as the c-axis was for the initial unit cell.

In Figure 4.12 the o.d.f. has been constructed in the [010] direction and the cage

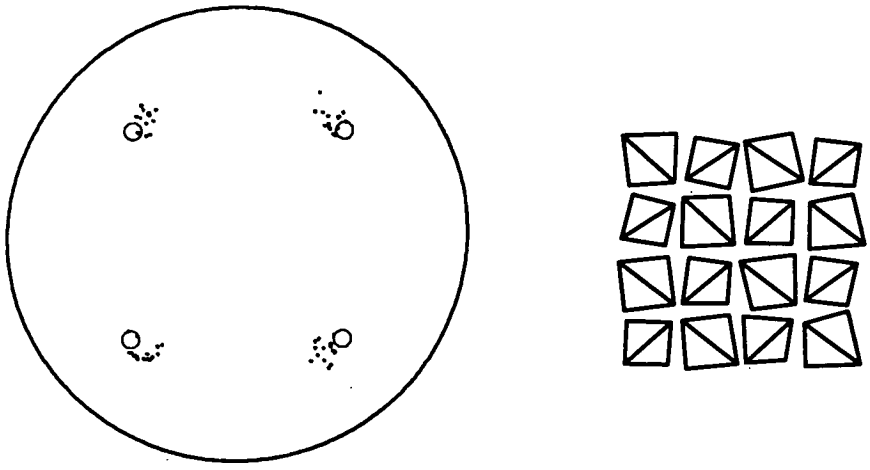

Figure 4.12. O.d.f. in [010] direction and centre-section in *ac* plane at 200K on cooling.

diagram shows *ac* planes, so that these figures are consistent with the direction of the unique axis. Both the o.d.f. and cage diagram are consistent with the ordering of the initial unit cell (Figure 4.11). The change in direction of the unique axis is acceptable, because the ensemble was returned to a tetragonal phase from a cubic phase in which the *a*, *b* and *c* directions are all equivalent so that any of these axes can become the unique axis when the ensemble passes through the reverse transition.

The order-disorder transition in the simulation of 32 molecule ensemble is reversible. Both the potential and volume in Figures 4.10(a,b) suggest hysteresis between the values recorded on heating and cooling. Hysteresis is often indicative of a first-order phase transition, but it is difficult to state this for certain since such a small ensemble is used. The reverse transition appeared to be completed at 300K, but a tetragonal phase was also approached near 440K, the transition temperature on heating. In a small ensemble such as this any fluctuation in the cell is more significant than for a larger ensemble and a single change of a molecular orientation can affect the overall order of the entire ensemble. It is possible therefore that the ordered tetragonal phase

was reforming at 440K but was disrupted by fluctuations in the ensemble such that the cubic phase was briefly re-entered.

The phase transition in the 32 molecule ensemble was reversible, whereas in the 256 molecule ensemble the phase transition could not be reversed in the simulation performed upon it. The difference in behaviour between these ensembles may be described as a finite-size effect. Why this effect occurs could be of considerable interest, but before an explanation can be proffered a more detailed examination of the disordering transition is required.

4.5 Reorientations

4.5.1 A model for reorientations

From initial investigations in the plastic phase it is clear that molecules make reorientational jumps between distinct orientations (*q.v.* Figure 4.8). Such a reorientation can be between an up and a down orientation or between symmetrically equivalent up or down orientations. In Section4.1 the up and down orientations were defined in terms of the alignment of molecular 3-fold symmetry axes and the [111] directions of the cubic unit cell. This alignment can be used to algorithmically define the orientation of a molecule.

In Figure 4.13(a), imagine that the faces of the cube are parallel to Cartesian axes so that the back top right-hand vertex of the cube has the co-ordinate $(1, 1, 1)$. The dashed tetrahedron has the 3-fold symmetry axis from its centre through the vertex at $(1, 1, 1)$ aligned with the [111] axis of the cube and the 3-fold through the vertex (-1,-1,1) with the $[\bar{1}\bar{1}1]$ axis of the cube. The alignment of these axes uniquely defines this particular (up) orientation of the tetrahedron.

By studying Figure 4.13(a) it is possible to see what rotations relate the various orientations of the molecule. For example, if the tetrahedron is rotated by 90° anticlockwise about the [001] axis then the 3-fold through $(1, 1, 1)$ is now aligned with the

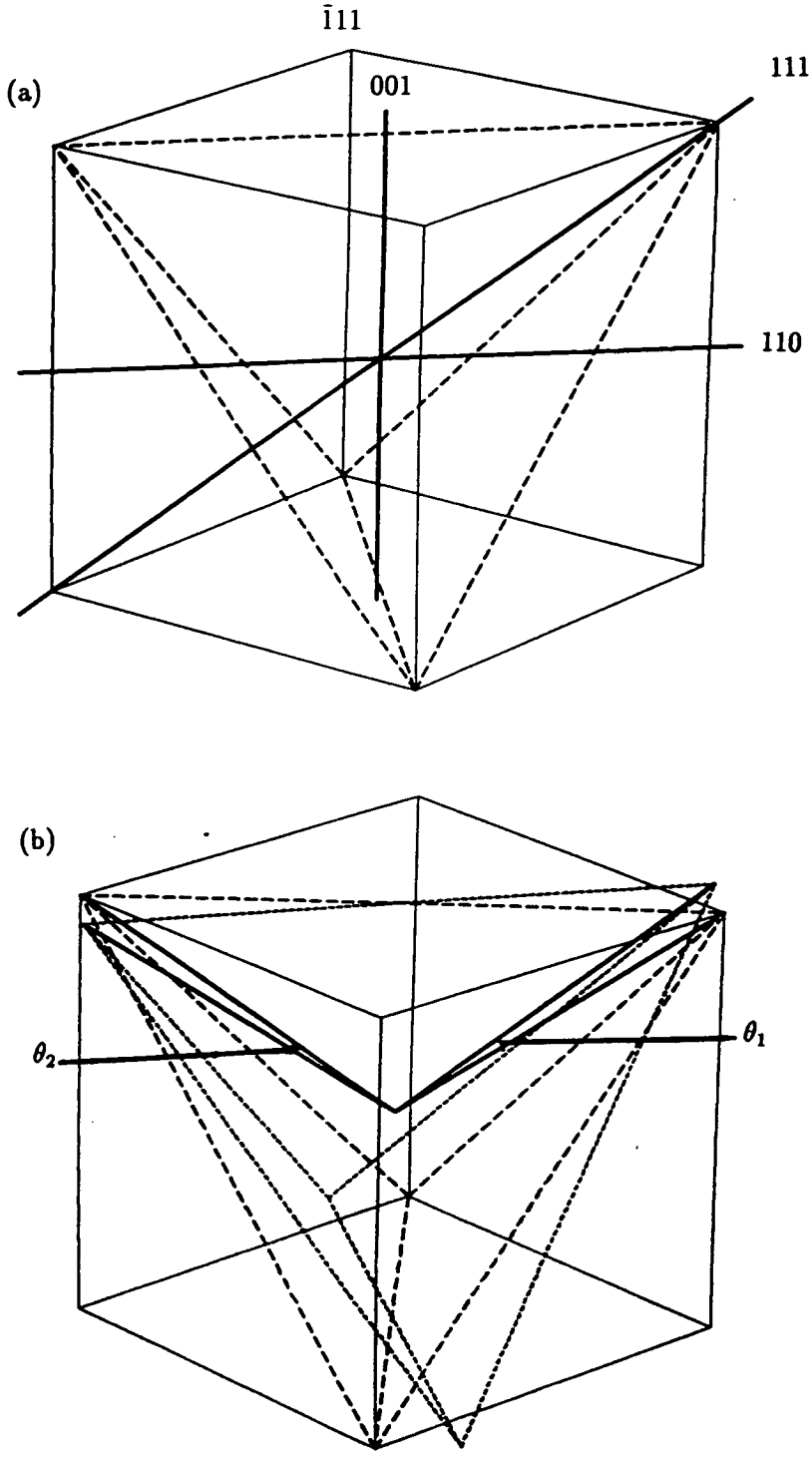

Figure 4.13. (a) tetrahedron in cube (b) slightly rotated tetrahedra.

[$\bar{1}11$] axis of the cube and the 3-fold through (-1,-1,1) with the [$1\bar{1}1$] axis of the cube; the tetrahedron is now in an inverted (down) orientation. If the tetrahedron is rotated by 120° about the [1, 1, 1] axis then the 3-fold through (1,1,1) obviously remains aligned with the [111] axis of the cube whilst the 3-fold through (-1,-1,1) is now aligned with the [$1\bar{1}\bar{1}$] axis of the cube. Under this rotation the molecule retains its up orientation but with 3-fold axes aligned with different [111] directions compared to its starting position.

If the tetrahedron in Figure 4.13(a) is the reference orientation, the orientation of a molecule may be described by the orientation of the two vertices which have position vectors $\vec{V}_{01}(1,1,1)$ and $\vec{V}_{02}$(1,-1,-1) for the unrotated tetrahedron. For a rotated molecule the position of the vertices $\vec{V}_{01}$ and $\vec{V}_{02}$ can be found from the transform matrix, T, derived from the quaternion of that molecule using (1.19). The transformed position vectors are $\vec{V}_1 = T\vec{V}_{01}$ and $\vec{V}_2 = T\vec{V}_{02}$.

Whether the molecule is in an up or down orientation can be defined by the particular cubic [111] directions with which $\vec{V}_1$ and $\vec{V}_2$ are aligned most closely. The position vectors for the cubic [111] directions associated with an up orientation are $\vec{A}_1$=(1,1,1), $\vec{A}_2$=(-1,-1,1), $\vec{A}_3$=(1,-1,-1) and $\vec{A}_4$=(-1,1,-1) and those associated with a down orientation are $\vec{A}_5$=(-1,-1,-1), $\vec{A}_6$=(1,1,-1), $\vec{A}_7$=(-1,1,1) and $\vec{A}_8$=(1,-1,1). If we take the dot products of $\vec{V}_1$ and the vectors $\vec{A}_{1...8}$ then $\vec{V}_1$ is most closely aligned to the [111] direction for which the angle between the vectors, θ_1, is a minimum, *i.e.*

$$\theta_1 = \min\left[\cos^{-1}\frac{\vec{V}_1 \cdot \vec{A}_i}{|\vec{V}_1||\vec{A}_i|}\right] \qquad i = 1...8. \tag{4.2}$$

If θ_1 is minimum for any $\vec{A}_i$ associated with an up orientation (i = 1...4) then the molecule can only be in an up orientation; conversely if θ_1 is minimum for any $\vec{A}_i$ associated with a down orientation (i = 5...8) then the molecule can only be in a down orientation. The orientation of a molecule is then uniquely defined by considering the

alignment of $\vec{V}_2$. The angle between $\vec{V}_2$ and the remaining possible [111] directions is

$$\theta_2 = \min\left[\cos^{-1}\frac{\vec{V}_2 \cdot \vec{A}_j}{\mid \vec{V}_2 \mid\mid \vec{A}_j \mid}\right] \qquad j \leq 4 \text{ if } i \leq 4, j \geq 5 \text{ if } i \geq 5, j \neq i \quad (4.3)$$

thus defining the alignment of $\vec{V}_2$. Using this method of defining orientations there will be six symmetrically equivalent descriptions of the up and of the down orientation, because the definition depends on uniquely choosing with which two out of a possible four directions a molecule is aligned.

To allow for a certain amount of orientational fluctuation away from an exact up or down orientation a molecule is defined to occupy a particular orientation only if the values of both θ_1 and θ_2 are less than 15° [59]. The choice of angle is arbitrary, but the angle must not be too large, as the definition would not be rigorous, nor too small, as normal thermal displacements of a molecule would cause spurious reorientations to be recorded. The angles θ_1 and θ_2 are determined for each molecule on each time-step. If either of θ_1 or θ_2 is greater than 15° then the molecule is considered to be reorienting. The reorientation is complete when both angles are again less than 15° for a certain orientation.

4.5.2 The Order-disorder Transition

We shall now use the model for the reorientation of adamantane molecules to re-examine the order-disorder phase transition in the 256 molecule ensemble. Figure 4.14(a) shows the average number of reorientations per picosecond recorded on heating, measured over 50ps of simulation time at each temperature. No reorientations are recorded up to 360K. At 380K a few reorientations are observed at a rate of 0.24ps^{-1} increasing to 0.94ps^{-1} at 400K. At 420K there is a considerable increase in reorientation rate to 3.96ps^{-1}. The reorientation rate continues to increase steeply as temperature rises.

If the orientation which a molecule occupies is totally random then any molecule

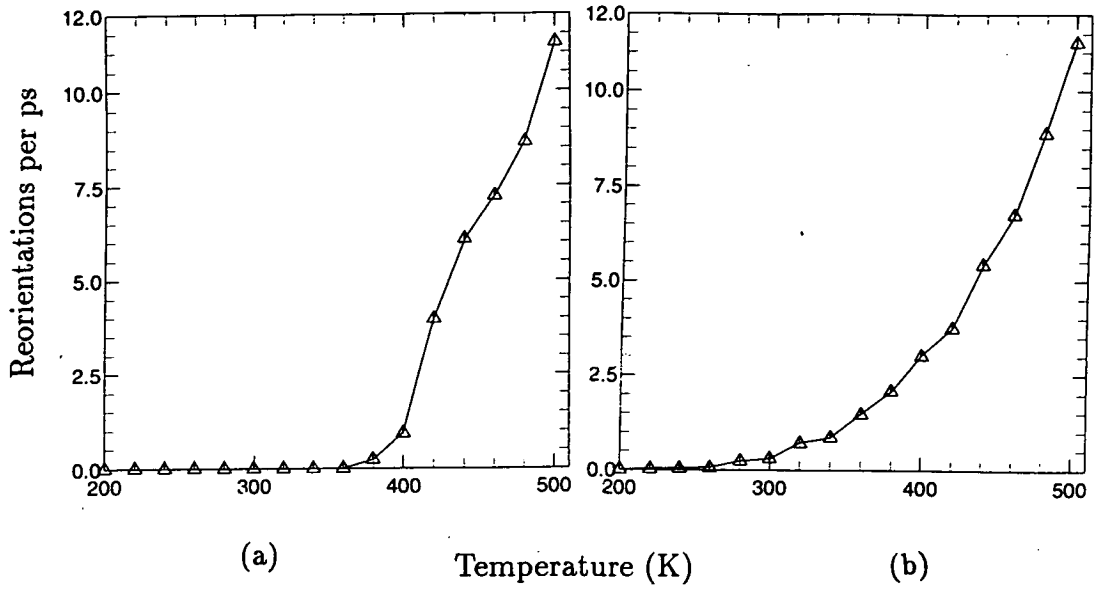

Figure 4.14. Number of reorientations recorded on (a) heating and (b) cooling.

would have equal probability of being in an up or a down orientation; on average half the molecules would occupy the up orientation and the other half the down orientation. Table 4.3 shows the occupation of the up and down orientations on heating, averaged on every tenth step over 2500 steps. Since there are only two possible orientations we may expect a Gaussian (normal) distribution for the number molecules occupying a particular orientation, the mean of which would be 128 and the standard deviation of which is given by $\sigma = \sqrt{Np(1-p)}$ where p=0.5 is the probability of a particular molecule being in an up or a down orientation and N=256×250 is the sample size used to calculate the values in Table 4.3; as a percentage σ=0.22%. The values for average occupation at all temperatures show a higher occupation of the down orientation than the up; in most cases the deviation of the down orientation from 50% is greater than the standard deviation for a entirely random distribution of orientations. This suggests some short-range order may persist in the plastic phase.

Temp.(K)	Up	%	Down	%	Temp.(K)	Up	%	Down	%
380	126.2	49.3	129.8	50.7	460	125.4	48.9	130.8	51.1
400	127.9	50.0	128.1	50.0	480	125.3	48.9	130.7	51.1
420	125.1	48.9	130.7	51.1	500	126.3	49.3	129.7	50.7
440	121.7	47.5	134.3	52.5					

Table 4.3. Average occupation of up and down orientations on heating.

Any short-range order would be signified by a correlation of the orientations occupied by neighbouring molecules, thus we shall define an **orientational correlation function (o.c.f.)**. By analogy with spin in an Ising model, a molecule in an up orientation is assigned a value of $s = +1$ and a molecule in a down orientation a value of $s = -1$. If we now consider a molecule i and its j nearest neighbours on the face-centred cubic lattice, so that $j = 1...12$, then the orientational correlation of that molecule is defined as

$$O_i = \sum_{j=1}^{12} s_i s_j \qquad s_{i,j} = \pm 1. \tag{4.4}$$

The range of values of orientational correlation are from -12 (all neighbours in different orientations) increasing in steps of 2 to the maximum value of 12 (all neighbours in the same orientation). The orientational correlation function is the probability distribution of the orientational correlations of all the molecules in the ensemble. This is determined by counting how many of the molecules have each of the 13 possible values of orientational correlation. Since there are only 256 molecules in the ensemble, and the change of orientations is highly dynamical, the o.c.f. was calculated on every tenth step over 2500 steps and a time averaged o.c.f. calculated for the equilibrated ensemble. The maximum possible value of the o.c.f. can of course only be as large as the total number of molecules. We shall use an o.c.f. normalised by dividing by the total number of molecules, so that the value of the o.c.f. gives the fraction of all molecules

with a particular orientational correlation.

In the ordered phase all molecules have eight of their twelve neighbours in inverse orientations and the other four in the same orientation; the orientational correlation of all molecules is therefore -4. The o.c.f. for the ordered ensemble consists of a delta function at -4. The loss of orientational order at the phase transition can be seen from the o.c.f.s in Figure 4.15. At 380K the few reorientations which occur produce some local disorder, evident from the decay of the peak at -4. At 400K the sharp peak at -4 has further decayed. At 420K, in the plastic phase, the o.c.f. is broader and now peaks at -2. Were the orientations adopted by the molecules in the plastic phase to be entirely random, the mean configuration of a molecule and its neighbours would have six in the same orientation and six in the inverse orientation; the o.c.f. would show a Gaussian distribution centred on 0. Since the o.c.f. peaks at -2, the correlation of neighbouring molecules is not entirely random, thus short-range order must persist in the plastic phase, when long-range order has been lost.

The o.c.f. at 500K is still slightly peaked at -2 but with values of 0.248 at -2 and 0.240 at 0, compared to values of 0.271 at -2 and 0.249 at 0 at 420K. Further heating therefore causes a shift of the o.c.f. towards 0. As temperature increases the increased rotational kinetic energy of the molecules and the lowering of the potential barrier to reorientation as the cell expands leads to a rise in the reorientation rate. The molecules reorientate so frequently they are beginning to act like rotators, the correlation between neighbouring molecules is lost and the o.c.f. shifts towards a random distribution.

4.5.3 Recooling

The average number of reorientations per picosecond recorded at temperatures on cooling are shown in Figure 4.14(b). Above 400K, in the plastic phase, reorientation rates are in agreement with those measured on heating. At 400K and 380K, the reorientation rates are 1.48ps^{-1} and 0.86ps^{-1} respectively, significantly larger than the rates measured at the same temperatures on heating. Unlike on heating, reorientations are

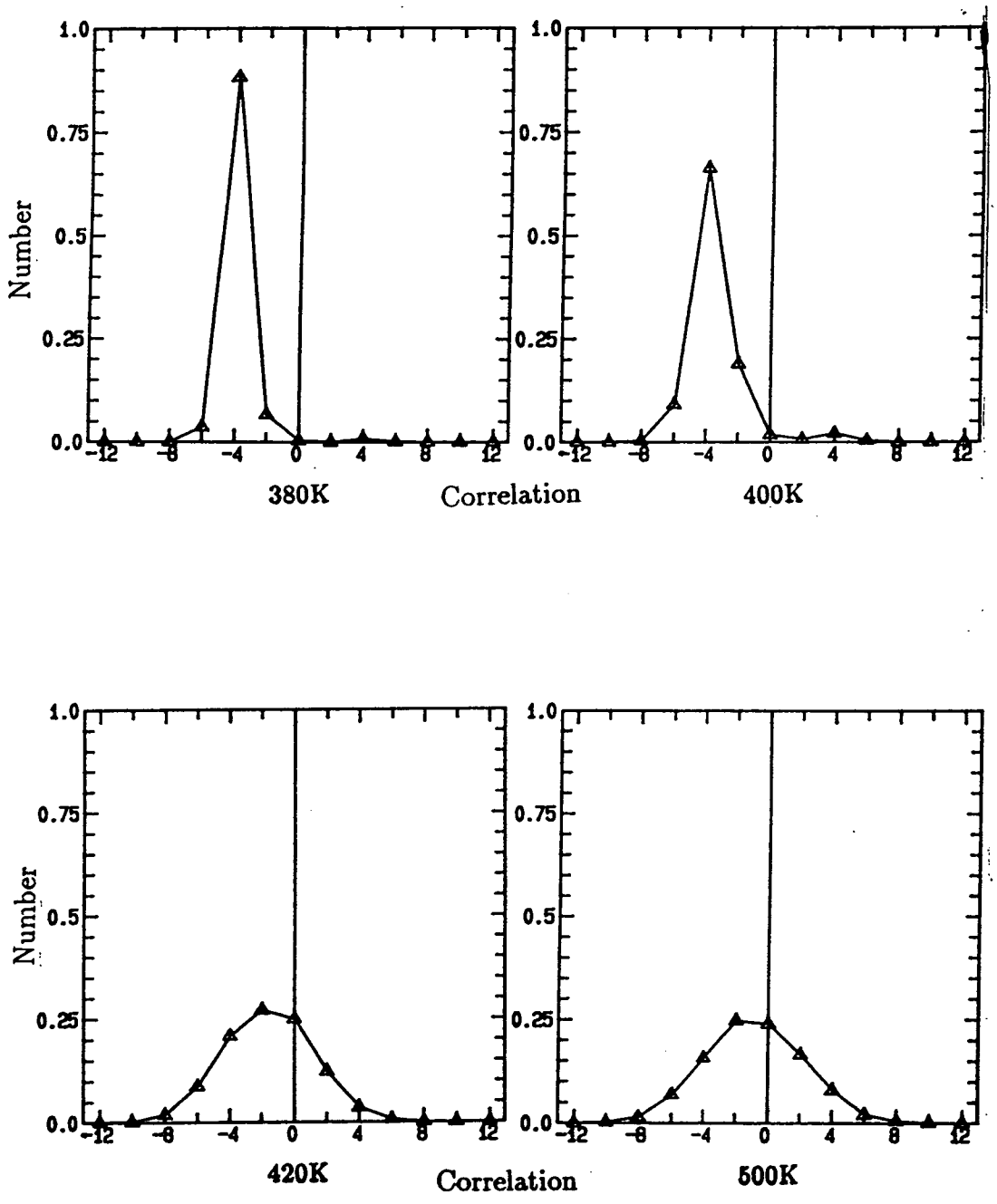

Figure 4.15. O.c.f. at 380K, 400K, 420K and 500K on heating.

Temp.(K)	Up	%	Down	%	Temp.(K)	Up	%	Down	%
500	126.6	49.5	129.4	50.5	340	131.4	51.3	124.6	48.7
480	135.3	52.9	120.7	47.1	320	126.2	49.3	129.8	52.1
460	122.2	47.7	133.8	52.3	300	120.7	47.1	135.3	52.9
440	129.1	50.4	126.9	49.6	280	131.5	51.4	124.5	48.6
420	127.1	49.6	128.9	51.5	260	133.0	52.0	123.0	48.0
400	124.1	48.5	131.9	51.5	240	130.0	50.8	126.0	49.2
380	127.8	49.9	128.2	50.1	220	129.0	50.4	127.0	49.6
360	130.2	50.9	125.8	49.1	200	129.0	50.4	127.0	49.6

Table 4.4. Average occupation of up and down orientations on cooling.

observed below 380K, in small and decreasing numbers, down to 220K. At 220K only four reorientations are recorded in 150ps of simulation time; at 200K no reorientations are observed over the same time.

In Table 4.4 the average occupation of the up and the down orientation on recooling are given. The orientation with the highest occupation fluctuates between up and down as temperature is reduced to 280K, below which temperature the up orientation retains the highest occupancy. On heating (Table 4.4) the down orientation always had a higher occupancy than the up orientation, however, on cooling the up orientation has the higher occupancy below 280K suggesting the localised order does not require the down orientation to be favoured, but rather that, over the time of measurement, one orientation is slightly favoured over the other. Below 280K the frequency of reorientation events has declined to the extent that the fluctuation between higher occupancy of up or down no longer occurs; the reorientational motions of molecules are beginning to freeze out. At 220K the average occupation of the up orientation is exactly 129 molecules and remains the same at 200K; the orientational freezing transition has occurred and there is no further change in the orientation of any of the molecules.

It was shown above that the ordered tetragonal phase is not regained on cooling from the plastic phase. Since reorientations are observed down to 220K, and the unit cell remains close to cubic, it can be argued that the ensemble remains in the plastic phase.

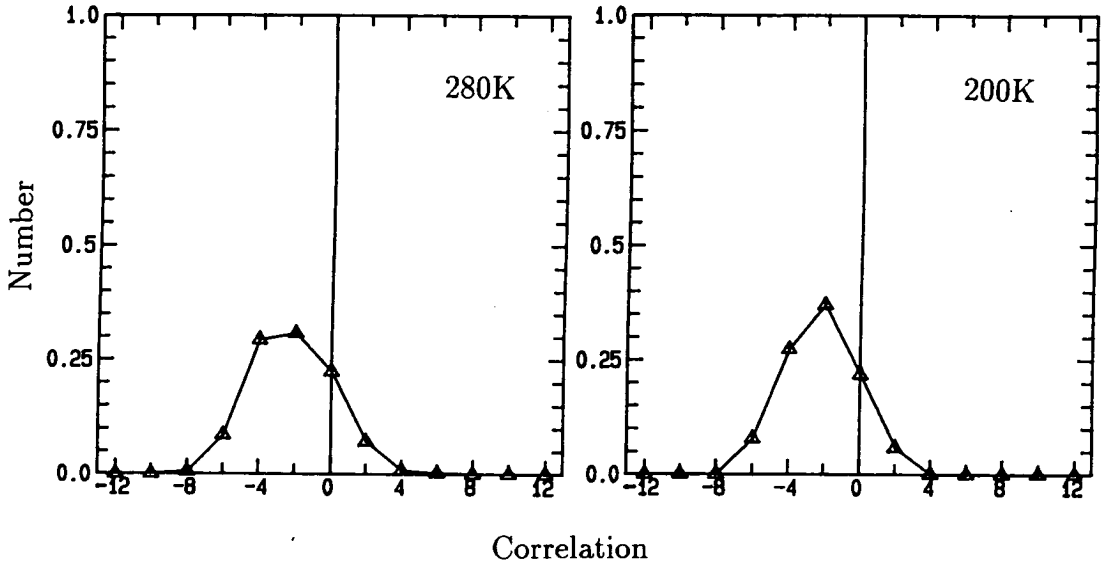

Figure 4.16. O.c.f. at 280K and 200K on cooling.

In Figure 4.16 the o.c.f. at 280K is peaked at -2 showing that localised orientational order is present in the recooled ensemble. On cooling to 200K the peak at -2 has sharpened, but there is no immediate evidence of a shift of the peak to the ordered correlation at -4.

4.6 An Order-disorder Transition using Monte Carlo

In the discussion of the molecular dynamics simulation we have used the nomenclature of Ising models in discussing the orientational phase transition of adamantane. In both the ordered and disordered phase of adamantane the molecules are most likely to occupy one of two orientations, these orientations being symmetrically inverse. In the Ising model of an anti-ferromagnet there is a transition from a lowest energy state, which involves an ordered configuration of up and down spins, to a state where the

arrangements of up and down spins becomes disordered. A model for adamantane will now be constructed based on the anti-ferromagnetic Ising model on a face-centred cubic lattice, and the order-disorder transition simulated using a Monte Carlo method. As might be expected, anti-ferromagnetic behaviour on a face-centred cubic lattice has been studied previously, first by Danelian [60] who studied the theory of the system based on the partition function. The system was later studied using Monte Carlo methods [61, 62], with applications to magnetic materials such as EuTe [63] and frustrated binary alloys [64]. None of the published work is general enough to be reassessed in terms of adamantane, hence new simulations will be performed so that analysis similar to that applied to the molecular dynamics simulations may be used.

4.6.1 Simulation Details

In the Monte Carlo model for adamantane only the orientational order-disorder transition will be considered. The molecular centres remain fixed on face-centred cubic lattice sites and the lattice parameter remains constant at a=9.333Å; the tetragonal to cubic transition is not included in the model. The molecules are restricted to be in only two possible orientations, the exact up and down orientations in the plastic phase as described in Section 4.1. The potential energy of interaction of a pair of molecules on nearest neighbour lattice sites will depend only on whether they are in the same or inverse orientations. The Williams potential with modified parameters is used to calculate the energy between nearest neighbour molecules on the lattice. Only two values of energy need be considered. Again using s=+1 for the up orientation and s=-1 for the down orientation, the energy of interaction $\mathcal{E}(s_i, s_j)$ for neighbouring molecules is

$$\mathcal{E}(+1,+1) = \mathcal{E}(-1,-1) = -1.68929\text{kcal/mole}$$

when both molecules have the same orientation and

$$\mathcal{E}(+1,-1) = \mathcal{E}(-1,+1) = -2.40291\text{kcal/mole}.$$

when the molecules have inverse orientations. The expression for the total energy of the ensemble is then

$$E = \sum_{i=1}^{N} \sum_{j=1}^{12} \mathcal{E}(s_i, s_j) \tag{4.5}$$

where 12 is the number of nearest neighbours on a face-centred cubic lattice.

The lowest energy state of the ensemble has the molecules on (0,0,0) and ($\frac{1}{2}$,$\frac{1}{2}$,0) lattice sites in up orientations and those on ($\frac{1}{2}$,0,$\frac{1}{2}$) and (0,$\frac{1}{2}$,$\frac{1}{2}$) lattice sites in down orientations, which is as close to the ordered tetragonal structure as the model allows. The simulations begin from an ensemble in the lowest energy state.

Changes in spin occupancy as temperature is changed are decided by means of the well-known Metropolis algorithm [1]. A 'sweep' of the ensemble is performed in which each spin is inverted in turn and the change in the total energy of the ensemble calculated, $\Delta E = E_n - E_{n-1}$, where E_n is the current total energy on the n^{th} sweep and E_{n-1} is the energy at the end of the previous sweep. If ΔE is negative, the energy of the ensemble has been lowered to a more energetically favourable state and consequently the change of the individual spin state is accepted; the change of that spin state has probability $p = 1$. If ΔE is positive then the probability of changing the spin state is calculated as

$$p = e^{-\frac{\Delta E}{k_b T}} \tag{4.6}$$

where T is the thermodynamic temperature of the ensemble and k_b the Boltzmann constant. As $T \to \infty$, $p \to 1$. A random number between 0 and 1, r, is generated; if

$p < r$ the change of spin state is rejected; if $p > r$ the change of spin state is accepted. This method allows less favoured energetic states to be reached, the probability of this happening increasing with temperature.

The main discussion of the Monte Carlo simulation will be based on an ensemble of 4×4×4 unit cells containing 256 molecules, so that a direct comparison in size with the 256 molecule molecular dynamics simulation can be made. Simulations on ensembles with 6×6×6 unit cells containing 864 molecules and 8×8×8 unit cells containing 2048 molecules are also performed so that finite size effects may be examined. At each temperature, 40,000 sweeps are performed to equilibrate the ensemble. The average total energy, with standard deviation as error, and the average normalised o.c.f. are then calculated over another 10,000 sweeps. The o.c.f. is the same as that defined previously (p.83).

4.6.2 The order-disorder transition

Figure 4.17 shows the average potential recorded at temperatures increasing in 10K steps, for the 256 molecule ensemble. Between 300K and 360K the potential rises steeply. Since the ensemble starts from a minimum energy state which is ordered as described above, the rise in potential must signify transition in the orientational order. The transition temperature may be defined as the midpoint of the range over which the potential rises steeply, *i.e.* 330K.

It may be helpful if first we can visualise the phase transition. Figure 4.18, like the earlier cage diagrams, shows two overlying *ab* planes viewed down the *c*-axis, with up oriented molecules represented by white squares and down oriented molecules represented by black squares. Remembering that this is a face-centred cubic lattice, in the initial configuration at 140K one layer has all its molecules in up orientations and the next has all its molecules in down orientations, giving the ordered structure a 'chess board' pattern. At 310K, below the transition temperature, the majority of that part of the ensemble shown in Figure 4.18 still shows the ordered pattern, but there are now

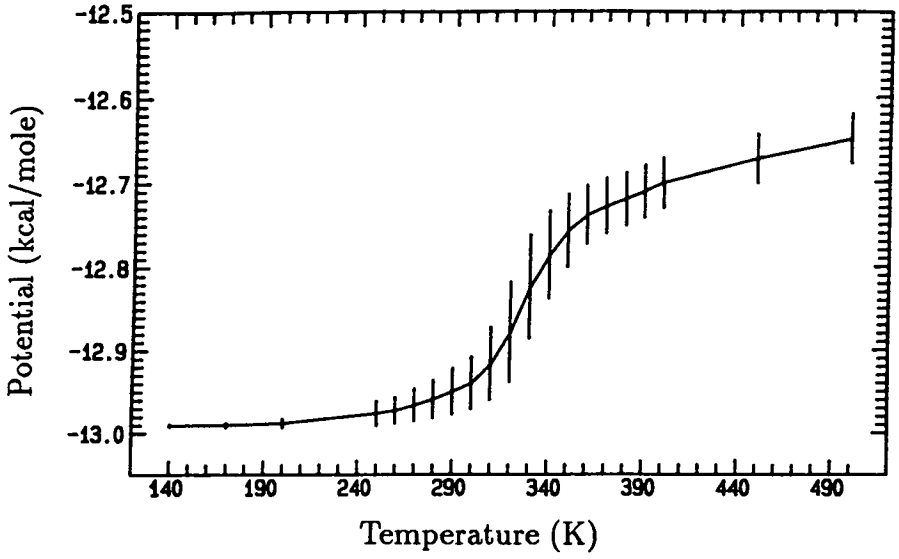

Figure 4.17. Average potential for 256 molecules on heating.

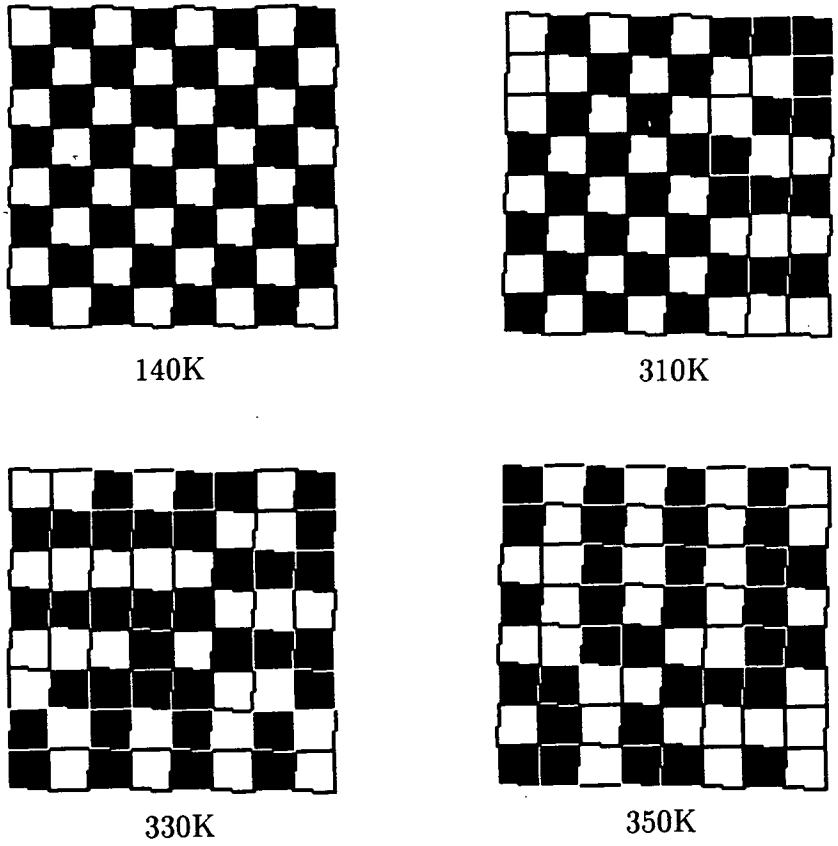

Figure 4.18. The Monte Carlo ensemble at 140K, 310K, 330K and 350K, on heating.

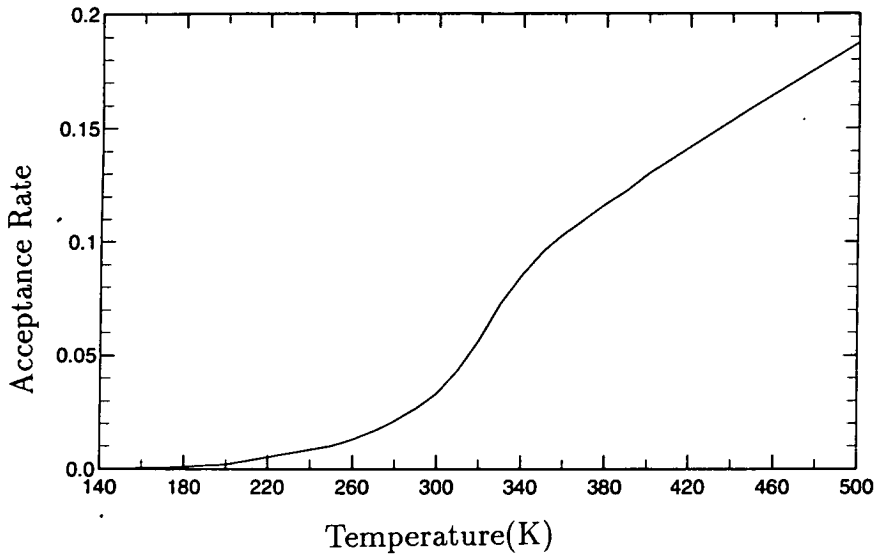

Figure 4.19. Acceptance rate for inversions of orientation.

significant areas where this order has been lost. At 330K the ensemble is obviously more disordered than at lower temperatures; there are no large ordered areas in the ensemble, the initial long-range order having been lost. Any further change in order at 350K is difficult to discern.

In the the molecular dynamics simulation the change in the dynamical state of the molecules was shown by a steep rise in the reorientation rate through the phase transition. The analogue of a reorientation in the Monte Carlo simulation is an inversion of molecular orientation, thus the number of inversions accepted per sweep, the acceptance rate, is analogous to the reorientation rate. Figure 4.19 shows the normalised acceptance rate (number accepted per molecule per sweep) calculated over 10,000 sweeps at each temperature. Since the probability of accepting an inversion rises exponentially with temperature the acceptance rate will always increase with temperature, however, Figure 4.19 shows that between 300K and 360K the acceptance rate rises

Temp. (K)	% Up	% Down	Temp. (K)	% Up	% Down
200	50.04	49.96	340	49.37	50.63
250	49.77	50.23	350	50.20	49.80
300	50.16	49.84	360	50.00	50.00
310	49.80	50.20	370	49.69	50.31
320	50.16	49.84	400	49.73	50.27
330	50.07	49.92	500	49.34	50.66

Table 4.5. Average occupation of up and down orientations on heating.

steeply through the phase transition, then levels off again once the disordered phase has been entered. There is therefore a change in the dynamical state of the molecules at the phase transition. More reorientations are made in the disordered phase than in the ordered phase by an amount that cannot be accounted for by the increase in temperature alone; the disordering transition is accompanied by an increase in the number of reorientations a molecule makes, so the disordered phase of the Monte Carlo simulation can be thought of as analogous to the plastic phase in the molecular dynamics simulation.

Table 4.5 shows the percentage occupancy of the up and the down orientation, from an average taken every 1000 sweeps over 10,000 sweeps of the equilibrated ensemble. If we again argue that the occupation of up or down orientations is Gaussian (p.81), then $N=256\times10$ and the standard deviation as a percentage is $\sigma=1.98\%$. The deviation from equal occupancy of orientations is at no temperature greater than this standard deviation. It may be concluded that both orientations are equally occupied on average, as for other Ising-like models.

A statistical analysis of the change in orientational order is provided by the o.c.f.s of the ensemble. As discussed earlier the o.c.f. for the initial ensemble shows a delta function at -4 with an amplitude of 1, if the o.c.f. is normalised. The o.c.f. at 200K has a peak at -4 with an amplitude of 0.989, slightly less than 1 since in a Monte Carlo

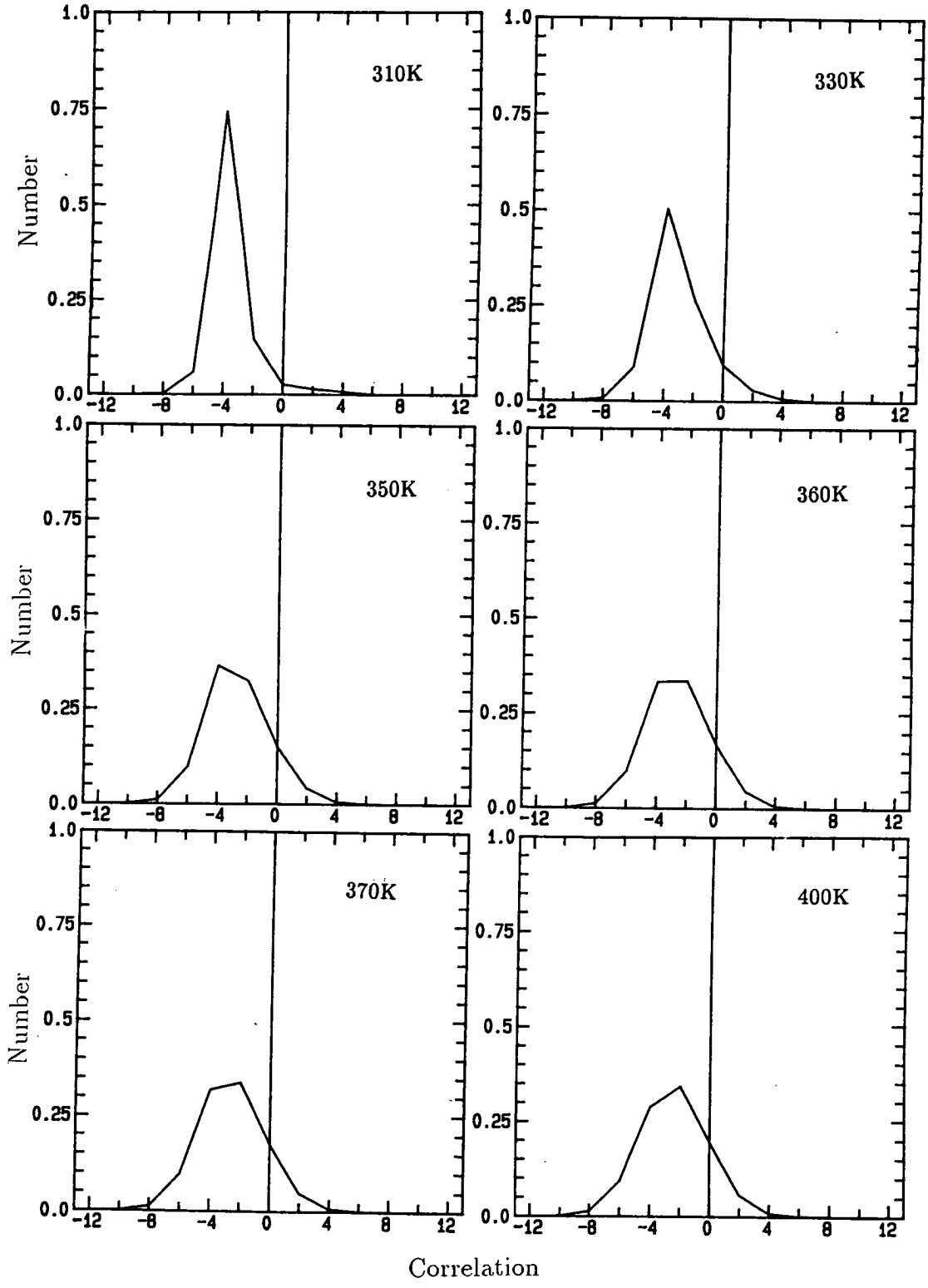

Figure 4.20. O.c.f.s at 310K, 330K, 350K, 360K, 370K and 400K on heating.

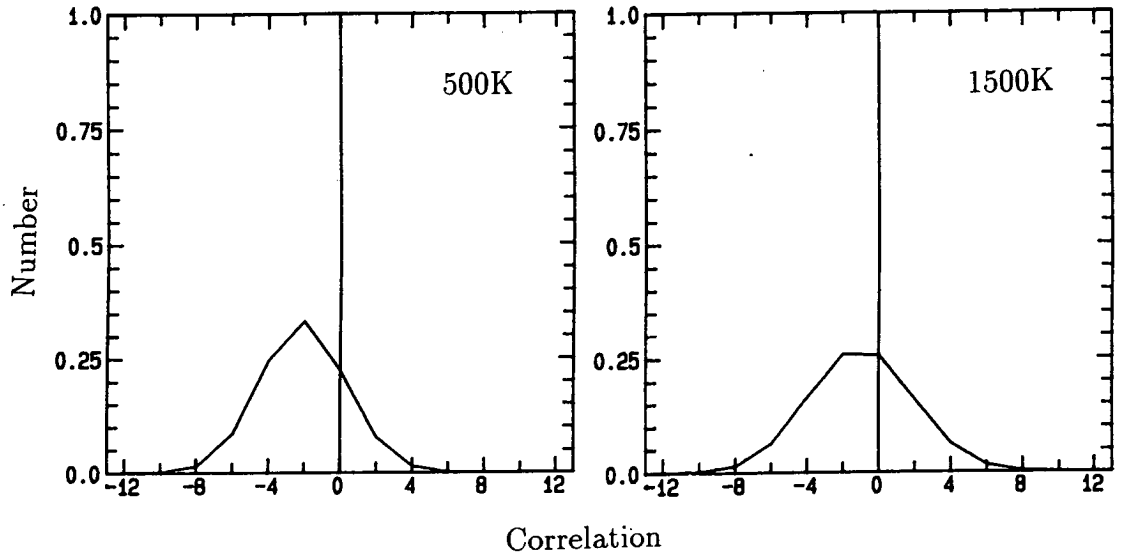

Figure 4.21. O.c.f.s at 500K and 1500K on heating.

simulation some inversions of orientation will be accepted even at very low temperatures. O.c.f.s through the phase transition are shown in Figure 4.20. Between 310K and 350K the peak at -4 decays; at 360K the values of the o.c.f. at -4 and -2 are about the same; by 370K the peak value is now at -2; with a further rise in temperature to 400K the peak at -2 increases. If we compare the o.c.f. at 400K in the Monte Carlo simulation to that at 420K in the molecular dynamics simulation (*q.v.* Figure 4.15) we can see that the peak at -2 in the Monte Carlo simulation is the more distinct.

If we compare the o.c.f. at 1500K to that at 500K (Figure 4.21), at 1500K the peak at -2 has disappeared and the values at -2 and 0 are approximately the same; the distribution shifts towards zero as temperature increases, indicating a loss of orientational correlations. In the molecular dynamics simulation it was argued that orientational correlation is lost when the molecules reorient so frequently that they act like rotators. Since there are only two orientation states in the Monte Carlo model rotator-like behaviour cannot occur. However, at 1500K the average number of inversions per molecule per sweep is 0.481, *i.e.* almost half the molecules invert their orientation over

a single sweep. At high temperature therefore, random inversions dominate and orientational correlations are lost. It can be argued that the loss of orientational correlation in the Monte Carlo simulation is due to the increase in acceptance rate in the same way as orientational correlation is lost in the molecular dynamics simulation due to the increase in reorientation rate.

4.6.3 Localised orientational order

In both the molecular dynamics and Monte Carlo simulations there is evidence that above the phase transition, although the initial long-range orientational order is lost, some localised orientational order persists. What is the nature of the order in the disordered phase of the Monte Carlo ensemble?

The assumption that there is localised orientational order present in the disordered phase is based on the fact that the o.c.f. in this phase peaks at -2, showing that there is a non-random correlation between the orientations of neighbouring molecules. In this simulation the energy lowering part of the Metropolis algorithm favours the configuration of the ordered phase being maintained, whilst random inversions create random disorder, thus there are ordered regions (with an o.c. of -4) and randomly disordered regions (with an o.c. of 0) in the ensemble such that the time averaged o.c.f. has a mean o.c. of -2, the average of -4 and 0; these ordered regions shall be referred to as ordered domains. In the initial ensemble a molecule has its four neighbours in the *ac* plane and in the *bc* plane in the inverse orientation (an o.c. of -4 in each of these planes) and its remaining four neighbours in the *ab* plane in the same orientation (an o.c. of +4 in that plane). We shall refer to this ensemble as being ordered in the [001] direction, the direction in which ordering is unique. Since the simulation involves a face-centred cubic lattice, the equivalent [100] or [010] directions could have been chosen as the unique directions. When the ensemble enters the disordered phase it loses any 'memory' of the direction in which the order of the initial ensemble was established, thus should an ordered domain form in the disordered phase, the ordering of that domain can occur

Temp. (K)	% ordered	No. domains	Largest domain
200	99.9	1.0	256.0
250	99.4	1.0	255.8
280	96.2	2.01	193.9
300	88.6	2.05	176.5
310	87.2	2.28	167.6
320	74.3	2.83	134.8
330	68.1	3.27	126.8
340	55.0	3.94	94.8
350	49.1	4.31	79.3
360	43.0	4.18	65.2
390	33.2	4.05	47.3
400	28.7	3.82	40.7
410	28.2	3.80	38.5
430	24.6	3.52	33.7
450	21.5	3.26	29.1
470	19.7	3.06	26.5
500	16.8	2.79	23.0
700	8.18	1.53	13.5
800	6.75	1.28	12.0
1000	4.54	0.89	9.00
1500	2.92	0.59	6.35

Table 4.6. Percentage of ordered molecules and domains in ensemble on heating.

in any of the [100] directions. A molecule is therefore identified as having an ordered configuration of neighbours if its o.c. in two out of the three neighbour planes is -4 and the o.c. in the remaining plane is +4.

To identify ordered domains in the ensemble, all molecules which have an ordered configuration of neighbours as described above (*i.e.* an o.c. of +4 in one plane and -4 in the other two) are identified. All such molecules and the nearest neighbours of these molecules are considered to be in an ordered domain. A search of the ordered molecules is then made to determine how many domains are present and the size of each domain. Molecules are considered to be in the same domain if they are nearest neighbours and in ordered configurations which have the same direction of ordering. In Table 4.6 the average values of the percentage of the 256 molecules in the ensemble which are in

ordered domains, the number of separate domains, and the number of molecules in the largest domain are listed for some temperatures on heating. The average values are calculated from every tenth sweep over 10,000 sweeps.

At low temperatures almost all molecules retain the initial ordered configuration, *i.e.* the ensemble is a single domain. At 280K, as the phase transition is approached, there is a significant change in the order in the ensemble; the initial order remains predominant, but the ensemble has now split into two large domains, the larger containing about 194 molecules. Between 300K and 340K, going through the phase transition, the order is gradually lost and the largest domain is reduced in size. Above 350K, in the disordered phase, less than 50% of molecules are in ordered configurations. As temperature increases the size of the largest domain gradually decreases. The number of domains present increases going through the phase transition, reaches a maximum at 350K, then gradually decreases as temperature increases in the disordered phase; this can be understood by the initial single domain separating into several domains as order is lost and then the size of these domains being reduced as temperature increases, so that smaller domains disappear entirely.

At high temperatures, few molecules remain in ordered configurations. At 800K the average size of the largest domain is 12.0, fewer than the 13 required for a single ordered configuration, which means that on some sweeps there are no ordered configurations and the ensemble is therefore randomly disordered. The continued diminution of domains as temperature increases explains the shift in the peak of the o.c.f. from -2 towards 0 (Figure 4.21). In the disordered phase, the correlation between neighbouring molecules is strongest from 360K to 500K, which is the temperature range over which ordered domains of significant size can still be identified. It may therefore be concluded that the localised orientational order is due to the persistence of ordered domains in the disordered phase.

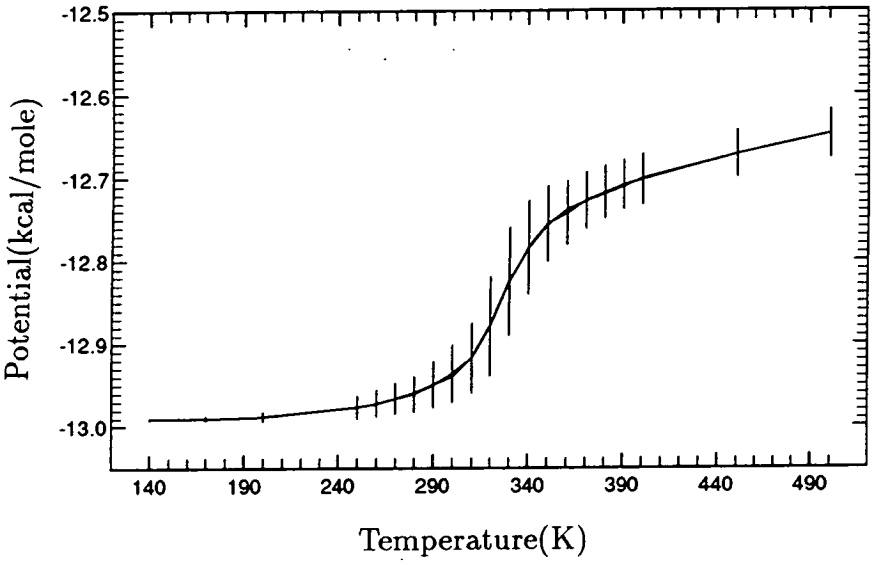

Figure 4.22. Average potential for 256 molecules on cooling.

4.6.4 Recooling

Starting from the final ensemble at 500K, the 256 molecule ensemble was recooled to 140K, using the same equilibration procedure as used on heating. Figure 4.22 shows the average potential recorded on cooling, superimposed on the values recorded on heating. The two sets of values almost exactly match, so there is no evidence of hysteresis in the phase transition. The o.c.f.s below the phase transition, in Figure 4.24, show the regrowth of the peak at -4 as the ensemble is cooled. At 200K the amplitude of the o.c.f. at -4 is 0.989, the value found on heating. In Figure 4.23 at 280K regions with the ordered configuration can be identified which is consistent with the apparent re-establishment of order in the ensemble, but in the final configuration at 140K it can be seen that the full order of the initial ensemble has not been regained on cooling. The ordered configuration is apparent, but in at least two separate domains.

Using the same analysis method as before the statistics of domain formation on

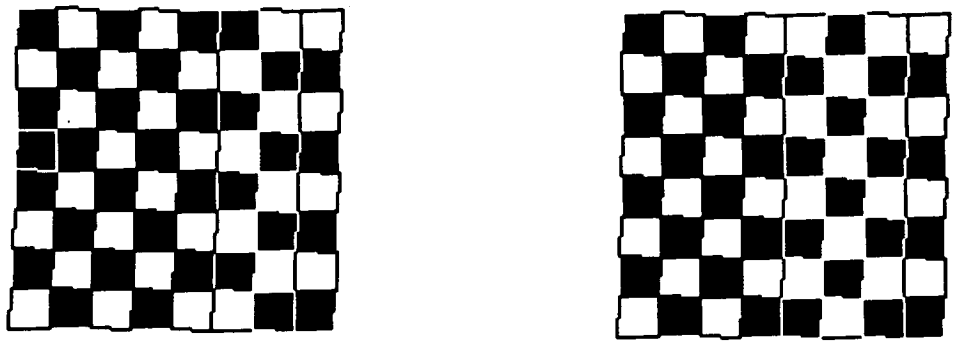

280K 140K

Figure 4.23. The Monte Carlo ensemble at 280K and 140K on cooling.

recooling through the phase transition can be examined. The average values for the percentage of the 256 molecules in the ensemble which are in ordered domains, the number of separate domains and the number of molecules in the largest domain, calculated from every tenth sweep over 10,000 sweeps are listed in Table 4.7. Between 350K and 310K, returning back through the phase transition, there is a significant increase in the percentage of molecules in ordered orientations and the size of the largest domain. Below 280K the ensemble remains separated into exactly two domains. In the final configuration two domains containing 136 and 120 molecules are identified. Re-examining the ensemble at 140K in Figure 4.23, the smaller domain may be identified in three (vertical) layers to the right of centre, and the larger domain is to left-hand side and the last vertical layer on the right (remembering periodicity).

The configuration of a molecule and its neighbours at the domain boundary must obviously be different from the ordered configuration in the bulk of the domain. Since the potential energy and the o.c.f. of for the multi-domain ensemble found on recooling have been observed to match the potential energy and the o.c.f. of the single domain structure on heating, the orientational correlation, and therefore the potential energy, of a molecule at a domain boundary must be the same as for a molecule in the bulk of a domain. Let us examine the ensemble at 140K in Figure 4.23 and consider the

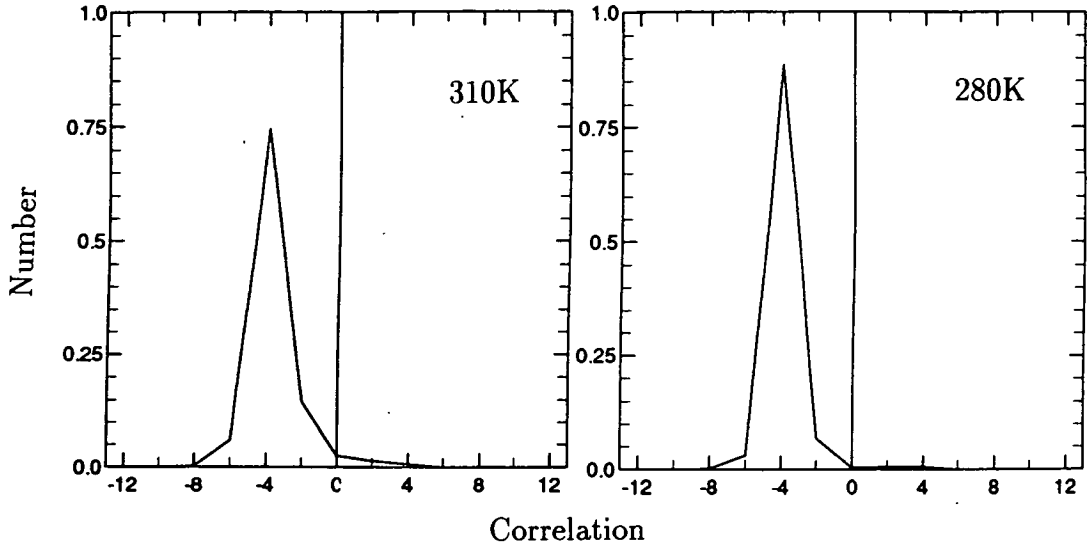

Figure 4.24. O.c.f.s at 310K and 280K on cooling.

Temp. (K)	% ordered	No. domains	Largest domain
450	21.8	3.28	29.7
400	30.1	3.83	42.4
380	34.8	4.12	50.7
360	41.7	4.20	63.4
350	47.5	4.25	76.0
340	58.3	3.90	98.5
330	65.8	3.31	115.9
310	88.0	2.76	124.3
300	84.5	2.03	159.5
280	88.3	2.40	143.4
270	98.2	2.00	137.9
250	99.1	2.00	137.5
200	99.9	2.00	136.3
140	100.0	2.00	136.0

Table 4.7. Percentage of ordered molecules and domains in ensemble on cooling.

configuration of a molecule at the domain boundary and its 12 neighbours. In the *ab* plane two of the neighbours, which are in the bulk of the domain, are in the same orientation and the other two neighbours, which are in the next domain, are in the inverse orientation, giving an orientational correlation of 0 in this plane. The same is true for the four neighbours in the *ac* plane. In the *bc* plane, however, the four neighbouring molecules, all of which are in the same domain, are in the inverse orientation, giving an orientational correlation of -4 in this plane. The overall orientational correlation at a domain boundary is therefore 0+0+(-4)=-4, which is the same as for the bulk.

In the disordered phase small domains with order in any or all of the [100] direction may be identified. These domains are prevented from growing by random inversions of orientation. When recooled, orientational order is re-established by growth of certain of these domains. When two domains ordered in different directions grow together orientational frustration occurs at the boundary between these domains. For example, if a domain ordered in the [100] direction meets a domain ordered in the [001] direction, ordering in the [100] direction requires molecules in *bc* planes all to have the same orientation, whereas ordering in the [001] direction requires the molecules at face-centre sites in the *bc* planes, *e.g.* $(0\frac{1}{2}\frac{1}{2})$, to have the inverse orientation from corner sites,*e.g.* (000). The molecule at (000) will therefore require one orientation to join the [100] domain and the inverse orientation to join the [001] domain, hence frustration. Such frustration may be resolved by a smaller domain joining a larger domain or, when two large domains meet, by the formation of a domain boundary which has the same potential energy as the bulk.

Since they have the same potential energy, the multi-domain ensemble found on recooling and the initial single-domain ensemble are degenerate. This degeneracy is consistent with the work of Danelian, who found a face-centred cubic anti-ferromagnet of N spin states with zero-field and nearest-neighbour interactions to have 2^R degenerate ground states, where $R = N^{\frac{1}{3}}$, this degeneracy being due to 'partial long-range order'. In the ground state of the simulations discussed above the partial long-range

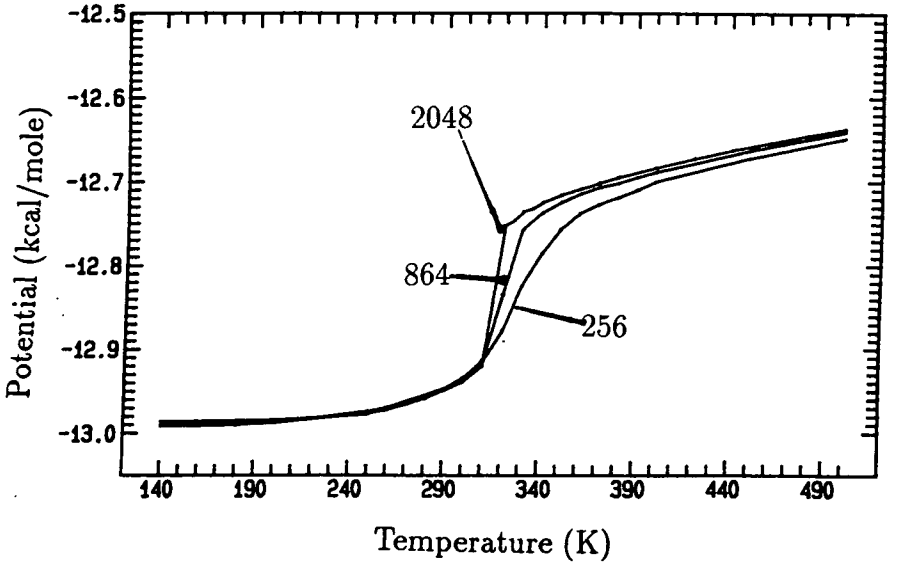

Figure 4.25. Average potential for 256, 864 and 2048 molecule ensembles.

order is comprised of several domains each exhibiting long-range order. The initial single-domain ensemble is a special ground state, which is analogous to the single crystal of adamantane in the ordered tetragonal phase.

4.6.5 Finite-size effects

In the molecular dynamics simulations it was found that finite-size effects have an important influence on what happens in the simulation of a phase transition. It is therefore opportune to check for finite-size effects in the Monte Carlo model. Figure 4.25 shows the average potential measured on heating for 256, 864 and 2048 molecule ensembles. In each simulation temperature is increased in 10K intervals from 140K to 500K. By defining the transition temperature as the mid-point of the temperature range over which the potential changes most steeply, the transition temperature was found to be 330K in the 256 molecule ensemble. In the 864 molecule ensemble the phase transition occurs between 310K and 330K, giving a transition temperature of 320K. For the 2048 molecule ensemble there is an obvious discontinuity in the potential between 310K and 320K. The transition temperature is therefore 315±5K, where an error in the value

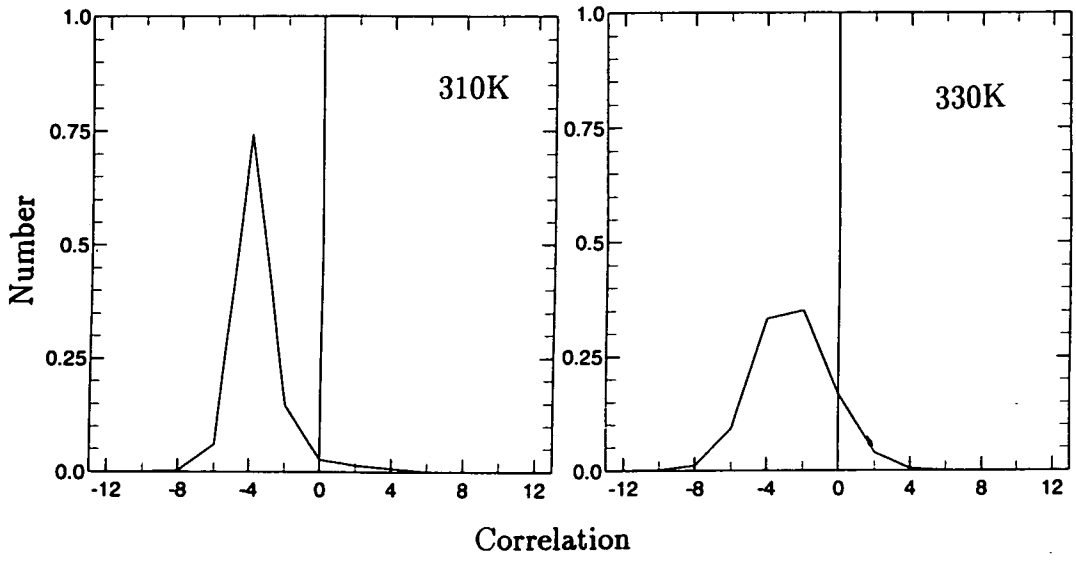

Figure 4.26. O.c.f.s at 310K and 330K on heating, for 2048 molecules.

Temp. (K)	% ordered	No. domains	Largest domain
140	100.0	1	2048
300	96.7	1	1981
310	83.6	3	1270
320	48.7	35	128
330	41.0	39	123
350	37.6	30	109
400	24.7	28	59
500	18.3	27	43

Table 4.8. Percentage of ordered molecules and domains in ensemble on heating for 2048 molecules.

has been stated as it is now certain that the phase transition occurs in the 10K range between 310K and 320K. As expected therefore, the transition temperature decreases as the size of the ensemble is increased.

Does an increase in size affect the short-range order? From Figure 4.26 it can be seen that, for the 2048 molecule ensemble between 310K and 330K, going through the phase transition the peak in the o.c.f. shifts from a sharp peak at -4 to a broad peak at -2, as for the 256 molecule simulation but over a smaller temperature range. Tables 4.8 and 4.9 give the statistics of domain formation in the 2048 molecule ensemble

Temp. (K)	% ordered	No. domains	Largest domain
330	31.5	34	76
320	51.7	24	641
310	93.7	3	1085
280	98.9	3	1144
200	99.9	3	1143
140	100.0	3	1152

Table 4.9. Percentage of ordered molecules and domains in ensemble on cooling for 2048 molecules.

on heating and cooling respectively; to reduce computation, the values in these tables were measured from the final configuration at each temperature.

On heating, at 310K the ensemble has split into 3 domains as the phase transition is approached. Immediately above the phase transition, at 320K, fewer than 50% of the molecules are in ordered configurations, the size of largest domain has been reduced by a factor of ten, and the number of domains increases, so there are now many smaller domains. Further heating reduces both the number of molecules in ordered configurations and the number of domains, as the smaller domains are removed.

On cooling, immediately above the transition, at 320K, a large domain has formed. Below the phase transition, at 310K, the small domains have grown together to form three large domains and a large majority of molecules are in ordered configurations. The three domains are retained with further cooling, resulting in an ensemble in which all molecules are in ordered configurations in three domains comprising 1152, 704 and 192 molecules.

It can be concluded from this analysis that the localised orientational order in the disordered phase and domain formation on recooling are not finite-size effects. The main finite size effects are a lowering of the transition temperature and the transition becoming more first-order, *i.e.* a discontinuous change in order between consecutive temperatures, as the size of the simulation is increased. A first-order transition in this system is consistent with previous simulations [62].

Temp. (K)	% ordered	No. domains	Largest domain
360	100.0	1.00	256.0
380	98.1	1.00	255.1
400	95.9	1.00	253.0
410	89.8	1.00	239.3
420	7.16	1.36	13.75
440	4.27	0.92	7.71
460	2.63	0.56	6.37
480	3.83	0.68	9.10
500	3.97	0.76	8.25

Table 4.10. Number of ordered molecules and domains in molecular dynamics ensemble for 256 molecules on heating.

4.7 Domains in the Molecular Dynamics Simulation

The Monte Carlo simulations have provided a possible model for short-range order in the plastic phase of adamantane. To verify this model we must find whether ordered domains can be identified in the molecular dynamics simulation. For the simulation on the 256 molecule ensemble the final configuration at each temperature is considered and each molecule defined to be in either an up or a down orientation depending on which orientation that molecule's orientation is closest to. The method for finding ordered domains in the Monte Carlo simulation can then be applied to the molecular dynamics simulation.

Table 4.10 lists the percentage of molecules in ordered configurations, the number of ordered domains in the ensemble, and the size of the largest domain on heating. Below the phase transition the ensemble remains a single domain; between 380K and 410K this domain is reduced in size by a few isolated reorienting molecules. At 420K the order of the ensemble has changed completely; few molecules remain in ordered configurations; on average there is more than one domain, but the average size of the largest domain is only just greater than one ordered configuration of 13 molecules. If the phase transition is defined by the change in order then the transition occurs

between 410K and 420K. At temperatures above 420K there is less than one domain on average and the domain size is less than 13 molecules, hence there must be times when there are no ordered domains in the ensemble.

The same formation of ordered domains observed immediately above the phase transition in the Monte Carlo simulations is not observed when the plastic phase is entered in the molecular dynamics simulation. The observation of a few isolated molecules adopting the ordered configuration is similar to the behaviour observed above 700K in the 256 molecule Monte Carlo simulation. In Figure 4.27 the o.c.f. at 500K in the molecular dynamics and 1500K in the Monte Carlo simulation, both for 256 molecules, can be seen to have very similar distributions. From this it can be concluded that the plastic phase found on heating in the molecular dynamics simulation is analogous to the high-temperature regime of the Monte Carlo simulation; in both cases the molecules reorient rapidly so that only small short-lived domains can form and there is only a weak correlation between the orientations of nearest neighbour molecules. The only temperature at which greater than one domain was observed in the molecular dynamics simulation was 420K, immediately above the phase transition. It is possible that the splitting of the single large domain into several small domains is the mechanism for the loss of order in the molecular dynamics simulation as it was found to be in the Monte Carlo simulation, however, this must occur in a very narrow temperature range near the transition temperature and is thus difficult to examine in detail in a molecular dynamics simulation of this size.

Table 4.11 lists average values of the percentage of molecules in ordered configurations, the number of ordered domains in the ensemble, and the size of the largest domain, on cooling. Between 480K and 420K the statistics are similar to the statistics for the same temperatures on heating. Below 400K there is a significant presence of ordered domains in the ensemble, although the size and number of these domains fluctuates with temperature down to 240K. Now let us compare the statistics on domain formation from 400K to 240K in the recooled molecular dynamics ensemble to those for

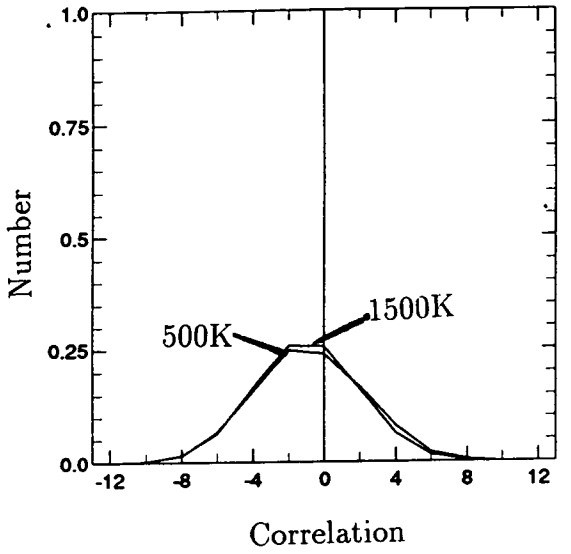

Figure 4.27. O.c.f.s from molecular dynamics at 500K and Monte Carlo at 1500K.

Temp. (K)	% ordered	No. domains	Largest domain
480	3.90	0.80	7.73
460	5.41	1.05	9.88
440	4.19	0.86	8.79
420	7.37	1.32	13.36
400	11.7	1.67	22.34
380	14.7	2.69	22.17
360	12.2	2.19	19.28
340	16.5	2.32	30.54
320	13.6	1.87	21.98
300	16.3	2.66	24.42
280	31.0	3.73	31.79
260	28.4	3.00	29.18
240	26.8	3.00	27.00
220	26.8	3.00	27.00

Table 4.11. Number of ordered molecules and domains in molecular dynamics ensemble for 256 molecules on cooling.

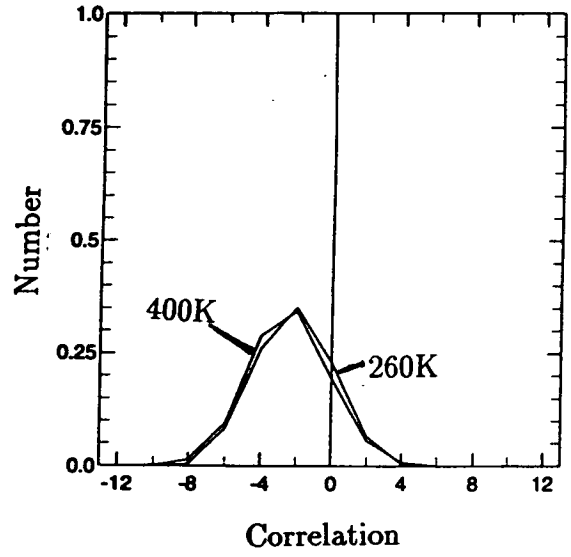

Figure 4.28. O.c.f.s from molecular dynamics at 260K on cooling and Monte Carlo at 400K on heating.

the disordered phase in the Monte Carlo simulation, from 400K to 500K in Table 4.6; the percentages of ordered molecules and the number and size of domains are of the same order. In Figure 4.27 the o.c.f. at 260K on recooling in the molecular dynamics simulation and 400K on heating in the Monte Carlo simulation, both for 256 molecules, can be seen to have very similar distributions.

Above it was stated that the 256 molecule ensemble of adamantane when recooled remains in a plastic phase down to 220K. When this phase is cooled below the order-disorder transition temperature, although long-range order is not re-established, there is a change in short-range order; domains of significant size can be identified and there is a stronger correlation between the orientations of neighbouring molecules, similar to the short-range order in the low-temperature regime of the disordered phase of the Monte Carlo model. Unlike the Monte Carlo model, however, recooling does not return all

molecules to ordered configurations, even in a multi-domain structure. Further cooling in the molecular dynamics simulation freezes out the reorientational motion leaving only 26.8% of molecules in ordered configurations in three separate domains containing 27, 22 and 20 molecules.

The 32 molecule simulation is too small to provide statistics on domain formation, however, some interesting comparisons with the results of the 256 molecule Monte Carlo and molecular dynamics simulations can still be made. On recooling, the ordered 32 molecule ensemble had the b axis as its unique axis as opposed to the c axis initially; this is analogous to one of the domains in the recooled Monte Carlo ensemble having order in the [010] direction compared to the [001] direction initially. The largest domain found in the final recooled structure in the 256 molecule molecular dynamics simulation contains 27 molecules, similar to the number of molecules in the smaller simulation. In the 32 molecule simulation a single domain which includes all molecules in the ensemble is formed, long-range order is re-established, and the tetragonal phase is re-entered.

In the 256 molecule molecular dynamics simulation, although some growth of ordered domains is observed on cooling, the ensemble does not return to the ordered tetragonal phase, or to a multi-domain structure analogous to that found in the Monte Carlo simulation. This could be because the time required to anneal either of these structures is much longer than the simulation time. Another possibility is that, unlike the Monte Carlo, if an ordered domain forms it may cause a local tetragonal distortion in the ensemble, so that when domains grow together a domain boundary analogous to that found in the Monte Carlo simulation can not form; the frustration effect may then prevent further domain growth.

4.8 Conclusions

Molecular dynamics simulations were performed on ensembles comprised of 256 and 32 molecules of adamantane. In both ensembles a transition from an orientationally ordered tetragonal unit cell to an orientationally disordered cubic unit cell was observed on heating. In the 256 molecule simulation this transition occurred between 400K and 420K, while in the 32 molecule simulation the transition occurred between 420K and 440K. These transition temperatures are much higher than observed experimentally, which may be attributed to a finite-size effect, the transition temperature decreasing as the size of the ensemble increases, and by the over-estimation of the cohesive energy between a pair of molecules by the Williams potential used to model molecular interactions.

In the disordered phase the molecules occupy two possible orientations which are symmetrically inverse. This is a plastic phase in which the molecules reorient between symmetrically inverse or symmetrically equivalent orientations. There is a non-random correlation between the orientations adopted by a molecule and its twelve nearest neighbours. In the order-disorder transition, therefore, long-range orientational order is lost, but some short-range order persists in the plastic phase. Heating the plastic phase removes the short-range order. Comparison with a Monte Carlo model for adamantane, which is analogous to an antiferromagnetic Ising model on a face-centred cubic lattice, suggests that the short-range order is manifested as the temporary formation of small, orientationally ordered domains.

On recooling, the 32 molecule simulation can be returned to the ordered tetragonal phase, but the 256 molecule simulation remains in a disordered, near cubic phase which is plastic down to 220K. In the Monte Carlo model long-range order is re-established by the growth of certain of the small ordered domains from the disordered phase. There is evidence that similar domain growth mediates the reverse transition in molecular dynamics. In the 32 molecule simulation the entire ensemble forms a single domain

thus re-establishing long-range order. In the 256 molecule simulation domain growth is observed, but no domain is found to become large enough to re-establish complete or partial long-range order. This is probably due to either long annealing times being required or to frustration between domains with different directions of unique order which prevents overall domain growth.

Is the short-range order in the plastic phase predicted in the simulation experimentally observable? The ordered domains observed in the simulation have the same order as the tetragonal phase, but with uniques axes in the a, b and c directions, so will have $P\bar{4}2$ symmetry; the disordered regions in the plastic phase are consistent with the $Fm3m$ space group observed in experiments. Immediately above the phase transition in the 256 molecule simulation about 7% of molecules are in ordered domains. If domain size is scalable in the molecular dynamics simulation as it is in the Monte Carlo simulation, a sample of adamantane large enough to be used in experiment should contain domains of significant extent. In x-ray scattering experiments from such a sample one would expect mainly to observe scattering consistent with a face-centred cubic crystal with a $Fm3m$ space group and some less prominent scattering consistent with the $P\bar{4}2$ space group of the ordered domains. Reynolds [52] predicted ordering in the plastic phase with a $F\bar{4}3m$ space group, which is not consistent with the results of the simulation, however, his work has provided diffuse scattering intensities for certain reciprocal lattice vectors; diffuse scattering intensities at the same lattice vectors could be calculated from a simulation and the result compared to experiment. Otherwise, it would be possible to calculate from simulations intensities for powder diffraction patterns or Bragg reflections which may be compared to future experiments.

Regarding possible further simulations, we should consider the maxim attached to most speculative discussions of simulations; larger ensembles, longer simulation times. With longer simulation times at the correct temperature it should be possible to return the 256 molecule simulation from the cubic to the tetragonal phase. To simulate the transition from a cubic to a single tetragonal phase in a larger ensemble would require

a very long simulation time. However, it is possible that in a larger ensemble ordered domains would be able to form a localised tetragonal distortion reforming the ensemble into several tetragonal crystallites with unique axes in differing directions, analogous to the domains formed on recooling the Monte Carlo simulation. This form of crystallite formation has been observed in experiments on cooling a single crystal from the plastic phase [49]. The main advantage of simulating a larger ensemble is in studies of the plastic phase, providing better statistics on domain formation and a check on the scalability of domain sizes, and improving the resolution of theoretical scattering calculations.

Chapter 5

Buckminsterfullerene

Science and virtue, he held, are incompatible, and all sciences have ignoble origin. Astronomy comes from the superstition of astrology; eloquence from ambition; geometry from avarice; physics from vain curiosity.
Bertrand Russell on Jean-Jaques Rousseau.

5.1 Introduction

For many years carbon was known to exist in three forms, graphite, diamond and amorphous. Then in 1985 Kroto and co-workers, during work on spectroscopy of carbon clusters, noticed an unusually large number of clusters containing 60 atoms compared to the number of clusters with fewer or greater numbers of atoms; the 60 atom clusters must somehow be more stable than other clusters. The explanation proposed was that these clusters consisted of a closed cage of carbon atoms. After some deliberation, it was realised that the structure best able to accommodate 60 atoms has the geometry of a truncated icosahedron (Figure 5.1), consisting of 12 pentagonal faces and 20 hexagonal faces with each pentagon entirely surrounded by hexagons. The result is a molecule of a single element which is a near spherical hollow cage; the structure is not so surprising once it is realised that Association footballs are generally constructed from hexagonal and pentagonal patches in exactly the same fashion.

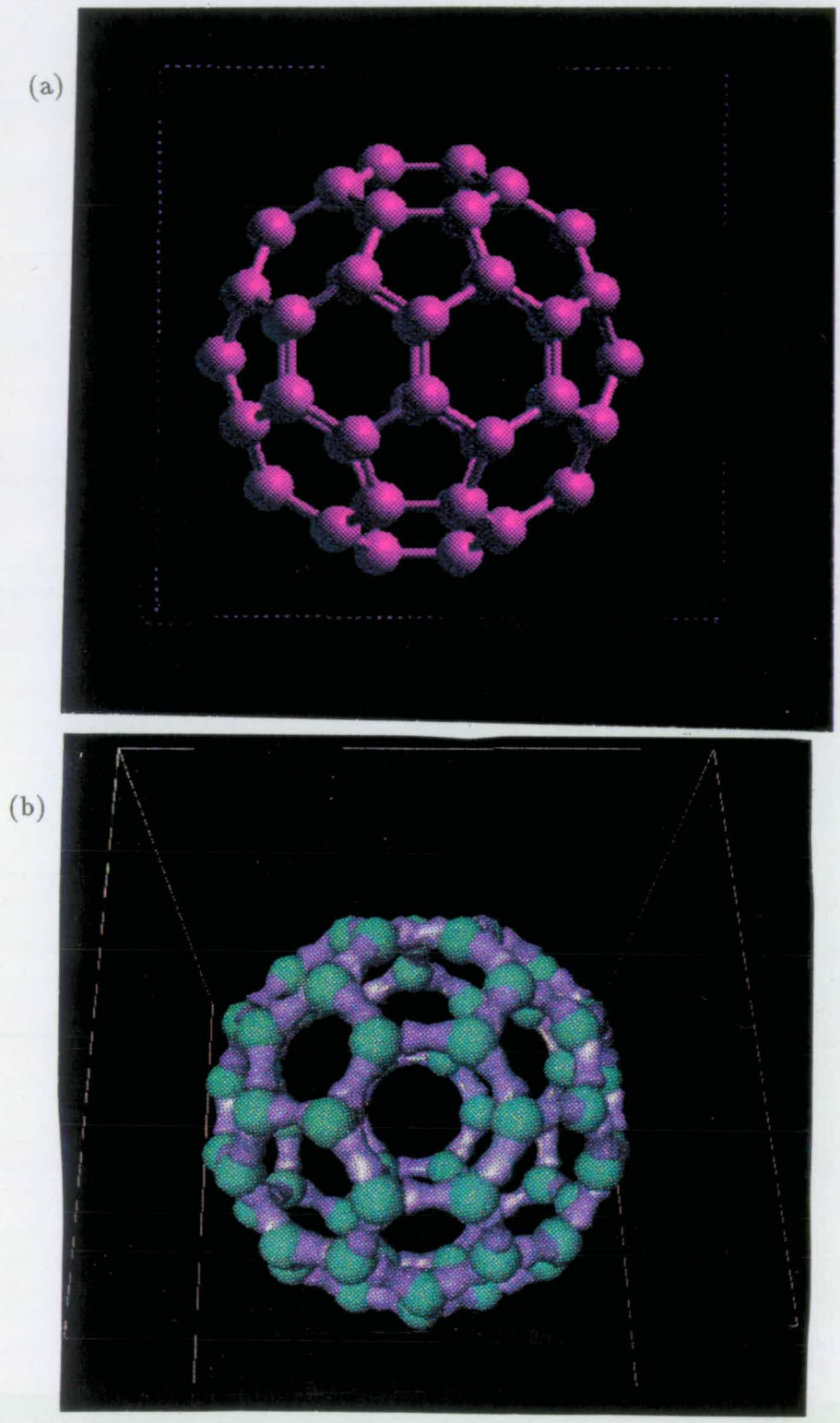

Figure 5.1. The C_{60} molecule (a) atoms (b) electronic structure.

Missing a wonderful opportunity for self-aggrandisement, Kroto resisted the temptation to try to call the new molecule 'Krotoene', preferring instead the somewhat unwieldy Buckminsterfullerene, after the American architect Richard Buckminster Fuller who designed geodesic domes with structures like C_{60}. This was the name the new molecule bore when it appeared on the front cover of Nature [65]. Attempts that it should be renamed after its resemblance to a piece of sporting equipment failed largely due to the trans-Atlantic language barrier, with both soccerene and footballene being suggested [1].

For the next few years after the initial discovery only a few more papers concerning C_{60} appeared, mostly concerning spectroscopy of carbon clusters and theoretical discussions of the proposed structure. Then in 1990 Krätschmer and co-workers managed to produce large enough quantities of C_{60}, by vapourising graphite with a high powered laser, so as to be able to grow C_{60} crystals from solution [66]. X-ray diffraction experiments on these fairly poor quality hexagonal shaped crystals showed almost spherical carbon cages with nearest neighbour centre-centre separation of 10.02Å and an average molecular radius of 7.1Å, consistent with the proposed structure of C_{60}.

Further X-ray and NMR experiments [67, 68] showed the molecules to be hollow cages with perfect icosahedral symmetry and that all atoms were equivalent, *i.e.* all bonded in the same way. It was found that there were 30 bonds of length 1.40Å connecting quasi-hexagonal faces and 60 bonds of length 1.45Å between quasi-hexagonal and pentagonal faces. Since carbon is tetravalent, it is often assumed that the shorter bonds have 2 electron pairs associated with them, and so are double bonds, while the longer bonds are single bonds with one electron pair. However, the difference in bond lengths is only 0.05Å which is less than is to be expected for conventional double and single bonds, but is more like the difference in length of neighbouring bonds in polyacetylene [69]. To distinguish, a bond connecting quasi-hexagons will be referred to as

[1] The French persisted in the latter for a while, Colombeau *et al.*, J.Phys.Chem. 96 p.22 1992.

a 6:6 bond and a bond connecting a quasi-hexagon and a pentagon will be referred to as a 6:5 bond.

The availability of macroscopic quantities for experiment and the confirmation of the molecular structure of C_{60} led to an enormous expansion of interest in the new molecule. Between 1985 and 1990 there were around 50 papers published on Buckminsterfullerene; in 1991 and 1992 over 500 papers appeared concerning the molecule, covering topics from the quantum mechanics of its structure to uses for the chemical compounds it can form. Of particular interest are compounds involving the C_{60} molecular crystal being doped with sodium or potassium, which are found to be superconducting at about 30K.

C_{60} is just one of a family of closed cage carbon molecules, which are now called Fullerenes [70]. Geometrically, a Fullerene molecule must have 12 pentagonal faces and any number of hexagonal faces, including 0 but excluding 1. The smallest possible Fullerene would be C_{20}, which is a dodecahedron, although this has never been observed probably because the bond angles required in its structure are too large for it to be stable. The largest observed Fullerene is C_{240}. After C_{60}, the next most abundant is C_{70} which has 25 hexagonal faces and is shaped like a rugby ball. Also of interest is C_{76} which shows chirality in the arrangement of its hexagonal faces [71].

5.2 C_{60} and its Molecular Crystal

When grown carefully from solution, molecular crystals of C_{60} with high purity (99.99%) are cubic close-packed, which may be anticipated for almost spherical molecules. At room temperature the unit cell is face-centred cubic with lattice parameter a=14.10Å and is in a plastic phase in which the molecules reorient [77]. The orientations of the molecules are disordered, so the space group is $Fm3m$ [72].

When cooled below 260K the rotational motion of the molecules gradually freezes out and an orientationally ordered phase is formed. The unit cell remains face-centred

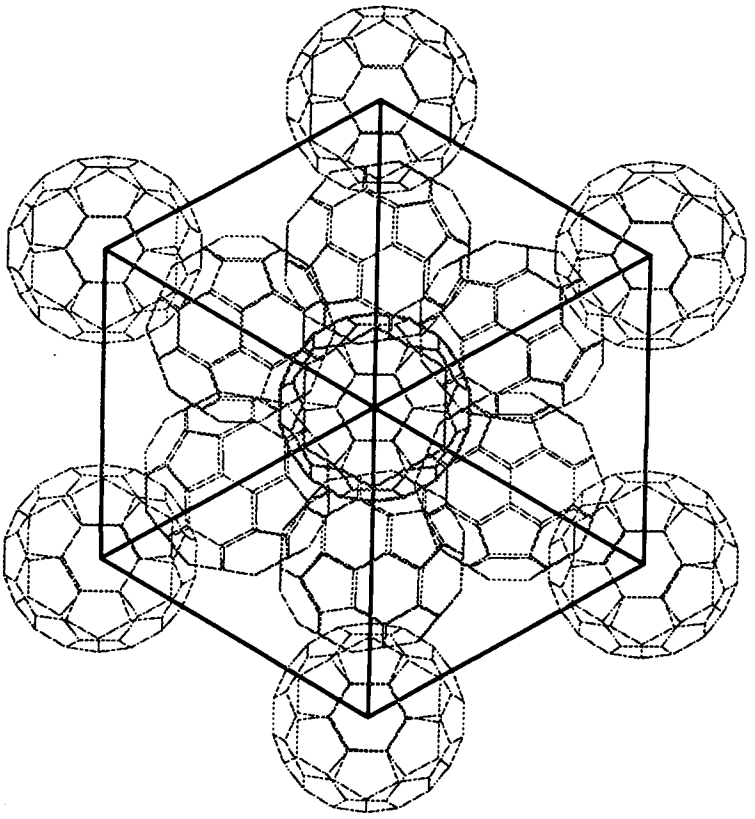

Figure 5.2. The low temperature unit cell viewed down [111].

cubic, with lattice parameter a=14.015Å at 90K, but the space group is now $Pa\bar{3}$, a primitive unit cell. This can be explained by the four molecules in the face-centred cubic unit cell adopting different orientations (Figure 5.2).

If we define an orientation of the C_{60} molecule such that three 2-fold axes (through the centres of 6:6 bonds) are aligned with the Cartesian x,y and z directions, four 3-fold axes (through the centres of quasi-hexagonal faces) are aligned with the [111] directions of the cubic unit cell. This orientation is that described by the molecular co-ordinates listed in Appendix B. The four distinct orientations of the molecules in the unit cell are described by a rotation of 22° clockwise about different [111] directions for each of the molecules. The molecule at $(0,0,0)$ rotates about [111], that at $(0,\frac{1}{2},\frac{1}{2})$ about $[\bar{1}1\bar{1}]$, that at $(\frac{1}{2},0,\frac{1}{2})$ about $[\bar{1}\bar{1}1]$, and that at $(\frac{1}{2},\frac{1}{2},0)$ about $[1\bar{1}\bar{1}]$.

Well below 260K a significant amount of orientational disorder is observed. The transition from the orientationally disordered phase to the orientationally ordered phase is continuous down to 90K, where an ordered static structure is observed [73]. In the ordered structure 67% of molecules adopt the sites described above with the remaining molecules adopting a minor site orientation which is similar to that above except the molecules are rotated by 82° about the [111] directions.

In terms of computational simulations, the discovery of C_{60} allowed different techniques developed over many years to be brought to bear on an entirely new subject. We shall now proceed to use some of these techniques, beginning with some calculations of the vibrational properties of the C_{60} molecular crystal.

5.3 Lattice Dynamics of C_{60}

5.3.1 General Theory

The concept of lattice dynamics should be familiar to anyone who has undertaken an undergraduate solid state physics course, however, since we have not used the method up until now, a brief discussion of the formulation of this method and its physical

significance is in order.

The problem is best introduced by first considering the simple example of a one-dimensional harmonic oscillator. A particle of mass m is subject to a potential ϕ which can be written as the Taylor expansion

$$\phi = \phi_0 + u(\frac{d\phi}{du})_0 + \frac{u^2}{2}(\frac{d^2\phi}{du^2})_0 + \frac{u^3}{6}(\frac{d^3\phi}{du^3})_0 + ... \tag{5.1}$$

where the zero subscript denotes evaluation at the position of minimum energy. Taking $(\frac{d\phi}{du})_0 = 0$ and assuming that the displacement, u, is small (the harmonic approximation), (5.1) can be written as

$$\phi = \frac{u^2}{2}(\frac{d^2\phi}{du^2})_0 \tag{5.2}$$

where the constant term has been removed and higher order terms are neglected. (5.2) is the harmonic term of the potential; higher order terms are anharmonic terms which are significant for large amplitude displacements. From (5.2) the angular frequency of simple harmonic motion can be obtained

$$m\omega^2 = (\frac{d^2\phi}{du^2})_0. \tag{5.3}$$

In a crystalline solid molecules are confined to definite sites in a unit cell and are subject to a potential due to the particles on the surrounding lattice. In a perfect crystal at 0K the site occupied by a molecule in the unit cell will be at the position for the minimum energy state possible according to the potential interaction with the rest of the crystal. Essentially this is an array of particles confined in periodic potential

wells. If given a small random displacement from their minimum energy positions these particles will oscillate. A quantised oscillation is called a phonon. For molecules, phonons have translational and rotational characteristics, and all such phonons have wave vectors in the first Brillouin zone. The superposition of many phonons create travelling waves on the lattice; these waves are dispersive, *i.e.* the frequency changes with spatial position. The variation of the frequencies of the phonon modes with wavevector is called the dispersion curve.

Let us now leap ahead and formulate a general equation for the determination of the dispersion curve. The expression for the displacement of molecule k in unit cell l can be written in the form of a general expression for a travelling wave

$$\mathbf{u}(kl) = \mathbf{U}(k\mathbf{q}) \exp[i(\mathbf{q} \cdot \mathbf{r}(kl) - \omega(\mathbf{q})t)] \tag{5.4}$$

where $\omega(\mathbf{q})$ is the angular frequency of a phonon with wave vector $\mathbf{q}$. The displacement is defined in terms of 6 co-ordinates,

$$\nu_i = \sqrt{m_i} u_i$$

where for $i = 1, 2, 3$ these are translational co-ordinates and m_i is the molecular mass, and for $i = 4, 5, 6$ these are rotational co-ordinates and m_i are the principle moments of inertia of the molecule. If we assume that these displacements are small then, extending (5.3), the potential for molecule k in the harmonic approximation is

$$\Phi_{ij}(kl) = \sum_{k'l'_j} \frac{d^2\phi}{du_i(kl)du_j(k'l')} \tag{5.5}$$

where the sum is performed for all of the k' other molecules in all of the l' unit cells. In the computational model a pairwise additive potential, such as the Lennard-Jones

and Williams potentials discussed previously, can be used. The total value of Φ is evaluated by summing the values of second derivatives of the potential between all atoms in molecule k and all the atoms in its neighbouring molecules within a cutoff radius. The equations of motion for a molecule are

$$\ddot{\nu}_i(kl) = -\sum_{k'l'j} \frac{\Phi_{ij}(kl,k'l')}{\sqrt{m_i m_j}} \nu_j(k'l'). \tag{5.6}$$

Combining (5.4) and (5.6) we find

$$\begin{aligned} \omega^2 \mathbf{U}_i(k\mathbf{q}) &= \sum_{k'j} \mathbf{U}_j(k'\mathbf{q}) \sum_{l'} \frac{\Phi_{ij}(kl,k'l')}{\sqrt{m_i m_j}} \exp[i\mathbf{q}\cdot(\mathbf{r}(k'l') - \mathbf{r}(kl))] \\ &= \sum_{k'j} \mathbf{U}_j(k'\mathbf{q}) \mathbf{D}_{ij}(k,k',\mathbf{q}) \end{aligned} \tag{5.7}$$

which defines the mass reduced dynamical matrix $\mathbf{D}(k,k',\mathbf{q})$. If this matrix is evaluated explicitly for a particular reciprocal lattice vector $\mathbf{q}$ the eigenvalues of the matrix can be found by diagonalisation. As in (5.3), the square roots of the eigenvalues give the angular frequencies of the phonon modes. By repeating this procedure for a range of $\mathbf{q}$ vectors, in specific lattice directions in the first Brillouin zone, the dispersion relations for the crystal can be found.

For the complete formulation of the lattice dynamics of molecular crystals see Pawley [75]. Further details of the significance and intricacies of lattice dynamics can be found in the classic text by Born and Huang [76].

To calculate dispersion relations for a molecular crystal we need to know the size, shape and space group (symmetry) of the unit cell, and the orientations of the molecules. We also require a suitable potential with which to model the intermolecular forces. For most substances determining the details of the unit cell by experiment is possible, finding an accurate and computationally simple model for intermolecular

potential can prove harder. One use of lattice dynamics calculations is to test the validity of a potential model for the relevant experimental unit cell parameters and symmetry. An accurate potential should predict that the unit cell configuration found experimentally is the minimum energy configuration of the molecules for the potential used in computation and that the harmonic approximation is valid, *i.e.* there are no large amplitude displacements of the molecules. By comparing frequencies of phonon modes predicted by lattice dynamics calculation to experimental values for the same modes it is sometimes possible to fit potential parameters more accurately.

A stable unit cell configuration with an accurate potential will give positive eigenvalues of the dynamical matrix for all wave vectors in the first Brillouin zone. If negative eigenvalues are obtained this can mean the model of intermolecular potential is inaccurate or that the unit cell has considerable anharmonic properties such that the molecules are subject to large amplitude displacements. We shall now use lattice dynamics to test the validity of a simple model for the interaction of C_{60} molecules.

5.3.2 Lattice dynamics using the Williams potential

The simplest model for interactions between C_{60} molecules is a pairwise additive potential between the carbon atoms in a molecule and all the atoms in its neighbouring molecules. In lattice dynamics a molecule can be assumed rigid if there is no coupling between molecular vibrations and lattice vibrations, *i.e.* the frequency of molecular modes is much greater than those of lattice modes; this assumption is valid for C_{60} [74].

Using the modified parameters for the Williams potential for carbon-carbon interactions (Table 4.2), the dispersion relations for the ordered phase, with the $Pa\bar{3}$ space group and the unit cell configuration described on p.119, were calculated. The minimum potential for the unit cell was predicted to have a lattice parameter of a=14.14Å, which is close to the experimental value of 14.015Å. Since the unit cell contains four molecules with distinctly different orientations, and since there are three translational and three

(a)

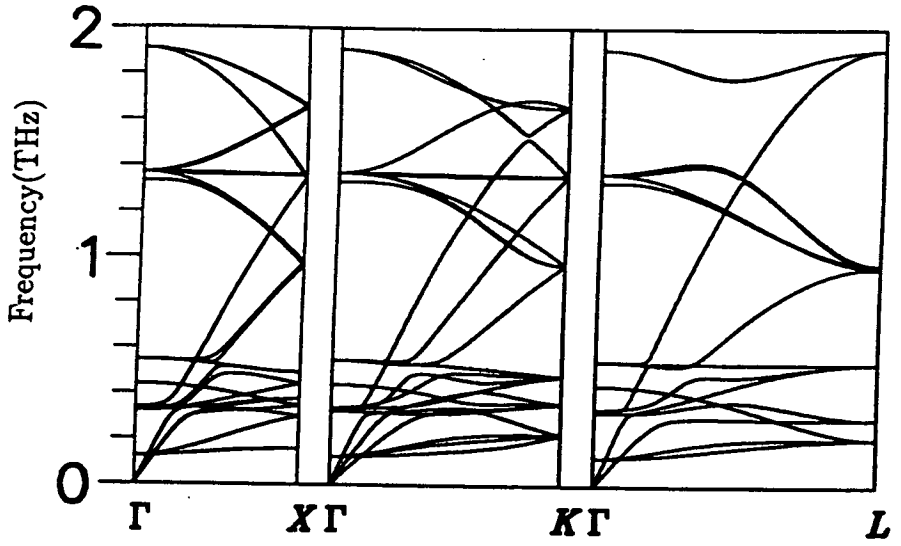

(b)

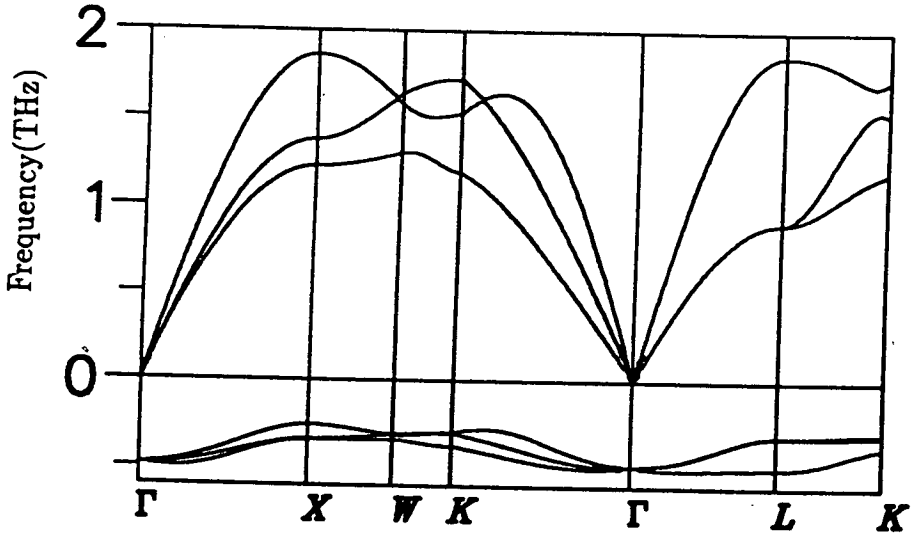

Figure 5.3. Dispersion relations for (a) $Pa\bar{3}$ (b) $Fm3m$.

rotational degrees of freedom associated with each molecule, a total of twenty-four phonon modes must be determined at any point in the Brillouin zone. The dispersion relations in the directions from $\Gamma[000]$ to $X[100]$, $K[\frac{3}{4}\frac{3}{4}0]$ and $L[\frac{1}{2}\frac{1}{2}\frac{1}{2}]$ are shown in Figure 5.3(a).

A detailed analysis of the phonon modes is not required for what we are to be concerned with. The most significant feature of these dispersion relations is that all the phonon eigenmode frequencies have real values. The $Pa\bar{3}$ symmetric unit cell configuration is therefore predicted to be stable for molecular interactions modelled by the Williams potential.

Using the same potential model, the dispersion relations for the plastic phase were then calculated. In this phase molecular orientations are disordered, and since the space group is $Fm3m$ the molecules in the face-centred cubic unit cell are indistinguishable from each other. In the calculation, to describe the unit cell configuration, we require only one molecular orientation, the choice of which can be arbitrary (the unrotated molecule described in Appendix B was used). There are six phonon mode frequencies to be calculated for points in the Brillouin zone. The minimum of potential for the unit cell was found for a lattice parameter of 14.23Å, compared to the experimental lattice parameter for the plastic phase of 14.1Å. The plastic phase dispersion relations are shown in Figure 5.3(b) in various directions between the points $\Gamma[000]$, $X[100]$, $W[1,\frac{1}{2},0]$,$K[\frac{3}{4},\frac{3}{4},0]$ and $L[\frac{1}{2}\frac{1}{2}\frac{1}{2}]$. In this figure eigenvalues with imaginary frequencies are plotted on the negative frequency axis for ease of representation.

The most obvious feature of the dispersion relations is that in all directions in the Brillouin zone three of the branches have positive frequencies and the other three branches have imaginary frequencies. The branches with positive frequencies all go to zero frequency at Γ and so must be the acoustic modes which are associated with translational motion; it must therefore be the rotational modes which are unstable. This means that, in the plastic phase, the molecules can make large amplitude rotational motions *i.e.* reorient.

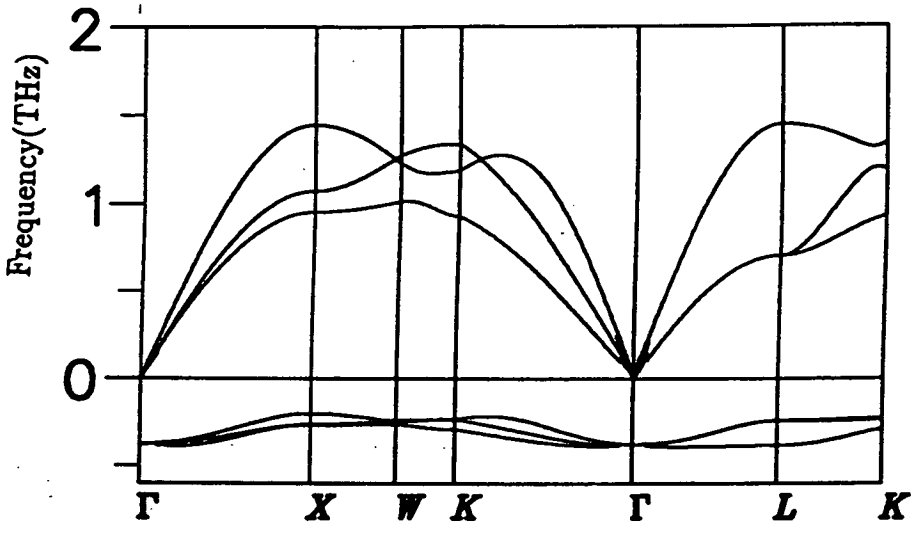

Figure 5.4. Dispersion relations for Fm3m, rescaled potential.

The results of our lattice dynamics calculations can be compared to the results of the inelastic neutron scattering experiments by Pintschovious *et al.* [78]. In such experiments the frequency of phonon modes can be determined from the energy which neutrons lose when scattered by collisions with phonons. Let us now compare the frequency of a mode from experiment to its calculated value. To do so we shall choose the highest frequency translational mode at the point $X[100]$ in the plastic phase (at 295K in experiment). The experimentally measured energy of this phonon mode is 6meV, which (by the Planck relation $h\nu$) corresponds to a frequency of 1.45THz. The calculated frequency is 1.879THz, of the correct order, but significantly larger.

For the model of molecular interaction to be accurate, the calculated values of frequency should match those in experiment. To do this the Williams potential function used must be modified. In (5.3) and (5.7) we can see that the (angular) frequency of a phonon mode is proportional to the second derivative of potential. The simplest method of modifying the potential is to rescale the magnitude of the second derivative

by rescaling the potential parameters which depend on energy by the factor which scales the square of the calculated frequency to the square of the experimental frequency. This factor is $(1.448)^2/(1.879)^2 = 0.6041$. The rescaled Williams potential parameters for carbon are therefore A=342.8kcal/moleÅ^{-6} and B=51952.6 kcal/mole.

The dispersion relations for the plastic phase unit cell were calculated using the rescaled Williams potential. The minimum of potential was again found for a lattice parameter of 14.23Å. The revised dispersion relations in Figure 5.4. can be seen to follow the same shape as before, but with reduced frequencies. The phonon mode at $X[100]$ is now calculated to have a frequency of 1.447THz, which is very close to the experimental value of 1.448THz.

From the lattice dynamics calculations it can be stated that the rescaled version of the Williams potential acting between carbon atoms in neighbouring molecules provides a reasonable model for the intermolecular forces between C_{60} molecules. We shall now proceed to employ this potential in a molecular dynamics simulation of an ensemble of C_{60} molecules.

5.4 Molecular Dynamics Simulations

5.4.1 The low temperature unit cell

The initial ensemble was set up with 4×4×4 face-centred cubic unit cells, with lattice parameter a=14.1Å, containing 256 molecules in total. The random initial velocities corresponded to a temperature of 50K. Random unit quaternions were generated so that initial molecular orientations would be random. During 3000 steps, with a time-step of 0.02ps, the unit cell was observed to undergo a distortion from cubic to tetragonal. After a further 3000 steps the potential energy of the ensemble had stabilised and equilibrium was assumed. The average unit cell was found to be nearly tetragonal with a=13.97(3)Å, b=13.99(2)Å and c=13.60(5)Å. In the equilibrated ensemble there is no evidence of the molecules reorienting.

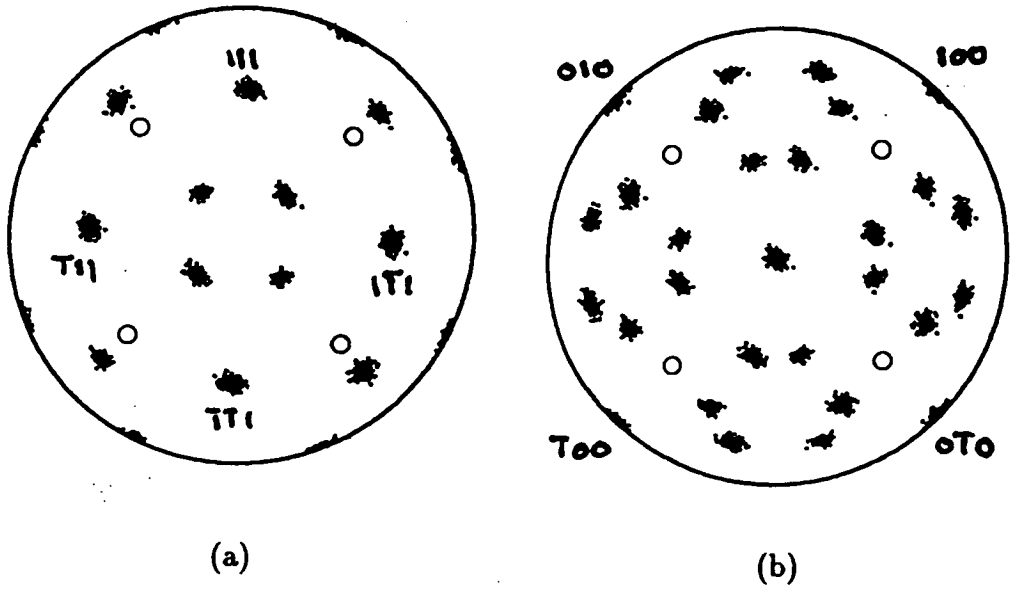

Figure 5.5. O.d.f.s of (a) 3-fold (b) 2-fold symmetry axes at 50K.

The unit cell found by molecular dynamics simulation is obviously not consistent with experimental results, however, it is still of interest to examine the orientational ordering of the molecules. To do this we can adapt the methods used for adamantane discussed in Section 4.3. In cage diagrams (*e.g.* Figure 5.6), the molecules are represented as icosahedra, the underlying symmetric shape of the C_{60} molecule. Again the two overlying *ab* lattice planes in the centre of the cell are shown, viewed down the *c*-axis. Since we are concerned with the orientations of icosahedrally symmetric molecules with respect to cubic and tetragonal unit cells, it is appropriate to consider the orientational distribution function (o.d.f.) of the 3-fold and of the 2-fold axes of symmetry of the molecules. A molecule of C_{60} has twenty 3-fold axes of symmetry, through the centres of each of its quasi-hexagonal faces, and has thirty 2-fold axes of symmetry, through the centres of 6:6 bonds. There will therefore be 10 points associated with each molecule in the o.d.f. of 3-folds and 15 points associated with each molecule in the o.d.f. of 2-folds.

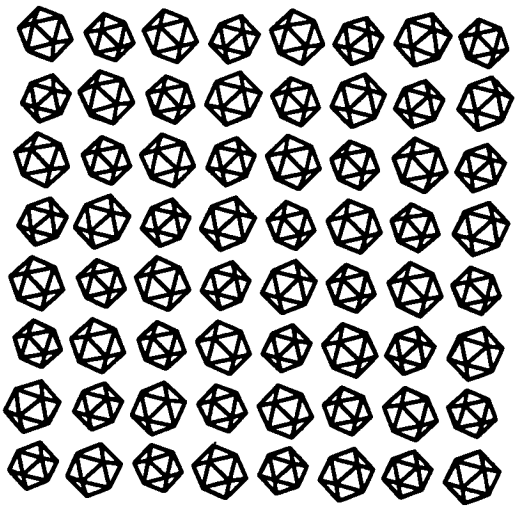

Figure 5.6. *ab* plane centre section at 50K.

Figure 5.5(a) shows the o.d.f. of 3-fold symmetry axes at 50K and Figure 5.5(b) the corresponding o.d.f. of 2-fold symmetry axes. In both o.d.f.s the points lie in distinct groups which indicates that the molecules are in ordered orientations. In Figure 5.5(b) there is a group of points in the centre of the circle showing alignment of 2-fold symmetry axes of the molecules and the *c*-axis of the tetragonal unit cell. If we count the number of groups of points on the o.d.f.s, where a group at the equator will count as half since it is in both hemispheres, we find that there are 16 on the o.d.f. of 3-folds and 27 on the o.d.f. of 2-folds, so that there must be at least two distinct molecular orientations present and that these orientations have four 3-fold and three 2-fold axes in common alignments.

In Figure 5.6 we can see that the upper-edge of each icosahedron is lying in the *ab* plane, so that the 2-fold symmetry axis through this edge must be aligned with the *c*-axis, the [001] direction, which is the 4-fold symmetry axis of the tetragonal unit cell. It is also evident that the upper-edges have have two distinct orientations with

respect to the a and b axes, *i.e.* the [100] and [010] directions. In Appendix B the co-ordinates listed correspond to the upper-edge of the icosahedra being aligned with the [010] direction. The two distinct orientations found in the tetragonal phase can be described by rotations of the molecule by 45° and by -45° about the [001] axis, so that the upper edge lies in the [110] or in the [$\bar{1}$10] direction respectively. These orientations are related by a 90° rotation about the [001] axis.

The tetragonal unit cell may be better defined if we consider the a and b axes of the tetragonal unit cell to be at 45° in the xy plane from the a and b axes of the molecular dynamics cell. The lattice parameters are now, a=b=9.88(9)Å and c=13.60(5)Å. In Figure 5.5(b), we can now see 2-folds aligned with the [100] and [010] directions, which are 2-fold symmetry axes of the tetragonal unit cell. In Figure 5.5(a) we can now see that the 3-fold symmetry axes of the molecule are aligned with the [111] directions of the tetragonal unit cell. Unlike a cubic unit cell, however, the [111] directions of a tetragonal unit cell are not 3-fold symmetry axes of that unit cell. There is no obvious arrangement of the orientations of molecules and their neighbours, so the orientation which a molecule adopts is most likely random. In the tetragonal unit cell the molecule at $(0,0,0)$ is indistinguishable from the molecule at $(\frac{1}{2},\frac{1}{2},\frac{1}{2})$ so the unit cell is body-centred tetragonal.

The results of this simulation are in agreement with those of Cheng and Klein [79, 80] who performed a simulation of 32 C_{60} molecules in 2×2×2 face-centred unit cells using a Lennrd-Jones potential between carbon atoms. Their model predicted a cubic phase above 340K in which molecules act as rotators. On cooling to 103K an ordered tetragonal phase formed.

As we have seen is previous chapters the application of periodic boundary conditions can, in certain cases, affect what phase an ensemble can adopt. In particular, in the 256 molecule simulation of adamantane (Chapter 4) the orientationally ordered tetragonal phase was stable when the simulation started from this phase, however, when cooled from the orientationally disordered cubic phase the tetragonal phase could

not be regained. We must therefore check whether the cubic $Pa\bar{3}$ phase remains stable for a molecular dynamics simulation started in that phase.

A 4×4×4 unit cell ensemble was set up in the cubic $Pa\bar{3}$ phase, with a=14.1Å and molecular orientations as described on p.119. A molecular dynamics simulation, using the same Williams potential model as before, was then performed for 6000 steps of time-step 0.02ps at 50K. The unit cell was found to transform from cubic to tetragonal with a=b=13.74(9)Å and c=14.07(7)Å. This unit cell is different from the unit cell resulting from the previous simulation discussed above, in which the a and b parameters were longer than the c parameter. To distinguish between the two different tetragonal phases we shall refer to the phase resulting from the simulation beginning with random orientations as Tetragonal I, and the phase resulting from the simulation beginning with the cubic $Pa\bar{3}$ structure as Tetragonal II. The volume of the unit cells in these two phases are very similar, with Tetragonal II having a volume only 0.08% larger than that of Tetragonal I. The average potential energy per molecule in Tetragonal I is -30.725 kcal/mole which is lower than that of Tetragonal II with -30.488 kcal/mole. The potential energy of Tetragonal II is 5% lower than the cubic $Pa\bar{3}$ configuration from which it formed.

Figure 5.7 shows the o.d.f.s of 2-folds in Tetragonal II in the [001],[010] and [100] directions, *i.e.* constructed with the equal area projection down the z, y and x axes respectively. The orientational ordering in Tetragonal II is significantly different from that in Tetragonal I (*cf.* Figure 5.5(b)). There are 54 groups of points on each o.d.f. in Figure 5.7, remembering we expect to see 15 2-folds for each molecule, this means there must be at least four different molecular orientations present in this ensemble. The tetragonal symmetry of the phase is evident from the 4-fold symmetric pattern in the [001] direction and the identical 2-fold symmetric patterns in the [010] and [100] directions, which are equivalent in a tetragonal unit cell. There is a large group of points at the centre of the o.d.f. in both the [010] and [100] directions showing an alignment of molecular 2-folds with 2-fold symmetry axes of the unit cell.

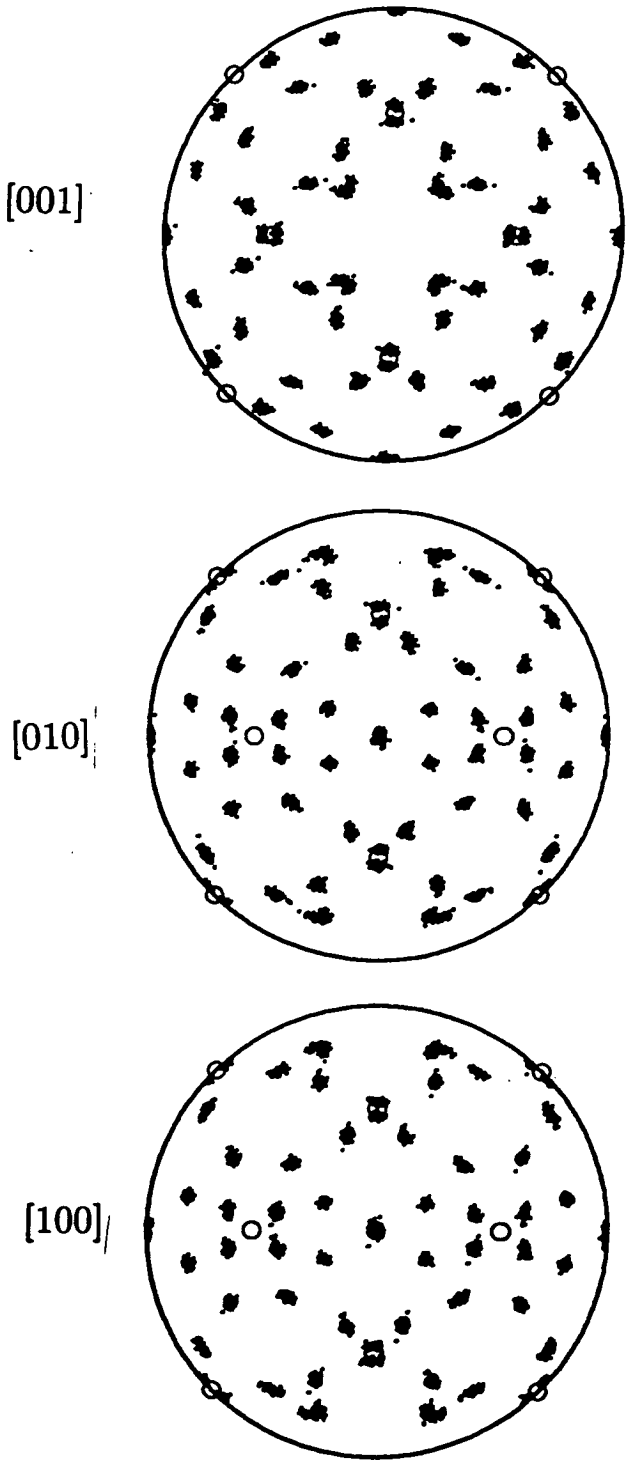

Figure 5.7. O.d.f. of 2-folds for Tetragonal II [001], [010] and [100] directions.

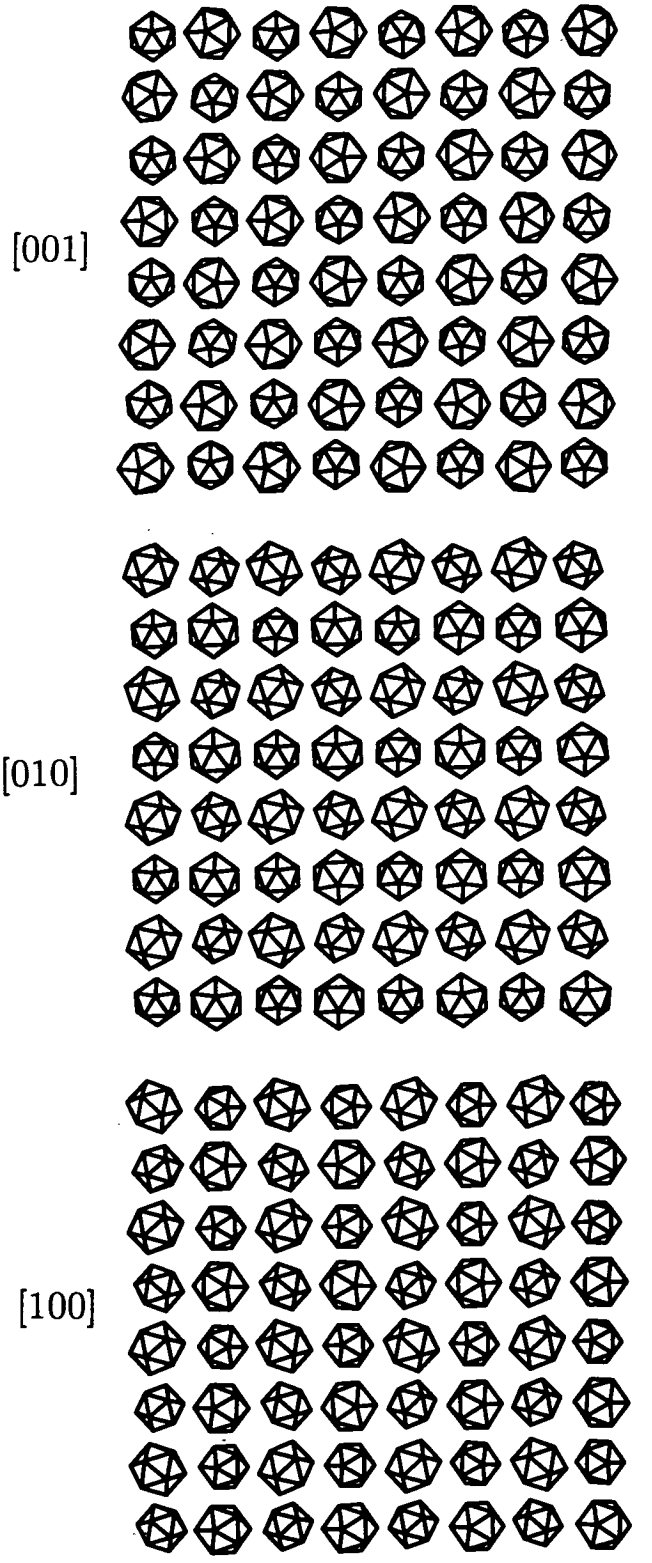

Figure 5.8. Central planes for Tetragonal II viewed in [001],[010] and [100] directions.

Figure 5.8 shows a centre section of the ensemble for planes perpendicular to the [010] and [100] directions, *i.e.* the *ac* plane and *bc* plane. Examining these figures we can see that molecules in alternate *ab* planes are aligned with the [010] direction (y-axis) and then the [100] direction (x-axis). The molecules are rotated by +45° or -45° about the [010] or [100] axis accordingly. If we again define the a and b axes to be at 45° in the xy plane to those of the molecular dynamics cell, then the tetragonal unit cell now has a=b=9.716Å and c=14.07Å. If the molecule at $(0,0,0)$ has a 2-fold aligned with the x-axis, which is now the [110] axis for this tetragonal unit cell, then the molecule at $(\frac{1}{2},\frac{1}{2},\frac{1}{2})$ has a 2-fold aligned with the $[1\bar{1}0]$ of the tetragonal unit cell (the y-axis). The [110] and $[1\bar{1}0]$ axes are 2-fold symmetry axes of the tetragonal unit cell. The orientations of the molecules at $(0,0,0)$ and $(\frac{1}{2},\frac{1}{2},\frac{1}{2})$ are related by a 90° rotation about the [001]. Since the molecule at the body-centre of the cell is in a distinctly different orientation to those on the corners the unit cell is primitive tetragonal, as for the ordered tetragonal phase of adamantane.

Using the Williams potential to model intermolecular forces has produced two distinctly different low temperature unit cells neither of which is consistent with experiment or the predictions from lattice dynamics calculations. The fact that both our simulations and those of Cheng and Klein produce similar results in different sized ensembles with similar but not identical potentials between carbon atoms tends to suggest that the tetragonal phase is neither a finite-size effect nor due to a minor deficiency in potential parameters, but rather that the pairwise additive van der Waals forces between carbon atoms is not an entirely adequate representation for the intermolecular forces between C_{60} molecules. Before we go on to examine why this may be we must first find whether the plastic phase behaviour can be successfully modelled using the Williams potential.

5.4.2 An order-disorder transition

The simulation of the order-disorder transition was started from the Tetragonal I ensemble equilibrated at 50K, since it has a lower potential energy than Tetragonal II at the same temperature. The temperature was increased to 200K and equilibrium re-established over 3000 steps, with time-step 0.02ps. The temperature was then increased in intervals of 20K, the same equilibration procedure being performed at each temperature. The average values of potential energy, volume per molecule and the a, b and c lattice parameters are shown in Figure 5.9. The c lattice parameter shows a steady expansion above 200K, and the a and b lattice parameters (which are coincident) show slight contractions above 340K, until at 580K all the lattice parameters have similar values. At 580K therefore, a transition from a tetragonal to a cubic unit cell is completed. Above 580K the unit cell remains cubic. Both the potential energy of the ensemble and the average volume occupied by a molecule show steady continual increases with temperature. There is no obvious discontinuous change in any of the parameters measured.

We must now examine the orientational ordering in the ensemble. Figure 5.10 shows the o.d.f. of molecular 2-folds at temperatures between 260K and 700K, while Figure 5.11 shows the molecules in the central ab planes at some corresponding temperatures. For later purposes the open circles on the o.d.f.s represent the cubic [110] directions. The o.d.f. at 360K is less ordered than that at 260K and has considerable numbers of points lying outwith the tetragonally ordered groupings. In Figure 5.11, at 260K the molecules retain their tetragonal orientations, with 2-folds aligned with the c-axis, whereas at 360K we can pick out several molecules which are no longer in that orientation (those outlined in boxes in Figure 5.11). At 360K some molecules are reorienting. We can observe how a molecule reorients by examining its orientational trajectory. To do this we use exactly the same method as for adamantane (p.69). Figure 5.12 show the orientational trajectory of two different molecules over the same

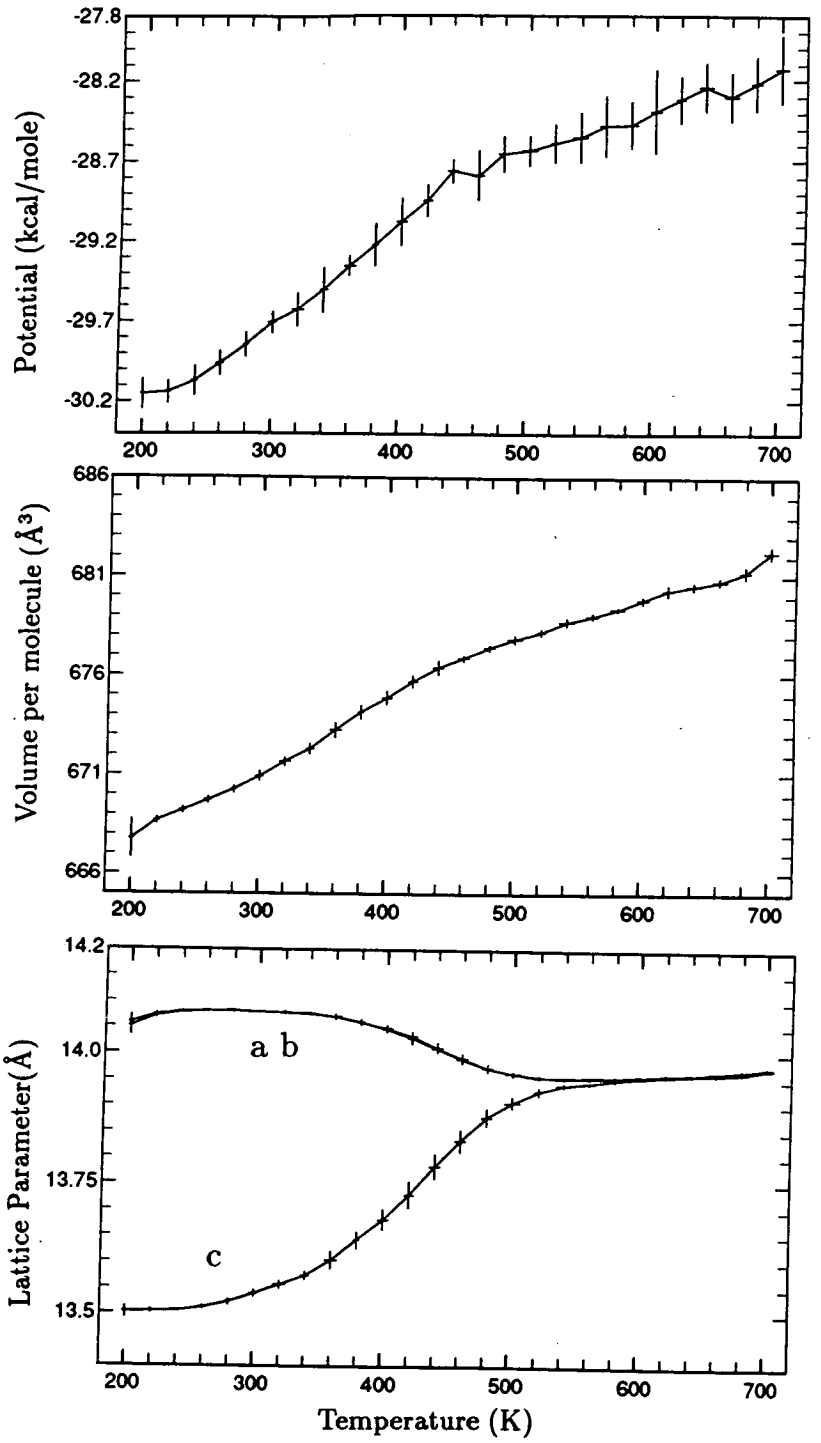

Figure 5.9. Average values of potential, volume per molecule and a, b and c lattice parameters against temperature, on heating.

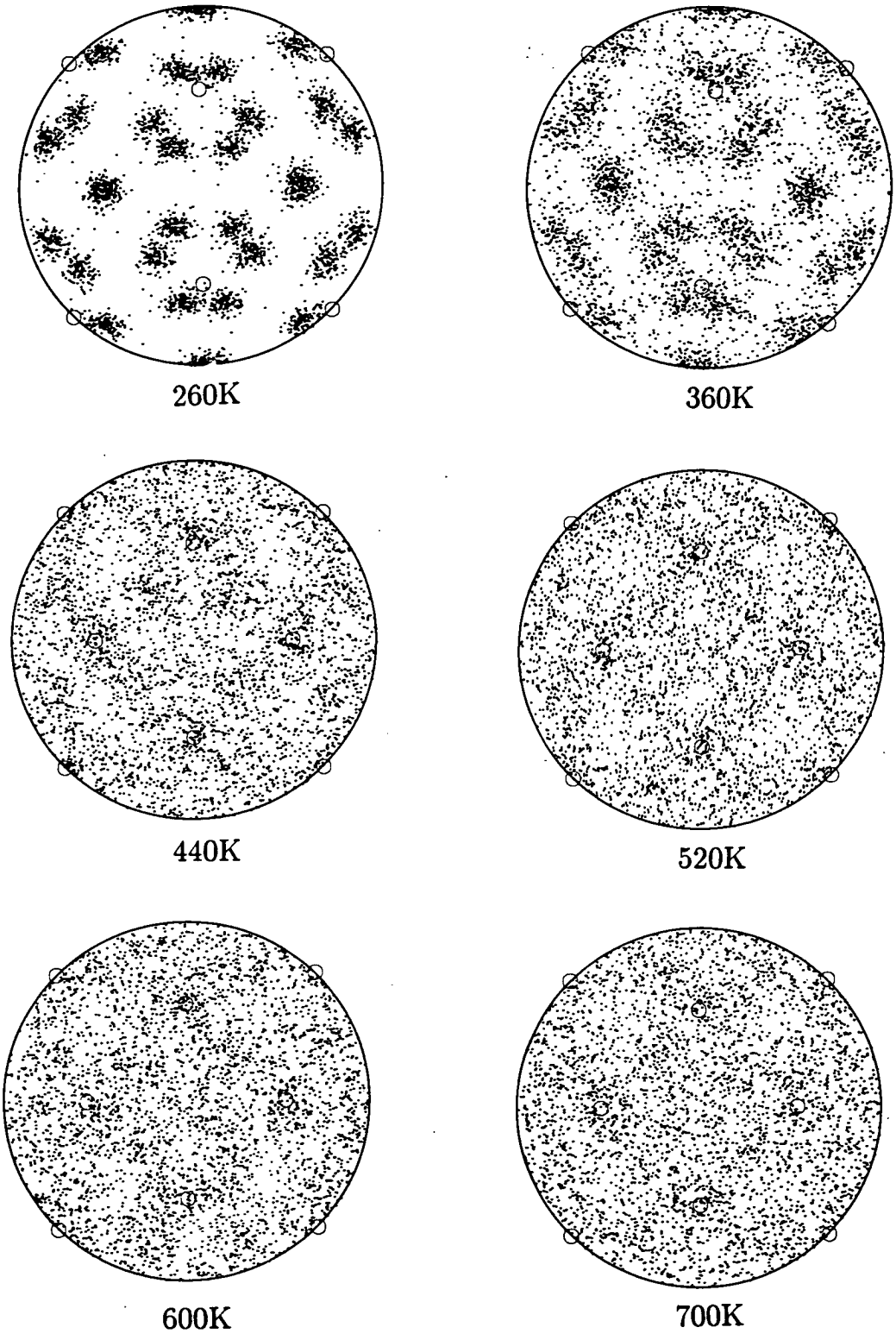

Figure 5.10. O.d.f.s of 2-folds at 260K, 360K, 440K, 520K, 600K and 700K.

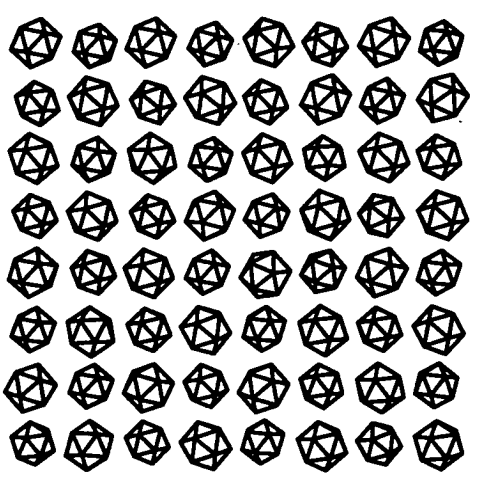

260K

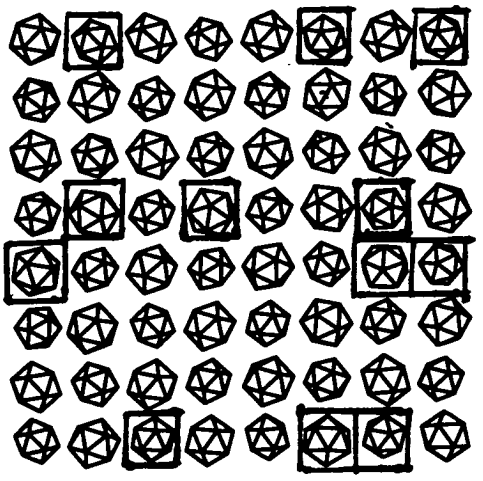

360K

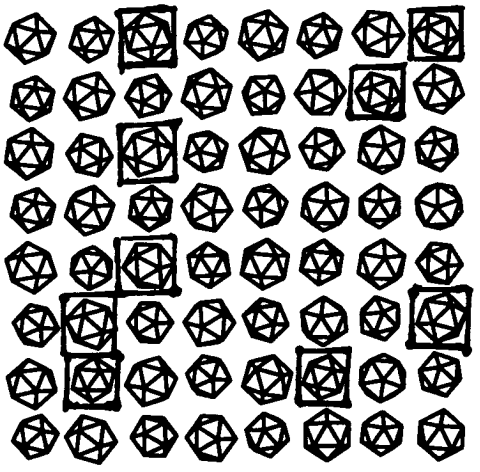

440K

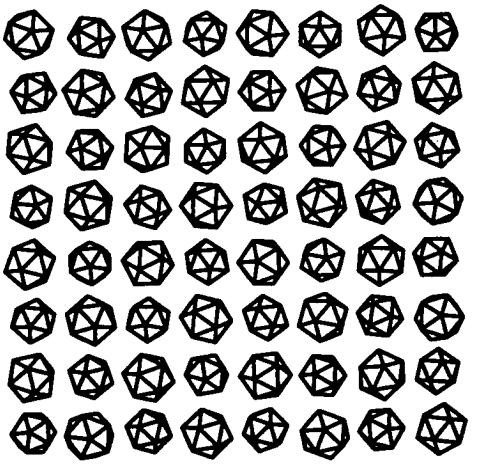

520K

Figure 5.11. *ab* plane centre section at 260K, 360K, 440K and 520K.

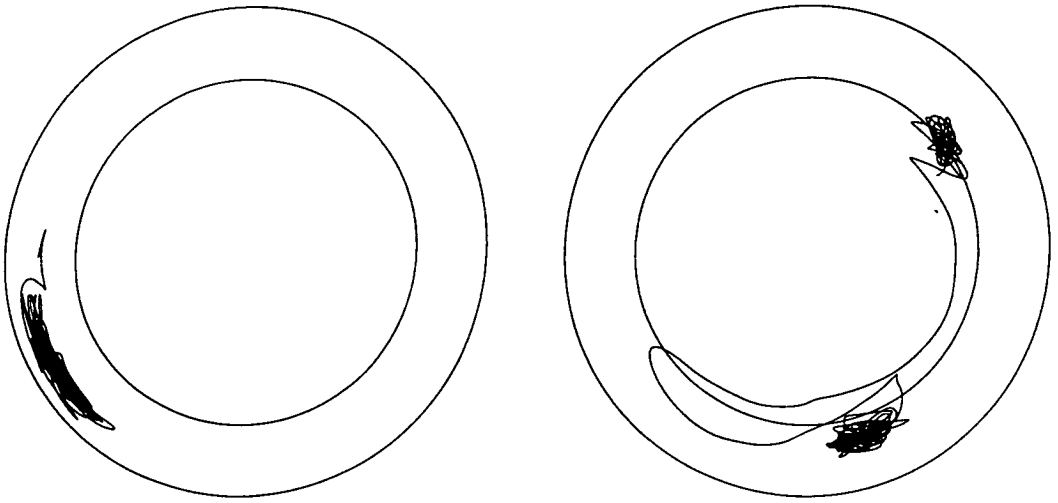

Figure 5.12. Orientational trajectories for two molecules at 360K.

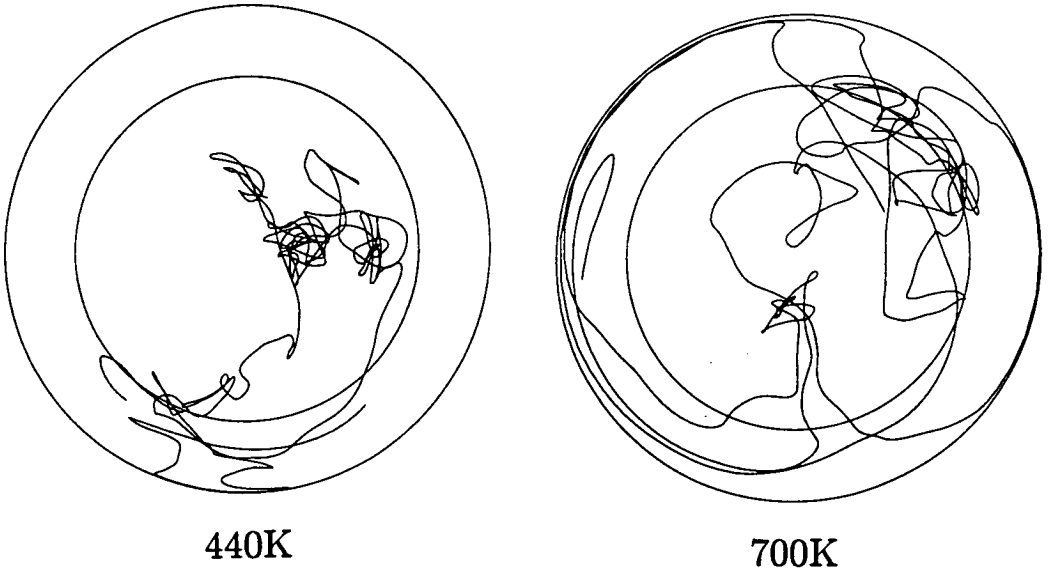

Figure 5.13. Orientational trajectories of a molecule at 440K and 700K.

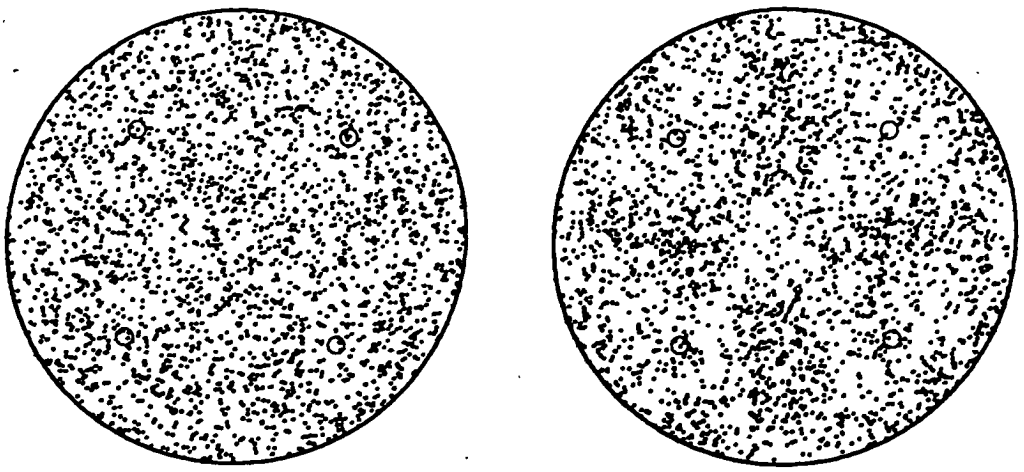

Figure 5.14. O.d.f. of 3-folds (a) random orientations (b) 600K.

120ps of simulation time at 360K. One molecule can be seen to remain in the same orientation for all the time of measurement, while the other makes a reorientational jump between two distinct orientations (*cf.* Figure 4.8).

In the o.d.f. at 440K, the groups of points associated with the orientationally ordered tetragonal ensemble have begun to merge. Most molecules are now reorienting with only a few remaining in the tetragonally ordered orientation (those in boxes in Figure 5.11). The orientational trajectory of a molecule at 420K, again over 120ps, in Figure 5.13, is longer and more random than those at 360K. At 520K the o.d.f. no longer has any obvious separate groups of points. Examining the molecules at 520K in Figure 5.11 only one or two could possibly be in the tetragonally order orientation. In the cubic phase at 600K and 700K the o.d.f.s show similar a distribution of points as the o.d.f at 520K, but more dispersed.

From the orientational analysis we may state that the observed transition from a tetragonal to cubic phase is a disordering transition in which molecules gradually leave

their low temperature orientations and begin to reorient. Above 580K the simulation predicts a face-centred cubic phase, with a=13.95(2)Å at 580K. This cubic phase is orientationally disordered and is a plastic phase in which the molecules have been shown to reorient; all molecules in the unit cell are indistinguishable and thus the space group is $Fm3m$. A cubic plastic phase is consistent with experiment and the lattice dynamics calculations in Section 5.3.2. We may conclude that the Williams potential provides a reasonable model for the cubic plastic phase of C_{60}.

Let us consider the plastic phase further. Figures 5.14(a) and (b) show the o.d.f. for molecular 3-folds of 256 randomly oriented molecules, and the o.d.f. for molecular 3-folds at 600K respectively. If we compare these figures we can see that the o.d.f. at 600K is not entirely random but that there is a higher density of points in some directions and an absence of points in others, suggesting there may be some underlying orientational order in the plastic phase. In Figure 5.14(b) there is a distinct lack of points in the vicinity of the cubic [111] directions, so the plastic phase order does not involve alignment of molecular 3-folds and the cubic [111] directions, as is found in adamantane. If we now re-examine the o.d.f. of molecular 2-folds at 600K in Figure 5.10 we can see, although there are no distinct groupings as in the ordered phase, there appears to be a higher density of points in the vicinity of the cubic [110] directions. In the cubic plastic phase therefore, there is a tendency for the molecular 2-folds to align with the [110] directions which are 2-fold symmetry axes of the cubic unit cell.

The plastic phase of C_{60} has been studied experimentally by David *et al.* [73] using neutron powder diffraction and by Blinc *et al.* [77] using NMR techniques. The results of both sets of experiments discount the molecules reorienting about cubic [111] axes, but support an alternative model involving molecules reorienting about cubic [110] axes. In this model the molecules have 6:6 bonds lying across [110] axes (*i.e.* the 2-folds through 6:6 bonds are aligned with [110] directions) and the molecules exhibit two reorientational motions, large amplitude rotations about [110] axes and discrete reorientational jumps in which molecules change which of their 2-fold symmetry axes

are aligned with [110] directions. Since there is still some alignment of the molecule with the unit cell the reorientations are not isotropic, *i.e.* the molecules are not free rotators. However, because the molecules rotate about a changing axis of rotation, there is no strongly favoured molecular orientation and the molecules are therefore close to being able to rotate unhindered. Blinc calls this reorientational behaviour quasi-isotropic.

Let us now compare the results of our simulations of the plastic phase to the quasi-isotropic model for reorientations from experiment. The lattice dynamical calculations for the plastic phase predicted no stable rotational modes and therefore that the molecules could make large amplitude rotations in any direction. Although the quasi-isotropic model predicts that molecules rotate about a fixed axis, the molecules also reorient such that the axis of rotation changes. The molecular orientation is not stable in the direction of the axis of rotation (the [110] directions) and so no stable rotational modes would be expected. The lattice dynamical calculations are therefore in agreement with the quasi-isotropic model. In the plastic phase in the molecular dynamics simulation we have seen that there is some alignment of molecular 2-folds with the cubic [110] directions, but that there is no strong orientational ordering, which is consistent with the quasi-isotropic model. In the orientational trajectory of a molecule at 300K (Figure 5.12) discrete reorientational jumps are evident. At 700K (Figure 5.13) the trajectory is indicative of molecular rotation, but since there is a higher density of the trajectory in some directions than others the rotation is not isotropic. A more detailed investigation of reorientational motion by molecular dynamics simulation would be required to confirm for certain whether the Williams potential model predicts the same reorientational motions as the quasi-isotropic model from experiment.

5.5 Discussion

Since lattice dynamics calculations using the Williams potential have predicted the cubic $Pa\bar{3}$ phase to be stable, this structure must be a local minimum energy unit cell configuration for C_{60} molecules interacting *via* the Williams potential. In molecular dynamics simulations, unlike lattice dynamics, large changes in the unit cell configuration and molecular orientations are possible, hence the C_{60} molecules can adopt a tetragonal unit cell configuration which has a lower potential energy compared to the cubic $Pa\bar{3}$ configuration.

We now require some ideas as to what potential can be used to successfully reproduce the cubic $Pa\bar{3}$ phase at low temperatures. After Cheng and Kleins' original papers there was considerable interest in this problem. The favoured approach was that, as well as the van der Waals forces between carbon atoms, there are also significant electrostatic forces between molecules. Sprik, Cheng and Klein [81] tested this by adding an extra interaction site for the Lennard-Jones potential at the centre of the 30 6:6 bonds. The results of their simulation using this model for intermolecular forces did produce an orientationally ordered cubic unit cell, but the orientations which the molecules adopted were not consistent with the required $Pa\bar{3}$ symmetry.

More realistic models of electrostatic forces involve placing discrete charges on certain sites on the molecule and calculating the resultant forces via the Coulomb potential,

$$\phi(r) = \frac{\mathcal{E}_0 q_i q_j}{r_{ij}} \tag{5.8}$$

where q_i and q_j are the charges on site i of a molecule and site j of a neighbouring molecule respectively which are separated by distance r_{ij}, and $\mathcal{E}_0$ is the permittivity of free space. Li, Lu and Martin [82] propose a model of the forces between C_{60} molecules

which involves a Lennard-Jones potential between carbon atoms and Coulombic interactions between charges of $q = -0.54e$ on the centre of 6:6 bonds and compensating charges of $q = +0.27e$ on the centre of the 60 6:5 bonds. By a static minimisation of the unit cell energy, they claim that the $Pa\bar{3}$ configuration is stable for this potential, however, as we have seen above a minimum of potential is not a guarantee of stability. It is also difficult to justify how positive charges can be place in the centre of bonds, which, as bonds should be, are occupied by negatively charged electrons. A similar model due to Burgos, Halac and Bonadeo [83] has charges of $q = -0.25e$ on the centre of 6:6 bonds, but this time with charges of $q = +0.625$ on the centres of pentagonal faces. Their claims for the validity of this potential in stabilising the $Pa\bar{3}$ configuration are again not based on a molecular dynamics simulation, but instead on calculating the equation of state. Heid [84] and Yildirim *et al.* [85] have both determined the electrostatic interaction between molecules by determining the electrostatic moments of a molecule according to icosahedral symmetry. Whatever the validity of this approach, however, the resultant description of intermolecular forces is too complicated to be applied in numerical simulations.

In a different approach, Girifalco [86] describes the interaction of C_{60} in the plastic and liquid phases by treating the molecules as spheres interacting by van der Waals forces and using the Lennard-Jones potential smeared out over the surface of such spheres to determine forces between molecules. Cheng, Klein and Caccamo [87] have used this potential to determine a liquid-solid (or more accurately liquid-plastic) phase diagram.

Since there has as yet been no conclusively successful description of the intermolecular forces between C_{60} molecules, it is appropriate to suggest some possible models. If electrostatic forces are genuinely a significant factor in molecular interaction, then any model of such forces should be consistent with the electronic structure of the molecule, *i.e.* the bonding between carbon atoms. Most of the electrostatic models discussed above assume the 6:6 bonds to be double bonds and the 6:5 bonds to be single bonds,

which would create a significant difference in charge densities between the two different bond sites. However, as stated earlier, the difference between the lengths of these bonds suggest that they are not what is conventionally understood as double and single bonding. The initial results of an *ab initio* calculation of the electronic structure of a C_{60} molecule [88] suggest that in fact there may be little difference in the charge density associated with each type of bond. To construct a model for the electrostatic interaction of C_{60} molecules, positive charge (with $q < +4e$) should be sited on atomic positions, since this is where the positively charged atomic nuclei are. Negative charges should be placed at the centre of each bond. The magnitude of the charge on the different types of bond should be similar, and of course be such that overall neutrality of the molecule is maintained. The problem with this model is that, because the pairwise additive potential for this model now requires $60^2 + 90^2$ calculations to determine the total force between two molecules, the computation required for a molecular dynamics simulation becomes prohibitive.

Although most of the suggestions for intermolecular potentials for C_{60} have so far been based on electrostatics there is as yet no direct evidence, either theoretical or experimental, that the electronic structure of C_{60} is polarized to a significant degree. Even if this is the case the high symmetry of the molecule means that is cannot be a dipole or quadrapole, but must have a higher electrostatic moment, which would mean that the overall Coulomb interactions would fall off with distance faster than the r^{-6} of the van der Waals forces. Indeed the molecule is a good approximation to a sphere with an even distribution of positive and negative charges on its surface, which by the laws of electrostatics is equivalent to equal amounts of positive and negative charge at the centre of the sphere and so the electrostatic moment would be zero.

Pairwise additive van der Waals type potentials have been used extensively to successfully model molecular crystals, adamantane in the previous chapter being a good example. That this method fails for C_{60} can most probably be attributed to the unusual structure of the molecule, in particular the fact that all atoms and bonds are on

the surface of a sphere; atoms and bonds on neighbouring molecules in crystalline C_{60} are all in close proximity to other atoms and bonds, compared to a molecule such as adamantane where it is only hydrogen atoms which are in in close proximity. For van der Waals type potentials the r^{-6} attractive term is a well known and well tested result from electrostatics. The repulsive terms in these potentials, however, rarely have a sound theoretical derivation and are most often chosen to have a convenient mathematical form with parameters fitted to experimental quantities such as lattice parameters or phonon frequencies, as shown earlier. The repulsive potential is intended to represent the complex quantum mechanical forces of repulsion when atoms and electrons approach each other. We may argue therefore that, rather than add discrete charges to atoms and bonds and use the classical Coulomb potential, it is the form of the repulsive forces which should be changed. Attractive van der Waals forces can only occur between atomic sites, however, the bond-bond interaction will be repulsive, so extra interaction sites for the repulsive potential should be added at the centre of bonds.

The simulations performed on C_{60} provided some curious, but interesting results. Further simulations would be worthwhile, as part of the general study of molecular crystals and in particular the problem of accurate representation of intermolecular potentials.

After the initial mad rush to explore the possibilities of C_{60} and the other fullerenes, scientific interest in the subject has declined considerably in the last two years. This has largely been due to the failure to find any practical application for the new material, despite suggestions as varied as superconductors and sunglasses. To the greater extent, therefore, C_{60} remains as a scientific curiosity, which is not necessarily a bad thing.

Appendix A

The adamantane molecule

The atomic co-ordinates of a molecule of adamantane are listed in Table A.1. The molecule is centred at (0,0,0) and all lengths are in Ångströms. The mass of a molecule of adamantane is 10×12+16×2=152 a.m.u. if the hydrogen is deuterium. The inertia tensor may be derived as follows

$$\tilde{I} = \sum m_i \begin{pmatrix} x_i x_i & x_i y_i & x_i z_i \\ y_i x_i & y_i y_i & y_i z_i \\ z_i x_i & z_i y_i & z_i z_i \end{pmatrix}$$

where m_i is the mass of atom i and x_i, y_i and z_i are the atomic co-ordinates relative to the molecules centre. For adamantane

$$\tilde{I} = \begin{pmatrix} 332.15386 & 0.0 & 0.0 \\ 0.0 & 332.15386 & 0.0 \\ 0.0 & 0.0 & 332.15386 \end{pmatrix} \text{a.m.u.Å}^2$$

Atom	x	y	z	Atom	x	y	z
C	1.77660	0.00000	0.00000	H	-2.40975	-0.63315	0.63315
C	0.00000	1.77660	0.00000	H	-0.63315	2.40975	-0.63315
C	0.00000	0.00000	1.77660	H	0.63315	2.40975	0.63315
C	-1.77660	0.00000	0.00000	H	-0.63315	-2.40975	0.63315
C	0.00000	-1.77660	0.00000	H	0.63315	-2.40975	-0.63315
C	0.00000	0.00000	-1.77660	H	-0.63315	-0.63315	2.40975
C	-0.88830	-0.88830	-0.88830	H	0.63315	0.63315	2.40975
C	0.88830	0.88830	-0.88830	H	0.63315	-0.63315	-2.40975
C	0.88830	-0.88830	0.88830	H	-0.63315	0.63315	-2.40975
C	-0.88830	0.88830	0.88830	H	-1.52145	-1.52145	-1.52145
H	2.40975	-0.63315	-0.63315	H	1.52145	1.52145	-1.54125
H	2.40975	0.63315	0.63315	H	1.54125	-1.54125	1.54125
H	-2.40975	0.63315	-0.63315	H	-1.54125	1.54125	1.54125

Table A.1. Atomic co-ordinates of adamantane.

Appendix B

The C_{60} molecule and units

Since the atomic positions in the C_{60} molecule correspond to the vertices of the well known geometric figure of a truncated icosahedron there is a simple method of generating the atomic co-ordinates. If a is the length of the 6:5 bond and b is the length of the 6:6 bond (a=1.45Å, b=1.40Å) then the radius of the molecules is

$$R = \sqrt{\lambda^2 \left(a + \tfrac{b}{2}\right)^2 + \tfrac{b^2}{4}}$$

where $\lambda = \frac{1+\sqrt{5}}{2}$ is the golden mean of antiquity. The symmetry of the molecule is $m\bar{3}$ so all atomic positions may be generated from the positions of only three atoms on the surface of the sphere

atom 1	$\frac{b}{2}$	0	$\lambda\left(a+\frac{b}{2}\right)$
atom 2	$\frac{a\lambda}{2}$	$\frac{a+b}{2}$	$\left[R^2-\left(\frac{a+b}{2}\right)^2-\frac{a^2\lambda^2}{4}\right]^{\frac{1}{2}}$
atom 3	$\frac{a\lambda^2+b}{2}$	$\frac{a}{2}$	$\left[R^2-\left(\frac{a\lambda^2+b}{2}\right)^2-\frac{a^2}{4}\right]^{\frac{1}{2}}$

These three atoms are linked by one 6:6 bond and one 6:5 bond. The 60 atomic co-ordinates can then be generated by cyclic combinations of all the permutations of positive and negative values of the three sets of co-ordinates above, i.e. $(\pm x, \pm y, \pm z)$, $(\pm y, \pm z, \pm x)$ and $(\pm z, \pm x, \pm y)$.

The C_{60} molecule has a mass of 60×12=720 a.m.u.. Using the method of deriving the inertia tensor given in Appendix A and the co-ordinates generated by the method given above the inertia tensor of the C_{60} molecule is

$$\tilde{I} = \begin{pmatrix} 6043.411 & 0.0 & 0.0 \\ 0.0 & 6043.411 & 0.0 \\ 0.0 & 0.0 & 6043.411 \end{pmatrix} \text{a.m.u.Å}^2.$$

The units used in this thesis,

Quantity	Unit	S.I. unit
length	Ångströms (Å)	10^{-10}m
time	picosecond (ps)	10^{-12}s
frequency	terahertz (THz)	10^{12}Hz
mass	atomic mass unit (a.m.u.)	1.6605×10^{-27}kg
potential energy	kcal/mole	0.043453eV

Bibliography

[1] Metropolis,N., *et al.*, J. Chem. Phys. **21** p.1087 (1953).

[2] Alder,B.J. & Wainright,T.E., J. Chem. Phys. **37** p.1208 (1957).

[3] Rahman,A., Phys. Rev. A **136** p.405 (1964).

[4] Kihara,T., Intermolecular Forces, Wiley (1978).

[5] Lennard-Jones, J.E., Proc. Roy. Soc (London) **A106** p.463 (1924).

[6] Ackland,G.J. *et al.*, Phil. Mag. A **56** p.735 (1987).

[7] Car,R. & Parinello,M., Phys. Rev. Lett. **55** p.2471 (1985).

[8] Kibble,T.W., Classical Mechanics, Longman (1985).

[9] Parrinello,M. & Rahman,A. Phys. Rev. Lett. **45** p.1196 (1980).

[10] Nosé,S. & Klein,M., Mol. Phys. **50** p.1055 (1983).

[11] Beeman,D., J. Comp. Phys. **2** p.130 (1976).

[12] Verlet,L., Phys. Rev. **159** p.98 (1967).

[13] Press,W.H., Flannery,B.P., Teukolsky,S.A. & Vetterling,W.T., Numerical Recipes, Cambridge University Press (1986).

[14] DuVal,P., Homographies Quaternions and Rotations, Oxford (1964).

[15] Pawley,G.S., Mol. Phys. **43** p.1321 (1981).

[16] Refson,K. & Pawley,G.S., Mol. Phys. **61** p.669 (1987).

[17] Cahn,R.W., Nature **323** p.668 (1986).

[18] Cotterill,R.M.J., J. Cryst. Growth **48** p.582 (1980).

[19] Hayes,W., Contemp. Phys. **27** p.519 (1986).

[20] Gleick,J., Genius:Richard Feynmann and Modern Physics, Little,Brown (1992).

[21] Kosterlitz,J.M. & Thouless,D.J. J. Phys. C **6** p.1181 (1973).

[22] Nelson,D.R. & Halperin,B.I., Phys. Rev. B **18** p.2318 (1978).

[23] Halperin,B.I. & Nelson,D.R., Phys. Rev. Lett. **41** p.121 (1978).

[24] Young,A.P., Phys. Rev. B **19** p.1855 (1979).

[25] Standburg,K.J., Rev. Mod. Phys. **60** p.161 (1988).

[26] Abraham,F.F., Physics Reports **80** p.339 (1981).

[27] Specht,E.D. *et al.* Phys. Rev. B. **30** p.1589-1592 (1984).

[28] McTague,J.P. *et al*, Phys. Rev. B. **25** p.7765 (1982).

[29] Heiny,P.A. *et al.* Phys. Rev. Lett. **48** p.104 (1982).

[30] Frenkel,D. & McTague,J.P., Phys. Rev. Lett. **42** p.1632 (1979).

[31] Ramirez,R. & Utrera,L., Phys. Rev. B **47** p.4555 (1993).

[32] Chui,S.T., Phys. Rev. Lett. **48** p.933 (1982).

[33] Saito,Y., Phys. Rev. B **26** p.6239 (1982).

[34] Combs,J.A., Phys. Rev. Lett. **61** p.714 (1988).

[35] Abraham,F.F., Phys. Rev. Lett. **44** p.463 (1980).

[36] Toxvaerd,S., Phys. Rev. Lett. **44** p.1002 (1980).

[37] Choquard,Ph., & Clerouin,J., Phys. Rev. Lett. **50** p.2086 (1983).

[38] Ashcroft,N.,W., & Mermin,N.D., Solid State Physics, Saunders College (1976).

[39] Mandell,M.,J., McTague,J.P. & Rahman,A., J. Chem. Phys. **64** p.3699 (1976).

[40] Mandell,M.,J., McTague,J.P. & Rahman,A., J. Chem. Phys. **66** p.3070 (1977).

[41] Hsu,C.S. & Rahman,A., J. Chem. Phys. **71** p.4974 (1979).

[42] Swope,W.C. & Andersen,H.C., Phys. Rev. B **41** p.7042 (1990).

[43] Oxtoby,D.W., J. Phys. Cond. Matt. **4** p.7627 (1992).

[44] Jäckle,J., Rep. Prog. Phys. **49** p.171 (1986).

[45] Jónsson,H. & Andersen,H.C., Phys. Rev. Lett. **60** p.2295 (1988).

[46] Wahnström,G., Phys. Rev. A **44(6)** p.3752 (1991).

[47] Hoheisel,C., Mol. Phys. **62** p.385 (1987).

[48] Ackland,G.J. & Vitek,V., Phys. Rev. B **41** p.10324 (1990).

[49] Nordman,C.E. & Schmitkons,D.L., Acta Cryst. **18** p.764 (1965).

[50] Amoureux,J.P., Bee,M. & Damien,J.C. Acta Cryst. **B36** p.2633 (1980).

[51] Yamamoto,S. & Hosokawa,T., J. Phys. Soc. Japan **63** p.1828 (1994).

[52] Reynolds,P.A., Acta Cryst. **A34** p.242 (1978).

[53] Meyer,M. & Ciccotti,G., Mol. Phys. **56** p.1235 (1985).

[54] Meyer,M., Marhic,C. & Ciccotti,G., Mol. Phys. **58** p.723 (1986).

[55] Yashonath,S. & Rao,C.N.R., J. Phys. Chem. **90** p.2552 (1986).

[56] Trew,A.S. & Pawley,G.S., Can. J. Chem. **66** p.1018 (1988).

[57] Ciccotti,G. *et al.*, Phys. Rev. Lett. **59** p.2574 (1987).

[58] Williams,D.E., J. Chem. Phys. **47** p.4680 (1967).

[59] Dove,M.T. & Pawley,G.S., Mol. Phys. **55** p.1147 (1985).

[60] Danelian,A., Phys. Rev. **133** p.1344 (1964).

[61] Binder,K., Z. Phys. B **45** p.61 (1981).

[62] Styer,D.F., Phys. Rev. B **32** p.393 (1985)

[63] Nowotny,R.M. & Binder,K., Z. Phys. B **77** p.287 (1989).

[64] Schweika,W., Binder,K. & Landau,D.P., Phys. Rev. Lett. **26** p.3321 (1990).

[65] Kroto,H.W., Heath,J.R., O'Brien,S.C., Curl,R.F. & Smalley,R.E., Nature **318** p.162 (1985).

[66] Krätschmer,W., Lamb,L.D., Fostiropoulous,K. & Huffman,D.R., Nature **357** p.354 (1990).

[67] David,W.I.F. *et al.*, Nature **353** p.147 (1991).

[68] Hawkins,J.M. *et al.*, Science **252** p.312 (1991).

[69] Cox,P.A., The Electronic Structure and Chemistry of Solids, Oxford (1987).

[70] Kroto,H.W., Nature **329** p.529 (1987).

[71] Ettl,R., Diederich,F. & Whetten,R.L., Nature **353** p.149 (1991).

[72] David,W.I.F., Ibberson,R.M., Dennis,T.J.S., Hare,J.P. & Prassides,K., Europhys. Lett. **18** p.219 (1992).

[73] David,W.I.F., Ibberson,R.M., Dennis,T.J.S., Hare,J.P. & Prassides,K., Europhys. Lett. **18** p.735 (1992).

[74] J. Yu, L. Bi, Kalia,R.,K. & Vashita,P., Phys. Rev. B **49** p.5009 (1994).

[75] Pawley,G.S., Phys. Stat. Solidi **49** p.475 (1972).

[76] Born,M. & Huang,K., Dynamical Theory of Crystal Lattices, Oxford (1954).

[77] Blinc,R., Seliger,J., Dolinšek,J. & Arčon,D., Phys. Rev. B **49** p.4993 (1994).

[78] Pintschovious,L. *et al.*, Phys. Rev. Lett. **69** p.2662 (1992).

[79] Cheng,A. & Klein,M.L., J. Phys. Chem. **95** p.6750 (1991).

[80] Cheng,A. & Klein,M.L., Phys. Rev. B **45** p.1889 (1992).

[81] Sprik,M., Cheng,A. & Klein,M.L., J. Phys. Chem. **96** p.2027 (1992).

[82] J.-P. Lu, X.-P. Li & Martin,R.,M., Phys. Rev. Lett. **68** p.1551 (1992).

[83] Burgos,E., Halac,E., & Bonadeo,H., Phys. Rev. B **47** p.13903 (1993).

[84] Heid,R., Phys. Rev. B **47** p.15912 (1993).

[85] Yildirim,T., Harris,A.B., Erwin,E.C. & Pederson,M.R., Phys. Rev. B **48** p.1888 (1993).

[86] Girifalco,L.A., J. Phys. Chem. **96** p.858 (1992).

[87] Cheng,A., Klein,M.L. & Caccamo,C., Phys. Rev. Lett. **71** p.1200 (1993).

[88] Clark,S.J., Private Communication.